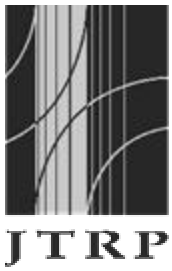

INVESTIGATION OF NOVEL ACOUSTIC BARRIER CONCEPTS PHASE I: CONCEPT DEVELOPMENT AND PRELIMINARY EVALUATION

Final Report
SQDH 2003 – 2;
FHWA/IN/JTRP-2003/9; HL 2003 - 6

By:
Luc Mongeau, Principal Investigator
J. Stuart Bolton, Principal Investigator
Sanghoon Suh, Research Assistant
The Institute for Safe, Quiet and Durable Highways
School of Mechanical Engineering, Purdue University

Sponsored by: The Institute for Safe, Quiet and Durable Highways, and
Joint Transportation Research Program,
Purdue University
The Toll Road District, Indiana DOT

In Cooperation With: University Transportation Program, and
Federal Highway Administration, U.S. DOT

Approved by: Robert J. Bernhard, Director
Vincent P. Drnevich, Co-Director
The Institute for Safe, Quiet and Durable Highways

June 2003

Technical Report Documentation Page

1. Report No.	2. Government Accession No.	3. Recipient's Catalog No.
SQDH 2003-2		

4. Title and Subtitle	5. Report Date
Investigation of Novel Acoustic Barrier Concepts Phase I: Concept Development and Preliminary Evaluation	June 2003
	6. Performing Organization Code FHWA/IN/JTRP-2003/9; HL 2003-6
7. Author(s) Luc Mongeau, J. Stuart Bolton, and Sanghoon Suh	8. Performing Organization Report No.
9. Performing Organization Name and Address The Institute for Safe, Quiet and Durable Highways Purdue University 140 S. Intramural Drive West Lafayette, IN 47907-2031	10. Work Unit No. (TRAIS)
	11. Contract or Grant No. SPR-2593
12. Sponsoring Agency Name and Address Joint Transportation Research Program Purdue University 550 Stadium Mall Drive West Lafayette, IN 47907 – 2051	13. Type of Report and Period Covered **Final Report**
	14. Sponsoring Agency Code

15. Supplementary Notes:
Prepared in Cooperation with the Indiana Department of Transportation, Federal Highway Administration, and University Transportation Centers Program

16. Abstract

In a previous research project [SQDH 2002-3; "Study of the Performance of Acoustic Barriers for Indiana Toll Roads,"] the influence of environmental factors and of advanced sound barrier concepts was investigated. The presence of temperature gradients over pavements was found to have a strong influence on sound propagation. Refraction of sound waves emitted by tire-road interactions in the vicinity of the ground also affects sound barrier performance. Modified ray tracing model suggested that prevailing winds have an influence on barrier performance at large distances. Randomized edge configurations were found not to improve barrier performance for traffic noise. Random edges simply scatter sound energy without any net noise reduction. Although the edge can be optimized for specific frequency components and locations, it appears that optimization for broadband noise control is difficult. The study also suggested that adding sound absorptive material along the barrier edge could enhance barrier performance.

The present study is the continuation of the latter effort to confirm the findings related to the sound absorptive treatment on the barrier through a more rigorous study and to apply the design concept to a realistic situation. A comparison was made between barriers that incorporated sound absorptive treatments and barriers with T-shaped tops. The results confirmed that a sound absorptive treatment near the barrier edge resulted in a performance improvement over corresponding rigid barriers. A design optimization study of the most effective shape of acoustic treatments concluded that a circular shape works best. The performance of two different acoustical materials was also compared. Use of glassfiber resulted in better performance in the high frequency region, while polyolefin foam with closed cells achieved a relatively large insertion loss at low frequencies.

Efforts were made to develop a numerical predictive model. The boundary element method was used to model the infinite size surrounding fluid effectively. The disadvantage of the boundary element model is the calculation load associated with the large number of elements required for high frequency analysis. A mesh optimization procedure was successfully implemented in the boundary element model to reduce the calculation time while satisfying the tolerances for analysis accuracy at each analysis frequency. Octave band averaging was also adapted to facilitate the comparison between the numerical results and experimental data. It was found that the results from the boundary element model agree relatively well with the experimental results up to 6300 Hz at selected locations. The insertion loss distribution proved the numerical model's capability of reproducing the rather complicated interference pattern on the receiver plane correctly at one-third octave band frequencies from 1000 Hz to 6300 Hz. Spatial-averaged insertion losses over different size receiver planes showed that the numerical model was less reliable when the averaging was done close to the ground level.

Preliminary measurements for an actual, real-size barrier were performed in South Bend, Indiana, to identify a measurement location that can be used to verify the effectiveness of the proposed add-on device. The add-on device was designed based on laboratory experiments and numerical studies, and was proven to be effective in a realistic highway environment. Federal Highway Administration (FHWA) Traffic Noise Model (TNM) was exercised for the comparison of the measurements. On-site measurements were performed to evaluate the absorptive treatment. Application of the treatment over a limited (6 m) region improved the performance of the barrier by 2 to 5 dB at the frequencies from 2000 Hz to 5000 Hz.

17. Key Word	18. Distribution Statement
sound barriers, traffic noise, sound propagation, sound absorptive material, acoustic treatment	No restrictions. This document is available to the public through the National Technical Information Service, Springfield, VA 22161

19. Security Classif. (of this report)	20. Security Classif. (of this page)	21. No. of Pages	22. Price
Unclassified	Unclassified		

TABLE OF CONTENTS

Page

LIST OF TABLES

LIST OF FIGURES

Figure Page

Figure Page

Figure Page

ABSTRACT

Suh, Sanghoon. Ph.D., Purdue University, December, 2002. Investigation of Novel Acoustic Barrier Concepts Phase I. Major Professor: Dr. Luc Mongeau and Dr. J. Stuart Bolton.

In a previous research project [SPR 2418; "Study of the performance of acoustic barriers for Indiana toll roads,"] the influence of environmental factors, and of advanced sound barrier concepts was investigated. The presence of temperature gradients over pavements was found to have a strong influence on sound propagation. Refraction of sound waves emitted by tire-road interactions in the vicinity of the ground also affect sound barrier performance. Modified ray tracing model suggested that prevailing winds have an influence on barrier performance at large distances. Randomized edge configurations were found not to improve barrier performance for traffic noise. Random edges simply scatter sound energy without any net noise reduction. Although the edge can be optimized for specific frequency components and locations, it appears that optimization for broadband noise control is difficult. The study also suggested that adding sound absorptive material along the barrier edge could enhance barrier performance.

The present study is the continuation of the latter effort to confirm the findings related to the sound absorptive treatment on the barrier through a more rigorous study and to apply the design concept to a realistic situation. A comparison was first made between barriers that incorporated sound absorptive treatments and barriers with T-shaped tops. The results confirmed that a sound absorptive treatment near the barrier edge resulted in a performance improvement over corresponding rigid barriers. A design optimization study of the most effective shape of acoustic treatments concluded that a circular shape works best. The performance of two different acoustical materials was also compared. Use of glassfiber resulted in better performance in

the high frequency region, while polyolefin foam with closed cells achieved a relatively large insertion loss at low frequencies.

Efforts were made to develop a numerical predictive model. The boundary element method was used to model the (infinite size) surrounding fluid effectively. The disadvantage of the boundary element model is the calculation load associated with the large number of elements required for high frequency analysis. A mesh optimization procedure was successfully implemented in the boundary element model to reduce the calculation time while satisfying the tolerances for analysis accuracy at each analysis frequency. Octave band averaging was also adapted to facilitate the comparison between the numerical results and experimental data. It was found that the results from the boundary element model agree relatively well with the experimental results up to 6300 Hz at selected locations. The insertion loss distribution proved the numerical model's capability of reproducing the rather complicated interference pattern on the receiver plane correctly at one-third octave band frequencies from 1000 Hz to 6300 Hz. Spatial-averaged insertion losses over different size receiver planes showed that the numerical model was less reliable when the averaging was done close to the ground level.

Preliminary measurements for an actual, real-size barrier were performed in South Bend, Indiana, to identify a measurement location that can be used to verify the effectiveness of the proposed add-on device. The add-on device was designed based on laboratory experiments and numerical studies, and was proven to be effective in a realistic highway environment. Federal Highway Administration (FHWA) Traffic Noise Model (TNM) was exercised for the comparison of the measurements. On-site measurements were performed to evaluate the absorptive treatment. Application of the treatment over a limited (6 m) region improved the performance of the barrier by 2 to 5 dB at the frequencies from 2000 Hz to 5000 Hz.

1. IMPLEMENTATION REPORT

The effect of an absorptive treatment on a barrier edge was investigated. Sound absorptive material was added on the barrier top without any rigid backing material. Scale model experiments were performed in the laboratory to verify the benefit of an absorptive treatment compared to a rigid extension. Numerical models based on the boundary element method were also developed for the optimal design of the prototype, although the optimal design was suggested based on the results from scale model studies. The proposed design was implemented on the vertical edge of a barrier at an existing barrier access gap. The comparison study showed that the add-on device increased the barrier performance at certain frequencies.

The design can be used for barrier applications where there is limitation on the barrier height. It could also be retrofitted to existing barriers to improve their performance. Access gaps between sections hurt overall barrier performance. The add-on sound absorptive material device can be easily retrofitted to an existing barrier so that overall barrier performance is not compromised by emergency exits and access gaps.

The scale factor between the realistic barriers and analysis with models needs to be studied with an emphasis on sound absorptive material. Experiments with scale models could be performed with a higher maximum frequency to cover a broader range of frequencies in a full-scale barrier. The field test was performed with a very limited length of absorptive treatment on a corridor-type gap between two barriers. More extensive study should be performed to prove the effectiveness of the proposed design with a more substantial installation on the top of the barrier. Investigation into cost and durability of the acoustic material should also be addressed.

2. INTRODUCTION

In a previous research project [1] conducted at the Ray. W. Herrick Laboratories at Purdue University, it was found that addition of sound absorptive material along a barrier edge could enhance the barrier's performance. The present work is the continuation of this effort, aiming to confirm the findings of the previous study through a more rigorous investigation, and to apply the design concept to more realistic situation. The optimal shape and material of the sound absorptive treatments for the real-size barrier were investigated experimentally, using physical models, and numerically. Preliminary on-site measurements using a prototype confirmed the effectiveness of treatment for an existing sound barrier.

Physical models were designed and absorptive edges were built to perform the experiment in an anechoic chamber. The physical models were about ten times smaller than actual barriers. The frequency was scaled accordingly in order to maintain the same ratio of barrier dimension and wavelength as in the case of full-size barriers. An array of 57 microphones was used, at various locations in the shadow region. A comparison was made between the performance of a straight barrier, a barrier with a T-shaped top, and one with an added absorptive treatment on its top. The insertion losses at different receiver points were compared. The insertion loss distribution over the shadow region was also investigated. The spatially-averaged insertion loss was calculated for all cases. It was found that the results from this study corroborated the previous findings. The effective shape of the sound absorptive treatment was then investigated to aid future design. It was found that a circular shape was best among the various absorptive treatment treated. Two different acoustical materials were compared. Glassfiber offered better performance at high frequency. Polyolefin foam with closed cells offered relatively large insertion losses at low frequency.

A numerical study was performed for rigid barriers. The numerical model was based on the boundary element method. Two different boundary element formulations were used. Because the thickness of the barrier is much smaller than its height or its length, the use of the direct formulation was hampered by the "thin body problem". Therefore, the indirect method was adopted. The computational cost increases rapidly with the number of elements. A large number of elements is required for accurate predictions at high frequency. A mesh optimization procedure was implemented to reduce the calculation time while satisfying resolution requirements at the frequency of interest. Frequency averaging over one-third octave bands was used to facilitate the comparison between numerical results and experimental data. It was found that the results from the boundary element model agreed well with the experimental results. The add-on device was designed based on those findings from experimental and numerical works.

A preliminary measurement was performed on a test site located along US 20 in South Bend, Indiana. The goal was to verify the effectiveness of an add-on device consisting of a porous material lining installed along one edge of an existing concrete road barrier. A Federal Highway Administration (FHWA) Traffic Noise Model (TNM) was developed to make a comparison between the measurement results and predictions. The test was performed to evaluate the performance of an absorptive treatment along the vertical edge of the barrier on the test site. A performance increase was observed at frequencies ranging from 2000 Hz to 5000 Hz. The results suggested that the design and implementation of absorptive barrier top treatments should be pursued in a future study. This approach is particularly attractive since it would be make it possible to design effective treatments that could be retro-fitted to existing barrier installations to improve their effectiveness in a cost-effective manner.

3. LITERATURE SURVEY

The report of the first part of this study [1] includes a summary of a number of research articles discussing: 1) analytical methods; 2) empirical models; and 3) experimental investigations related to noise barriers. In this section, the emphasis is on literature pertaining to the performance of sound absorptive treatments on the barriers.

Sound absorptive materials can be applied either on a large area of the barrier, or at specific locations. The entire surface of the barrier on the road side is often covered with sound absorptive material to reduce sound reflection off the barrier surface. This is usually done to minimize possible increases in sound pressure on the other side of the road, on which no barrier is installed, due to reflection off a single barrier. In addition, various kinds of devices have been proposed for treating barrier tops. Some installations involved the modification of the barrier edge with rigid material to minimize diffraction. Other studies have investigated the performance of sound absorptive treatments on the barriers. Research related to highway noise prediction models was also reviewed to improve the understanding of Federal highway traffic noise model used to represent the field measurements.

3.1. Sound absorptive barriers

Butler [2] was one of the first to suggest that lining the region in the immediate vicinity of the edge of a barrier with sound absorptive material could reduce the sound pressure level in the shadow zone. Rawlins studied barriers treated with strips having both infinitely small impedances [3] and finite impedances [4] using the Fredholm integral equation. He showed that a one- wavelength wide strip of absorbing material at the edge of a half-plane featured the same diffracted field as that behind a barrier covered with sound absorptive material. This implies that at low frequency, for

example at 100 Hz, the required width of the absorptive strip is about 3.4 m. This suggests that absorptive treatments are not effective when used to reduce the low frequency component of traffic noise. But the idea of covering a section of the barrier instead of the entire surface is promising for high frequencies.

Acoustic treatments on the road side of barriers have been used to reduce the reflected traffic noise when noise barriers are placed on one or both sides of a highway. Full scale experiments carried out by Watt [5] concluded that the performance of a 2 m high barrier was reduced by 4 dB(A) when another reflective barrier of a similar height was present on the other side of the road. Both sound absorptive barriers and tilted barriers were found to be effective in minimizing the degradation in barrier performance resulting from the presence of another barrier on the other side of the road. It is interesting to note, however, that Watts and Godfrey [6] later reported that the measured effects of applying absorptive materials to roadside barriers were generally less than 1 dB on the L_Aeq and L_A10 scales and that most recorded changes due to the application of absorptive treatments were not statistically significant.

3.2. Sound absorptive barrier tops

In 1991, Fujiwara and Furuta [7] presented a study that dealt with the excess attenuation of sound pressure levels provided by an absorptive treatment on the edge of a noise barrier. The velocity potential around the edge of a barrier can be regarded as an imaginary line source that creates the diffracted field on the rear of the barrier. Thus, suppression of the edge potential reduces the strength of the imaginary source, and consequently the pressure behind the barrier is decreased.

Okubo and Fujiwara [8] suggested a soft-surface cylinder consisting of open ended tubes arranged radially to avoid the problem of obtaining materials whose impedance is significantly less than that of air. It was reported that the performance of the installation was frequency dependent, and was poor at some frequencies. They performed a numerical analysis for various configurations of the "waterwheel" [9]. The

depth of the channel, the diameter of the waterwheel, and opening angle of the channel were varied in the two-dimensional numerical models. The depth of the channels and the diameter of the "waterwheel" influenced the center frequency and the lower limit of the frequency range where the improvement occurred. The opening angle of the channel affected the upper limit of the effective range. The same authors later studied the effects of channel depth, and the individual effectiveness of each channel. A new design with five channels with different depths placed on the upper half of a cylinder was suggested [10].

The combination of sound absorptive edges and multiple edges was also studied using a boundary element method by Fujiwara et al. [11]. Two cylindrical absorptive edges of 25 cm diameter, separated by 75 cm on the top of 3 m barrier improved the insertion loss by 2.5 dB compared to 50 cm diameter absorptive edges. Mőser [12] modelled a cylinder with a given surface impedance and studied the influence of the impedance on the barrier performance when the cylinder is used at the barrier top. Based on the theoretical study, a cylindrical "headpiece" in the form of a Helmholtz resonator with perforated shell was suggested. The acoustic intensity near the edge of the barrier and the insertion loss in the shadow zone was measured with and without covering on the headpiece installed on the barrier top to investigate the influence of the acoustic impedance on the barrier performance. Up to 10 dB reduction of intensity was measured near the cylindrical headpiece at the center frequency of the one third octave band at 800 Hz without a covering. The insertion loss measured when the cover was removed at diffraction angles from 0 to 60 degrees showed that the perforated cylindrical shell yielded a 1 to 5 dB improvement from 800 Hz to 2500 Hz compared to the case of the covered cylindrical headpiece.

3.3. Traffic noise models

For some time, traffic noise predictions have been performed using the FHWA approved STAMINA 2.0 highway noise prediction models, derived from the FHWA High-

way Traffic Noise Prediction Model [13]. The barrier calculations within STAMINA are based on the Kurze and Anderson equation [14]. In 1998, the FHWA released its new generation highway traffic noise prediction model called the Traffic Noise Model, or TNM [15]. TNM is designed to eventually replace the FHWA's prior pair of computer programs, STAMINA 2.0/OPTIMA. De-Jong's formula for barrier performance predictions is used in TNM [16]. Much care needs to be taken when designing a full-scale experiment to evaluate the performance of a noise barrier in highway locations. A traffic noise prediction model must be used to calculate the predicted sound pressure level, unlike the case of a scale-model or full-scale models in which arbitrary noise sources such as a loudspeaker can be used. In most cases, researchers did not measure the sound pressure level before the barrier was installed. The data without the barrier in place are often calculated by using a prediction model, which can itself be inaccurate. Rochat [17] performed roadside measurements at various locations in the United States and indicated that the calculated sound levels from Traffic Noise Model is usually within 1.5 dB of the measured levels. Comparisons between different traffic noise models used in the United States were performed by Wayson et al. [18].

Experiments on barrier performance have been performed at various laboratories with the objective of controlling the environmental variables such as wind, temperature gradients, turbulence, and finite impedance ground surfaces. Full-scale outdoor experiments have also been performed at several locations. Particular care should be taken when comparisons are made among different barrier designs since inevitably a number of environmental parameters cannot be controlled.

It can be seen from the literature review that detailed work combining both laboratory level experiments with numerical predictions and field measurements with a full size barrier has not been performed, although some research has been reported about the advantages of sound absorptive treatments applied to the surface of the barrier. In this study, three-dimensional boundary element models combined with scaled barrier experiments in a controlled laboratory environment with a microphone array were employed to evaluate the benefits of sound absorptive treatments. The

results from the first part of the research were utilized for the design of a sound absorptive treatment for a full size barrier along a highway.

4. EXPERIMENTS USING A PHYSICAL MODEL

A comparison between the insertion losses of barriers with absorptive edges and rigid barriers was made using small physical models in a laboratory environment. The optimal shape of the sound absorptive lining was investigated following the same procedures. Finally, the performance of two types of sound absorptive materials for the barrier top treatment was compared.

4.1. Experimental procedures

As shown in Figure 4.1, the configurations considered were: 1) a 5 cm linear extension of a rigid, uniform rectangular barrier; 2) a T-shaped barrier with a 5 cm wide top; and 3) a 7.5 cm high and 2.5 cm wide sound absorptive treatment with 2.5 cm overlap with the rigid barrier. For the third configuration, the 7.5 cm wide glassfiber strip was positioned on the source side of the rigid barrier. To eliminate the necessity of creating a perfectly reflecting plane, the model tests were carried out in an anechoic room, simulating a free field. According to the theory of image sources, the insertion loss of a barrier on a rigid ground is equal to the insertion loss of a barrier that is twice the height of the original barrier in open space. A steel rectangular plate was used in the experiment, with dimensions 74 cm $\times$ 244 cm $\times$ 3 mm. This barrier is equivalent to a 37 cm tall acoustic barrier on a rigid ground.

The experiments were performed in an anechoic chamber located at the Herrick Laboratories at Purdue University. The geometry of the experimental setup is shown in Figure 4.2 and Figure 4.3. A small loudspeaker, with a 2.5 cm diameter, was used as the sound source. A total of 57 microphones (Modal shop T130C21) were used along with an ICP sensor signal conditioner (PCB 442B119ICP) with 0 dB gain. The loudspeaker was located 50 cm from the barrier, along the centerline (the

x-axis in Figure 4.2). The 57 receivers were located 75 cm from the barrier and distributed between the barrier centerline and the boundary of the shadow zone, which was located approximately 90 cm above the centerline (i.e., $y = 90$ cm) at this point. The vertical spacing between the microphones was 5 cm, and three rows of microphones were separated by 50 cm. A pistonphone (G.R.A.S. Sound & Vibration 42AA) with an "octopus coupler" (RA0025) was used for microphone calibration. A personal computer in combination with a data acquisition frontend (Agilent E8403A) was used to acquire the microphone signals. The signals were processed using the software LMS CADA-X and MATLAB.

4.2. Data analysis

Typically, diffraction experiments are performed using transient input signals to facilitate the identification of the desired responses [19]. Spurious events can be easily identified and eliminated from the time domain signals by isolating events that are clearly caused by sound propagation between the sound source and the receiver. It was found that the impulse input yields a poor signal-to-noise ratio due to the loudspeaker's limited frequency response and dynamic range. As a result, a continuous random signal was used as the input signal. The disadvantage of using a continuous random input signal is the difficulty of identifying spurious reflections. This problem was avoided by using an inverse Fourier transform procedure. The details of this procedure were described at length in a previous report [1]. The time domain impulse response function can be calculated from the frequency domain transfer function measured between the loudspeaker input and each of the microphone outputs. A time domain window was the applied to the impulse response function. The latter results was Fourier transformed to obtain reflection-free transfer functions. The insertion loss of the barrier was calculated after the procedure described above by dividing the transfer function without a barrier by the transfer function with a barrier in place.

The insertion loss, defined as the sound pressure level reduction due to the presence of a barrier, is a widely used metric to evaluate the performance of acoustic barriers. One disadvantage of the insertion loss is that it is defined for one specific receiver location. Barrier performance may vary significantly with microphone location. The insertion loss metric was modified to evaluate the performance of acoustic barriers over an extended region over the y-z plane parallel to the barrier in the shadow region. A knowledge of the sound pressure level over a plane allows the calculation of the insertion loss distribution over the receiver plane at selected frequencies. It is also possible to calculate the spatially averaged insertion loss for any number of receiver points. This yields a space-averaged insertion loss over a section of a receiver plane. Spatially averaged insertion loss values were deemed, a useful, more "global" quantity for comparisons between different configurations.

Three different metrics were thus used to evaluate the performance of various barriers. The insertion losses at selected receiver points were first compared. Receivers 1 and 2 were located along the centerline (x-axis) or at the virtual ground level ($y = 0$ cm). Receiver 1 was in the middle of the barrier ($z = 0$) and receiver 2 was offset by 50 cm (z = -50 cm) (see Figure 2). Receivers 3 and 4 were placed at the same height, 30 cm, receiver 3 was at $z = 0$ cm, and receiver 4 was at z = -50 cm. The insertion loss distribution over the receiver plane was compared at selected center frequencies in one-third octave bands. This was done to identify the actual shadow region and possible focusing effects. The spatially averaged insertion loss was finally calculated to observe how the performance of each design varied with the size of the receiver plane on average.

4.3. Results

The insertion loss of the baseline barrier, the barrier with a height extension, the T-top barrier, and the barrier with a glassfiber edge are shown for various receiver locations in Figure 4.4. The results show that the absorptive treatment on the edge

of the barrier yields a significantly greater insertion loss than the other three configurations, especially in the frequency band from 3150 Hz to 8000 Hz. The performance enhancement produced by the absorptive extension was more than 10 dB relative to the straight barrier with the same height. Figure 4.4(a) and Figure 4.4(c) show that the sound absorptive extension increases the insertion loss particularly in the frequency band from 4000 Hz to 8000 Hz for the receivers at $y = 0$ cm on the centerline. The benefit of the absorptive edges decreases for the two receivers at $y = 30$ cm, as shown in Figure 4.4(b) and 4.4(d). However, glassfiber edges perform better than other designs at these receiver locations. The performance of the absorptive edge barrier is compared to that of rigid barriers in Figures 4.5, 4.6 and 4.7 in terms of insertion loss distribution. Figure 4.5 shows the insertion loss distribution over the receiver plane at the one-third octave band center frequency of 4000 Hz for four different barrier designs. The rigid T-top barrier generated relatively narrow regions of high insertion loss in Figure 4.5(c). In comparison, the insertion loss distribution in Figure 4.5(d) shows that a soft edge resulted in a larger region of higher insertion loss near the middle of the barrier. This trend also can be seen in Figure 4.6, which shows the insertion loss distribution for four different barriers at 5000 Hz. At 6300 Hz, the benefit of the absorptive edge barrier can be readily seen in Figure 4.7. At this frequency the region of improvement is almost up to half the height of the entire receiver plane: see Figure 4.7(d).

Figures 4.8, 4.9 and 4.10 shows the spatially averaged insertion losses over three different receiver planes. Figure 4.8 shows the insertion loss averaged for four barrier designs up to 30 cm in the receiver plane, i.e., the insertion losses from 21 microphones were averaged. Absorptive treatments yielded higher averaged insertion losses from 2000 Hz to 6300 Hz. When the averaging was done over a receiver plane of 60 cm height, i.e., two thirds of the entire shadow zone, the benefit of the absorptive top was reduced as can be seen in Figure 4.9. This shows that an absorptive treatment on the barrier edge is slightly more effective for the receivers deep in the shadow zone. The averaged-insertion loss over the entire receiver plane (Figure 4.10) shows that the

insertion loss of the soft top barrier was still better than other designs at frequencies from 2000 Hz to 6300 Hz.

4.4. Influence of shape of sound absorptive treatment

Glassfiber treatments with different shapes were tested to study the effects of the shape of the sound absorptive device attached to the edge of a barrier. A comparison was made between four different absorptive treatments shapes. The same amount of material was used for all cases. Figure 4.11 shows the four samples installed on the top of the scale barrier model. A square cross-section 10 × 10 cm, a circular section with a diameter of 11.25 cm, and two triangular sections with 15 cm long sides were tested. The distance between the barrier and the speaker was the same as before, i. e., 50 cm in front of the barrier. An array of 57 microphone located 75 cm behind the barrier was used. Note that the identical treatments were installed on the top and the bottom of the barrier to satisfy the symmetry requirements for the experiment. A steel wire mesh with 5 cm square grid was used to contain the glassfiber material. The cross section of the sample was not uniform along the barrier edge due to the deformation of the wire mesh. This resulted in complicated interference and thus peaks and dips in the insertion loss curves at each receiver point were identified. The space-averaged insertion loss is believed to be more representative of barrier performance than the local insertion loss at each microphone for comparisons. Both the insertion loss distribution and the space-averaged insertion loss were compared.

The insertion loss distribution for all four different shapes at 1600 Hz, shown in Figure 4.12, shows that the circular shape is most effective and creates larger regions of high insertion loss. The same trend can be seen in Figure 4.13 at the frequency of 5000 Hz. The averaged insertion loss over the receiver plane from $y = 0$ cm to y= 30 cm shows that the circular shape treatment is clearly superior from 1250 Hz to 2000 Hz when the average is performed over one-third of the receiver plane: see Figure 4.14. The inverted triangular performs better than the circular shape near the

frequencies of 2500 Hz, 6300 Hz and 8000 Hz. At the frequencies of 4000 Hz and 5000 Hz, the circular shape works better than the inverted triangle by 2 to 5 dB. Averaged insertion losses for the four different cases over the region from $y = 0$ cm to 60 cm are shown in Figure 4.15. The averaged insertion loss for the circular treatment yields a larger insertion loss from 1000 Hz to 2000 Hz, and from 4000 Hz to 5000 Hz. It should be noted that at 4000 Hz and 5000 Hz the performance of the circular shapes is worse than the inverted triangle model but the difference is smaller compared to the averaged insertion loss from Figure 4.14. The insertion loss averaged over the entire measurement plane for four samples of different shapes is shown in Figure 4.16. It can be seen that the circular model yields the most balanced performance over a wide frequency range among the four designs.

4.5. Influence of sound absorptive material

Glassfiber is widely used in noise control applications requiring sound absorption. The sound absorption processes involves within glassfiber convert sound wave energy into heat. This occurs as sound waves propagate through the pores, or around and through the fibers. When the glassfiber is exposed without appropriate coating material it can absorb water and its performance is then degraded.

Polyolefin, closed-cell foams (also known as "QUASH") offers advantages compared to other conventional sound absorptive materials. QUASH products have good sound absorption at low and medium frequencies, the frequencies of interest in many industrial applications and the frequencies that are most difficult to absorb for conventional materials. And because QUASH products are made from polyolefins and have closed cells, they do not absorb water as much as conventional materials like fibers, polyurethane foams, and melamine foams. In addition to that, QUASH is also ultraviolet resistant, which is desired for outdoor application. The atmospheric advantage of QUASH for outdoor installation is an important factor in consideration of an actual design implementation.

A 5 cm wide steel plate 244 cm long was added to create a rigid, linear extension of the base plate for the comparison. A steel frame with a mesh size of 5 cm was used to build the circular glassfiber addition. The diameter of the frame was 10 cm and one layer of 2.5 cm thick glassfiber was used. Note that the circular shape was adopted based on the results reported in the previous section. The QUASH material was cut to produce a rectangular shape of 6.4 cm by 10 cm. The idea here was to have an additional 5 cm extension to the base plate with the three different materials. Note that more material was used for glassfiber and QUASH samples compared to the rigid extension. But the same amount of material was used for the samples of glassfiber and QUASH. The aim is to compare the performance of two different materials and the rigid extension is used only for reference. The loudspeaker and the microphone array were placed at the same location as before.

The insertion loss is compared at selected microphone locations in Figure 4.17. Figure 4.17(a) and Figure 4.17(c) show the insertion loss in the middle of the scale barrier model ($y = 0$ cm). It can be seen that glassfiber performs better at frequencies between 2500 Hz and 8000 Hz than any other designs. The difference between the glassfiber and QUASH was almost 20 dB at these frequencies. QUASH performs better at low frequencies, from 1000 Hz to 2000 Hz. Both of the absorptive additions yield greater insertion losses than the rigid extension barrier at all frequencies at these two receiver locations. The insertion loss comparison at $y = 30$ cm is shown in Figures 4.17(b) and 4.17(d). At this height the glassfiber still yields a larger insertion loss at frequencies from 3150 Hz to 8000 Hz, but the difference has been reduced from more than 20 dB at $y = 0$ cm to 5 dB at this height. The QUASH yields a larger insertion loss at lower frequencies consistently.

To assess the overall performance of the different barrier designs, the insertion losses were plotted over the complete receiver plane for several one-third octave bands. The insertion loss distribution is plotted at 2000 Hz in Figure 4.18. It shows that the QUASH design created a high insertion loss region of larger size over the receiver plane than other designs. At higher frequency, for example, 5000 Hz, the glassfiber

created a larger region of greater insertion loss than QUASH: see Figure 4.19. It is interesting that both the acoustic treatments were comparable at some frequencies as shown in Figures 4.20(c) and 4.20(d). glassfiber and QUASH perform better than a barrier model with a rigid extension at this frequency. The decrease in effectiveness of the acoustic treatments with increased distance from the barrier, z, is the result of untreated barrier sides as shown in Figures 4.20(c) and 4.20(d).

The receiver plane, which is 90 cm high and 100 cm wide, was then divided into three sections. The insertion losses at multiple numbers of microphones were averaged to generate the space-averaged insertion loss over the section of the receiver plane. Figure 4.21 shows the averaged insertion loss over 21 microphones from the $y = 0$ cm to 30 cm. It can be seen that the QUASH gives the largest insertion loss on average from 1000 Hz to 2500 Hz. Glassfiber is more effective in reducing the sound pressure level in the frequency range from 3150 Hz to 10000 Hz. It can be clearly seen that the two kinds of acoustic treatment give larger insertion losses than a rigid extension which shows a larger insertion loss than the base barrier by 2 - 3 dB except at the octave band at 3150 Hz. Figure 4.22 shows the averaged insertion loss over two-thirds of the receiver plane, from $y = 0$ cm to $y = 60$ cm. The same trend can be seen here: the QUASH performs better than glassfiber at low frequencies and glassfiber results in larger insertion losses at the frequencies from 4000 Hz to 8000 Hz. The averaged insertion loss over the entire receiver plane is shown in Figure 4.23. It should be noted that the two different types of material produced approximately the same amount of benefit over the rigid barriers at frequencies higher than 10000 Hz. It would be ideal to incorporate the two different materials for optimal acoustic performance over a wide frequency range.

These results confirmed that a barrier with a sound absorptive material near the edge yields better performance than barriers with rigid extensions. It was found that the shape of the sound absorptive material affects barrier performance. A circular shape was found to yield better results. A comparison between the glassfiber and

QUASH identified the frequency range for each material where the performance is best.

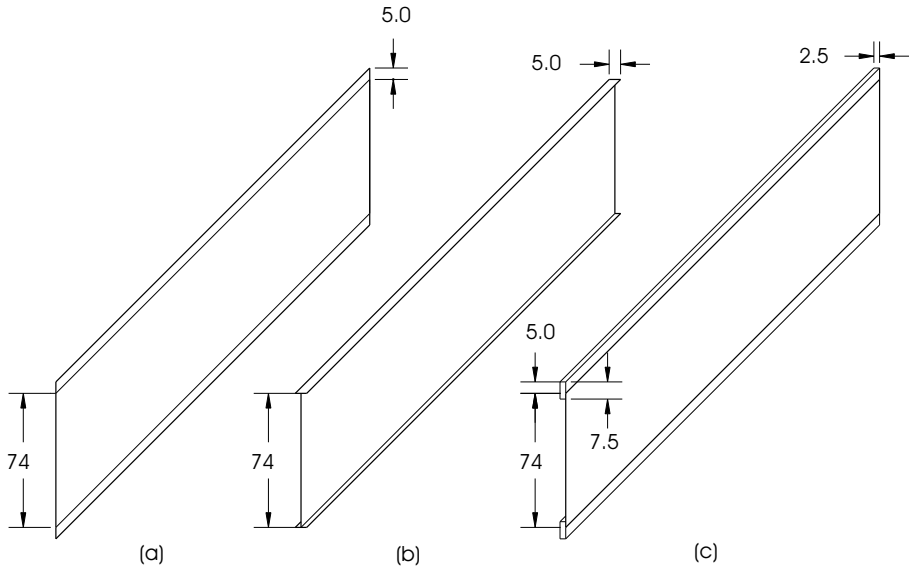

Figure 4.1. Geometry of the barrier designs considered: (a) rectangular barrier with a 5 cm linear extension, (b) rectangular barrier with a 5 cm wide T top, (c) rectangular barrier with a sound absorptive edge.

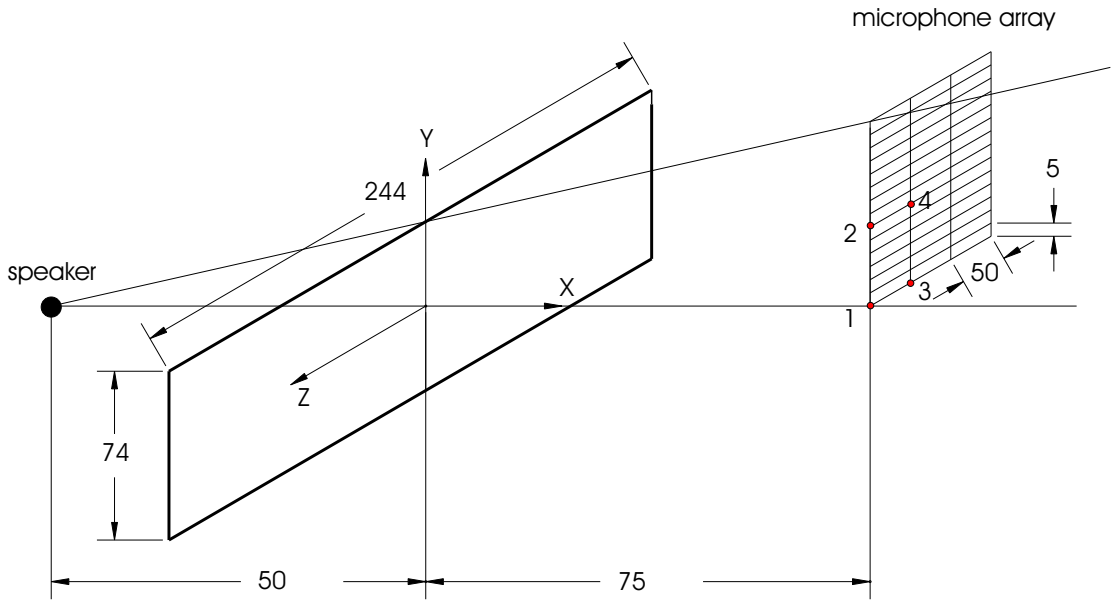

Figure 4.2. Schematic of the experimental setup (All dimensions are in cm). The numbers 1, 2, 3 and 4 indicate the receiver points used for the local insertion loss comparisons.

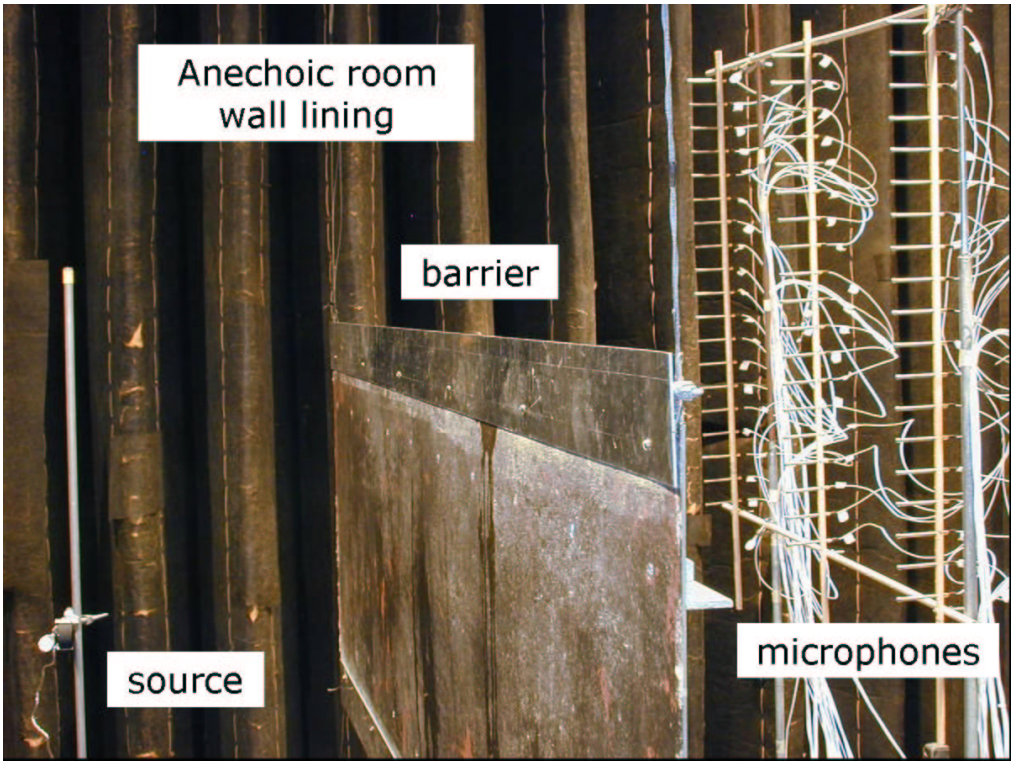

Figure 4.3. Picture of the experimental apparatus.

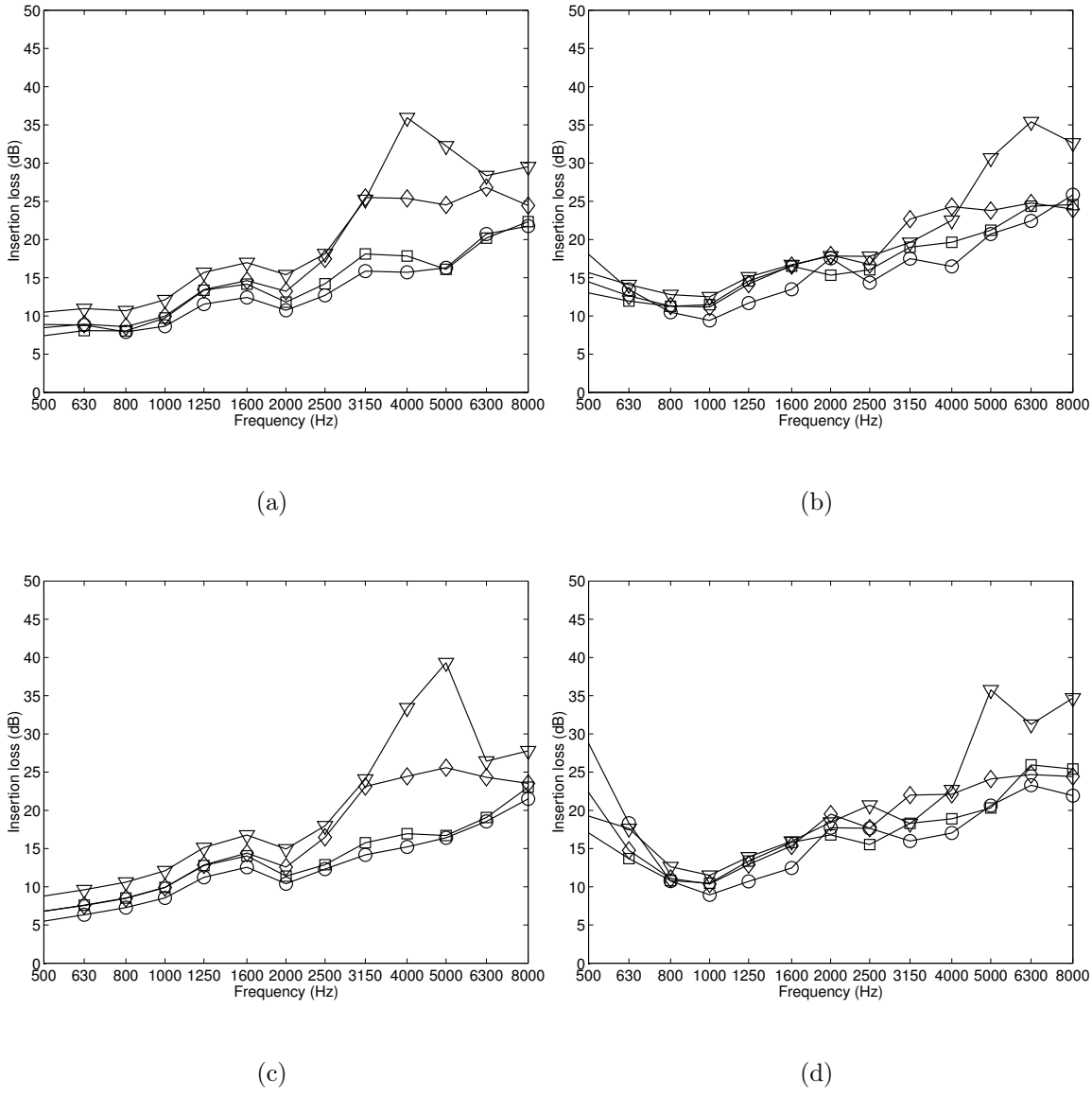

Figure 4.4. Insertion loss vs. frequency: '$\circ$': baseline barrier; '$\square$': 5 cm linear extension; '$\diamond$': 5 cm wide T-top; '$\triangledown$':5 cm glassfiber edge: (a) receiver 1 at $y = 0$ cm and $z = 0$ cm, (b) receiver 2 at $y = 30$ cm and $z = 0$ cm, (c) receiver 3 at $y = 0$ cm and $z =$ -50 cm, (d) receiver 4 at $y = 30$ cm and $z =$ -50 cm.

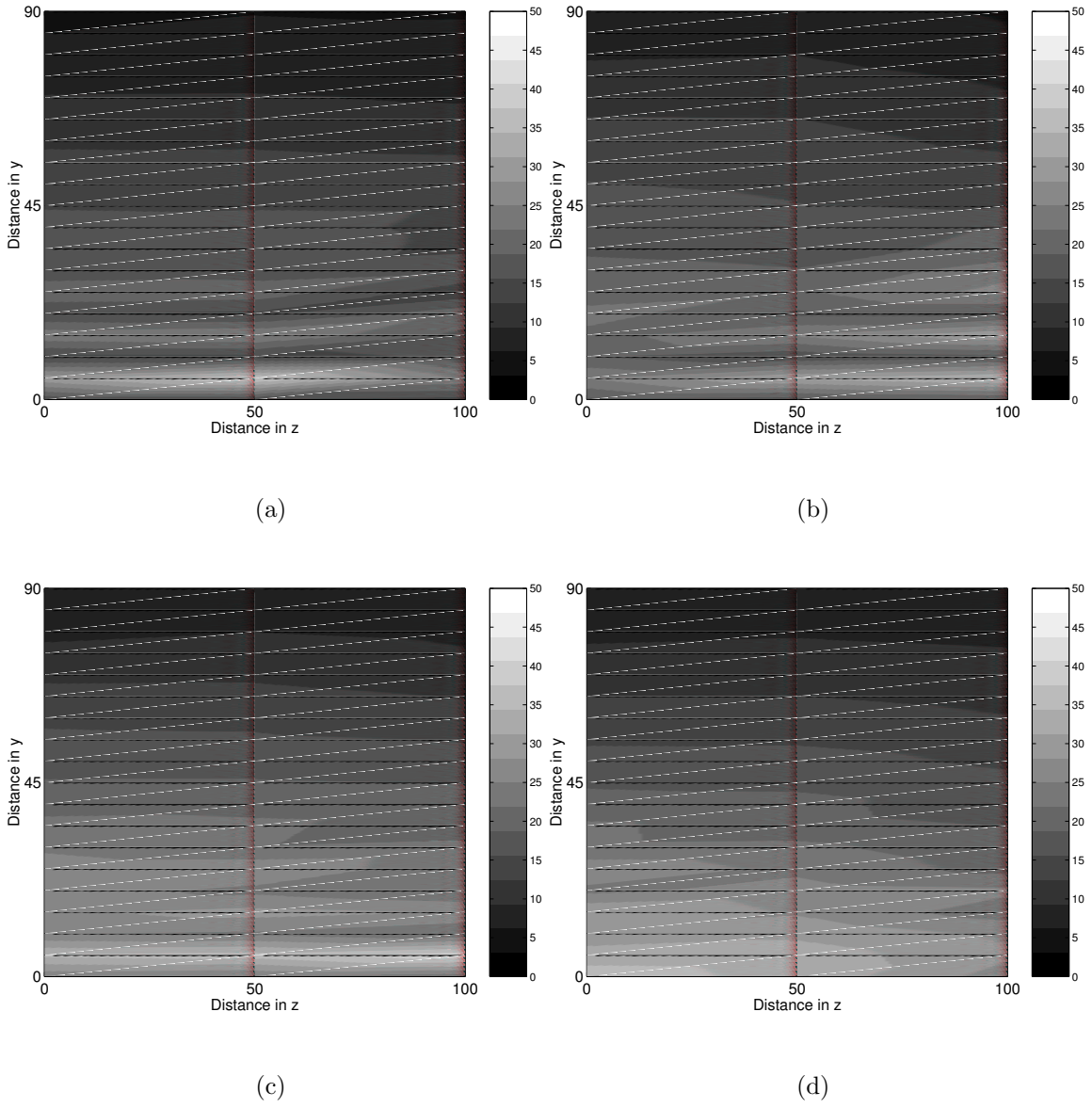

Figure 4.5. Insertion loss distribution over the receiver plane at the one-third octave band center frequency of 4000 Hz: (a) baseline barrier, (b) 5 cm linear extension, (c) 5 cm wide T-top, (d) 5 cm glassfiber edge.

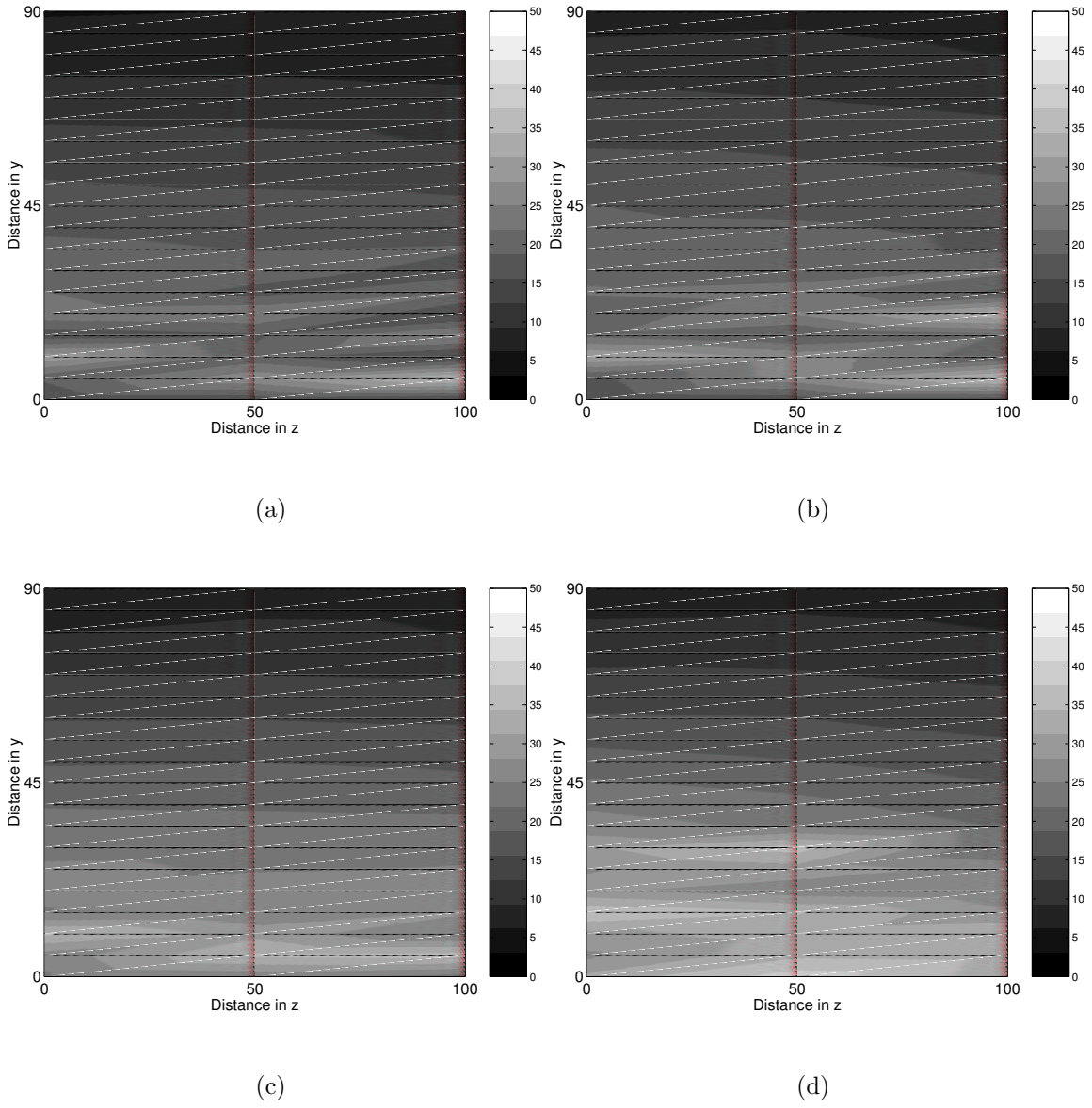

(a) (b)

(c) (d)

Figure 4.6. Insertion loss distribution over the receiver plane at the one-third octave band center frequency of 5000 Hz: (a) baseline barrier, (b) 5 cm linear extension, (c) 5 cm wide T-top, (d) 5 cm glassfiber edge.

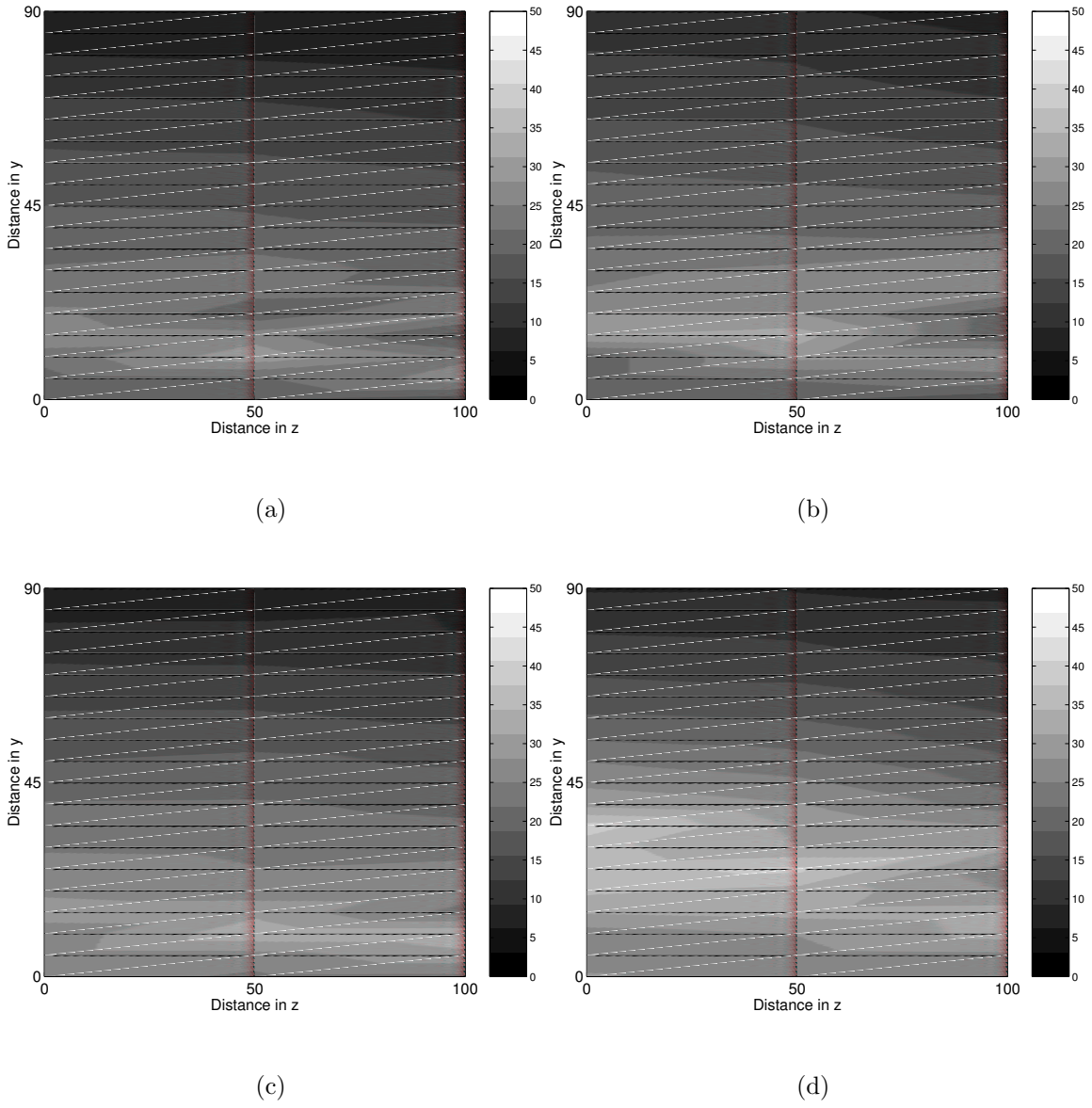

(a) (b)

(c) (d)

Figure 4.7. Insertion loss distribution over the receiver plane at the one-third octave band center frequency of 6300 Hz: (a) baseline barrier, (b) 5 cm linear extension, (c) 5 cm wide T-top, (d) 5 cm glassfiber edge.

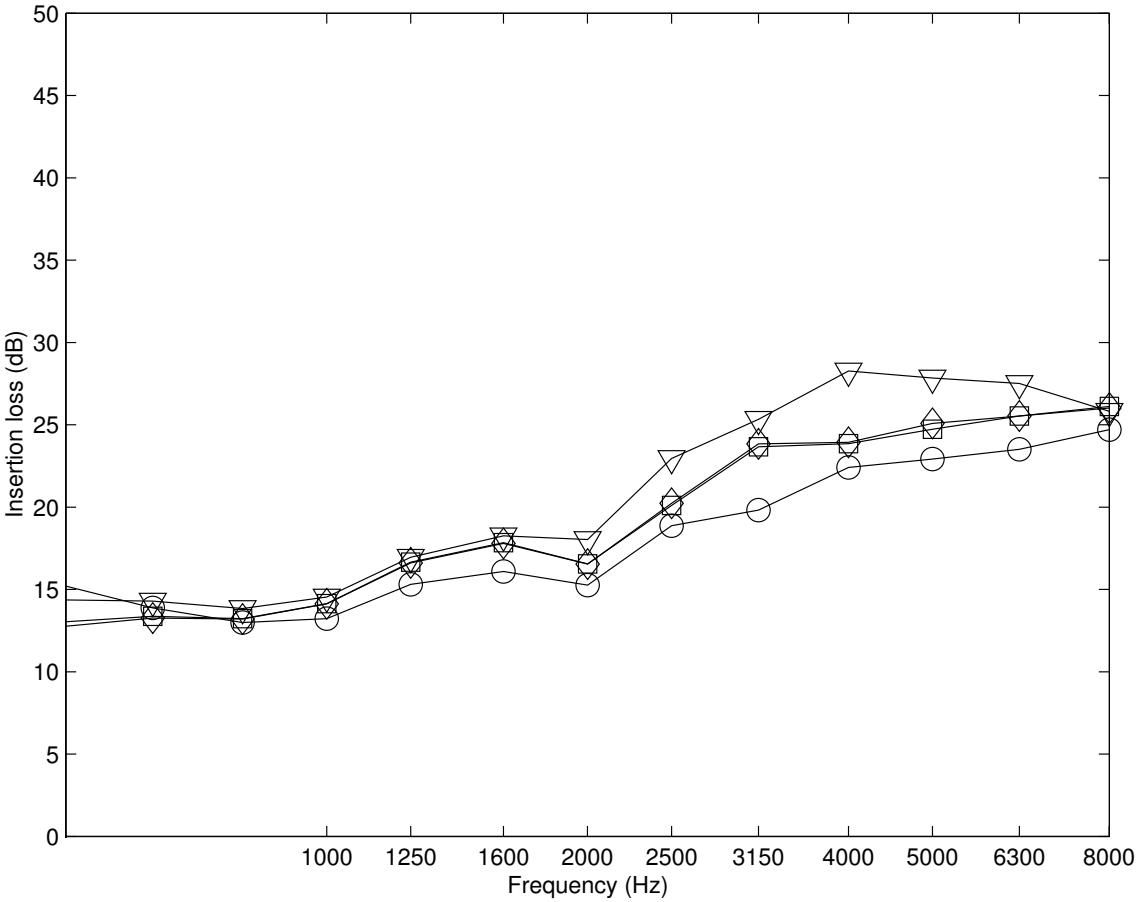

Figure 4.8. Space-averaged insertion loss over the receiver plane to the height of 30 cm (21 microphones): '$\circ$': baseline barrier; '$\square$': 5 cm linear extension; '$\diamond$': 5 cm wide T-top; '$\bigtriangledown$': 5 cm glassfiber edge.

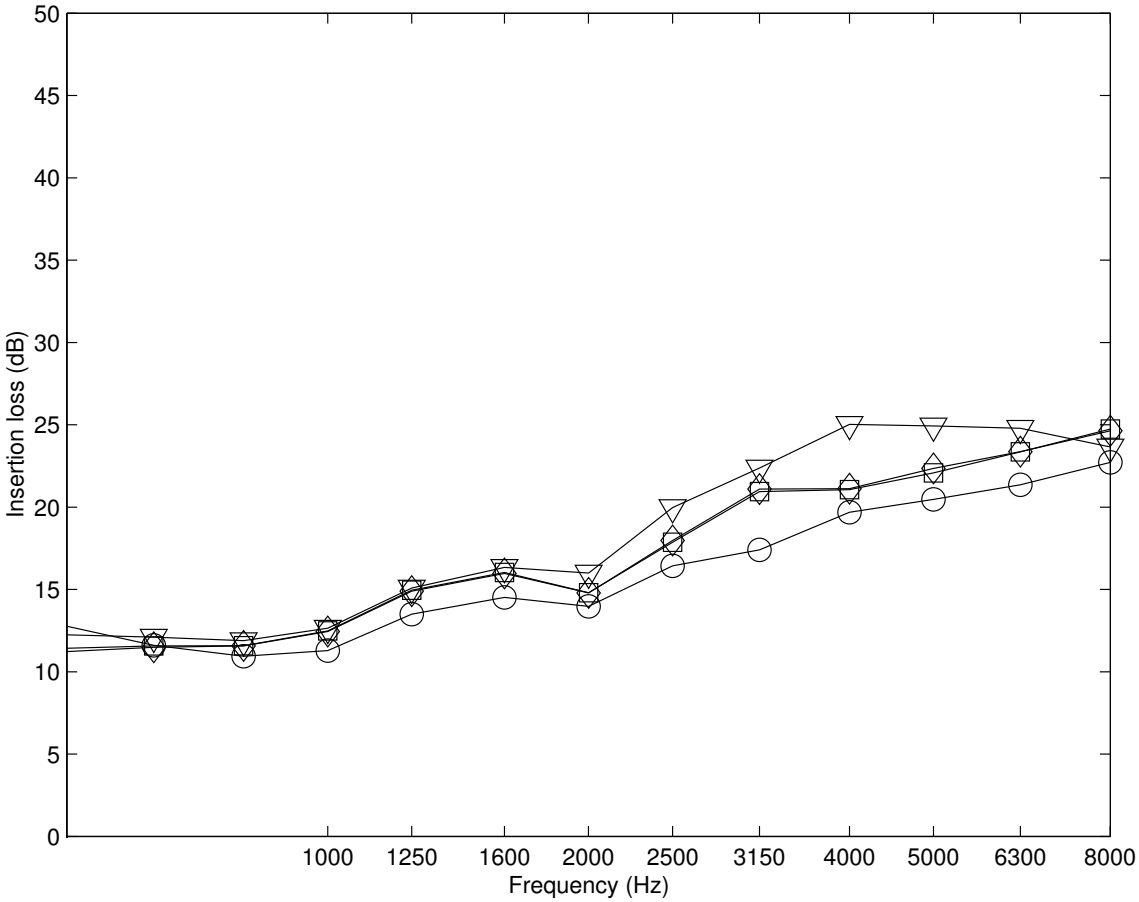

Figure 4.9. Space-averaged insertion loss over the receiver plane to the height of 60 cm (42 microphones): '$\circ$': baseline barrier; '$\square$': 5 cm linear extension; '$\diamond$': 5 cm wide T-top; '$\bigtriangledown$': 5 cm glassfiber edge.

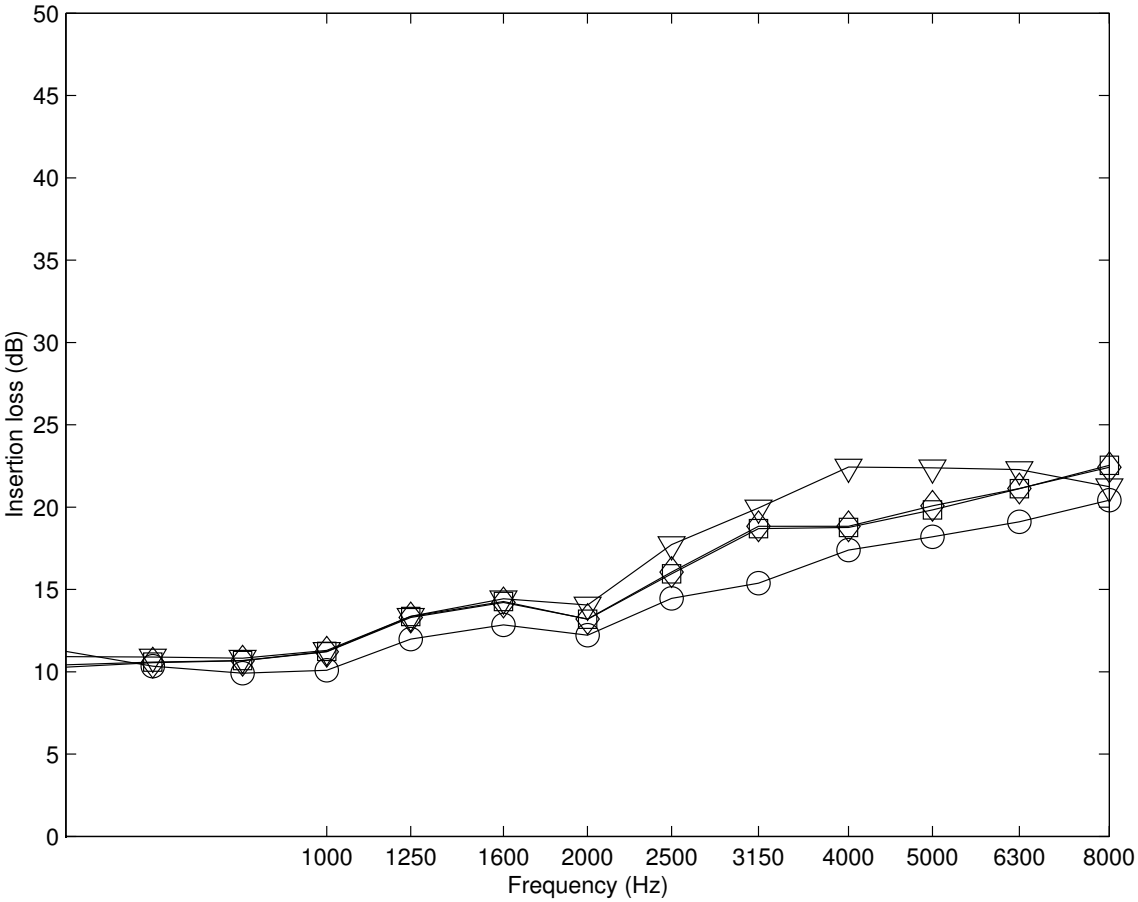

Figure 4.10. Spaced-averaged insertion loss over the receiver plane to the height of 90 cm (57 microphones): '$\circ$': baseline barrier; '$\square$': 5 cm linear extension; '$\diamond$': 5 cm wide T-top; '$\bigtriangledown$': 5 cm glassfiber edge.

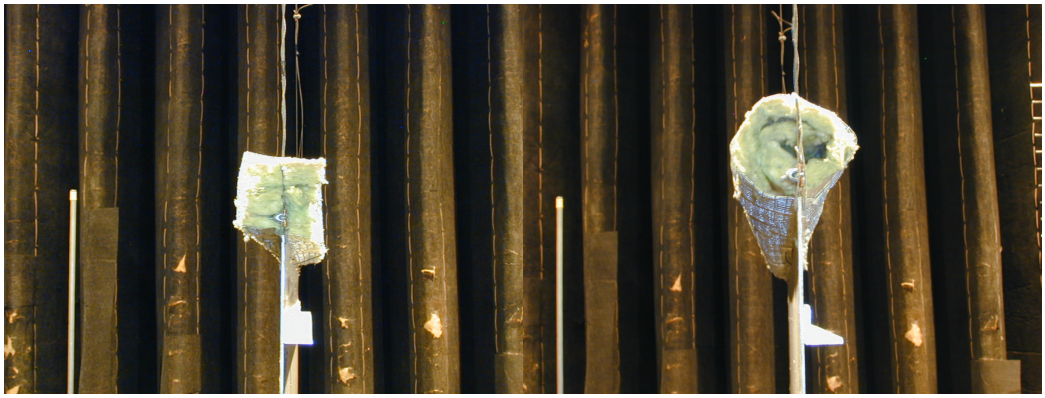

(a) (b)

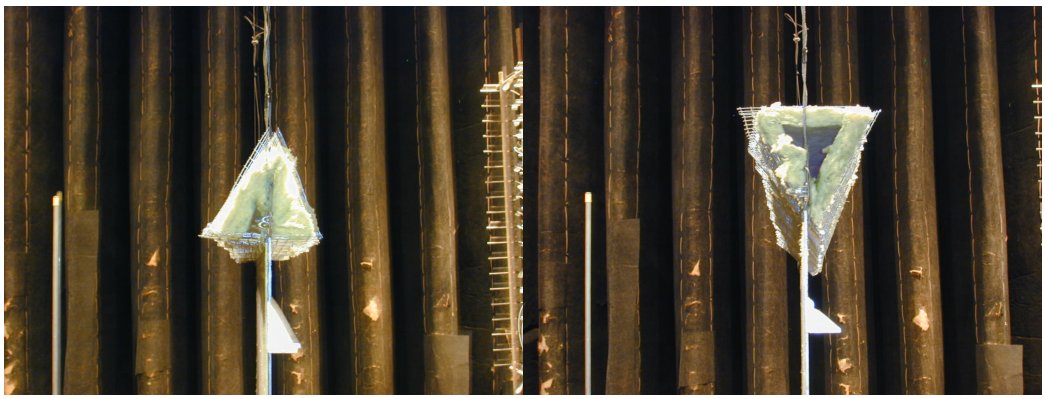

(c) (d)

Figure 4.11. Shapes of absorptive top installed on the barrier edge: (a) square, (b) circle, (c) triangle, (d) inverted triangle.

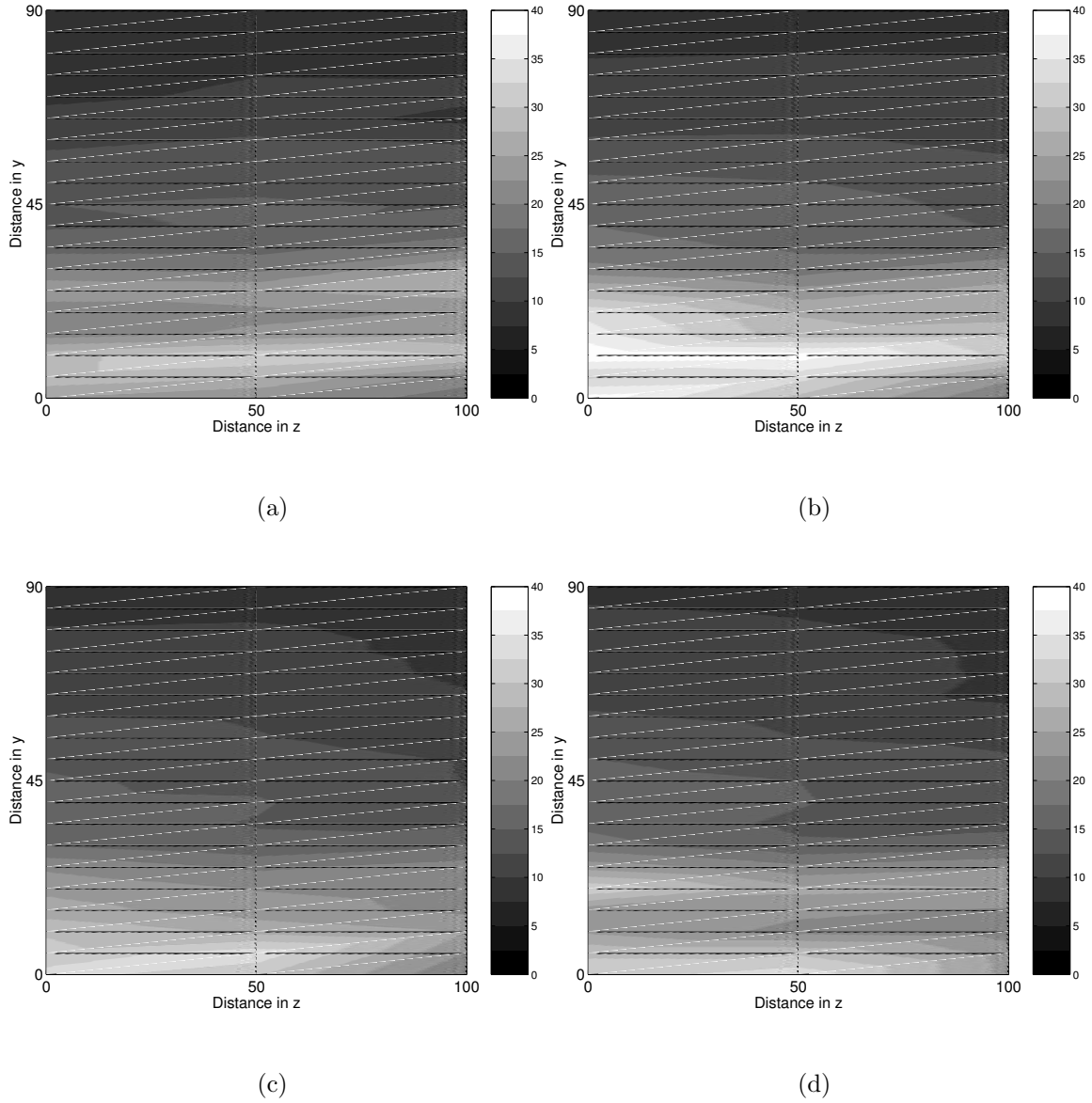

(a) (b)

(c) (d)

Figure 4.12. Insertion loss distribution over the receiver plane at the one-third octave band center frequency of 1600 Hz: (a) square, (b) circle, (c) triangle, (d) inverted triangle.

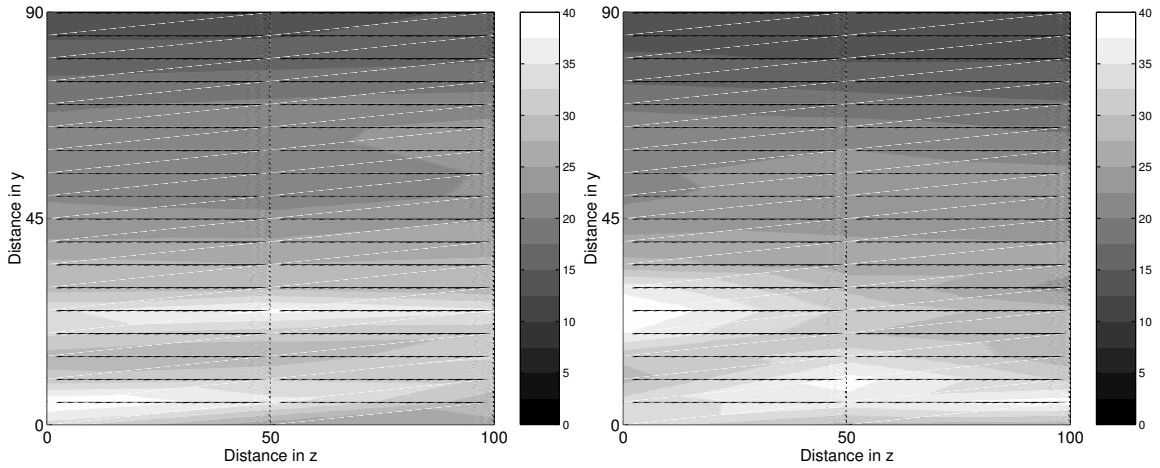

(a) square.

(b) circle.

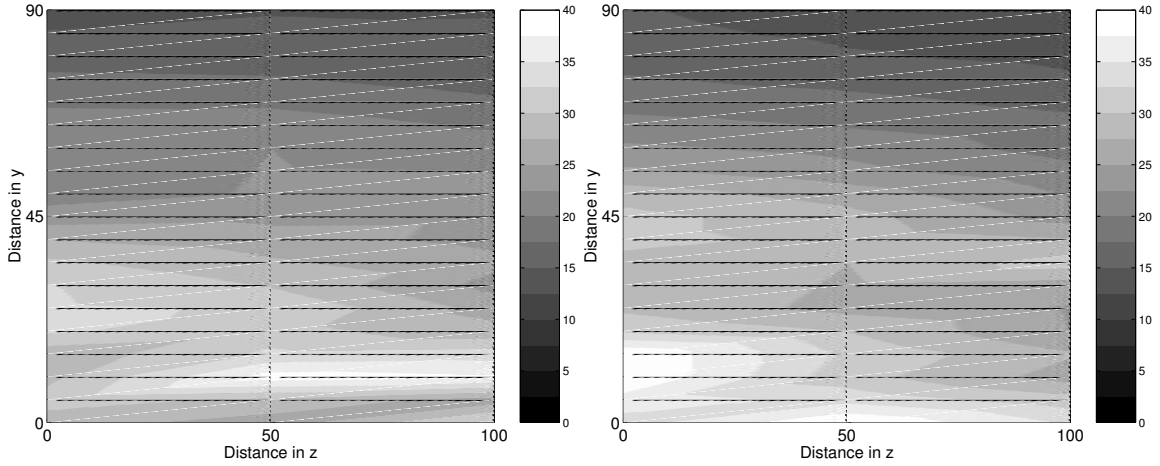

(c) triangle.

(d) inverted triangle.

Figure 4.13. Insertion loss distribution over the receiver plane at the one-third octave band center frequency of 5000 Hz.

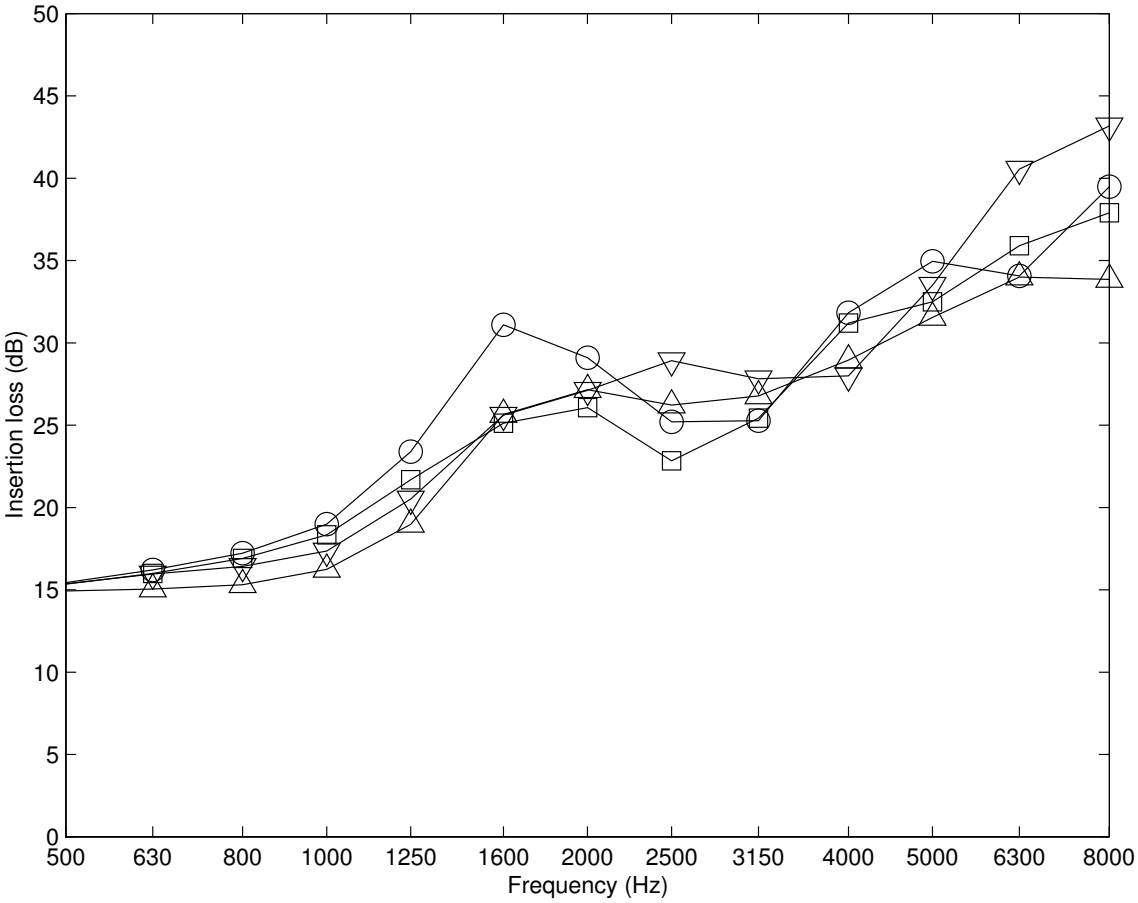

Figure 4.14. Space-averaged insertion loss over the receiver plane to the height of 30 cm (21 microphones): '□': square; '∘': circle; '△': triangle; '▽': inverted triangle.

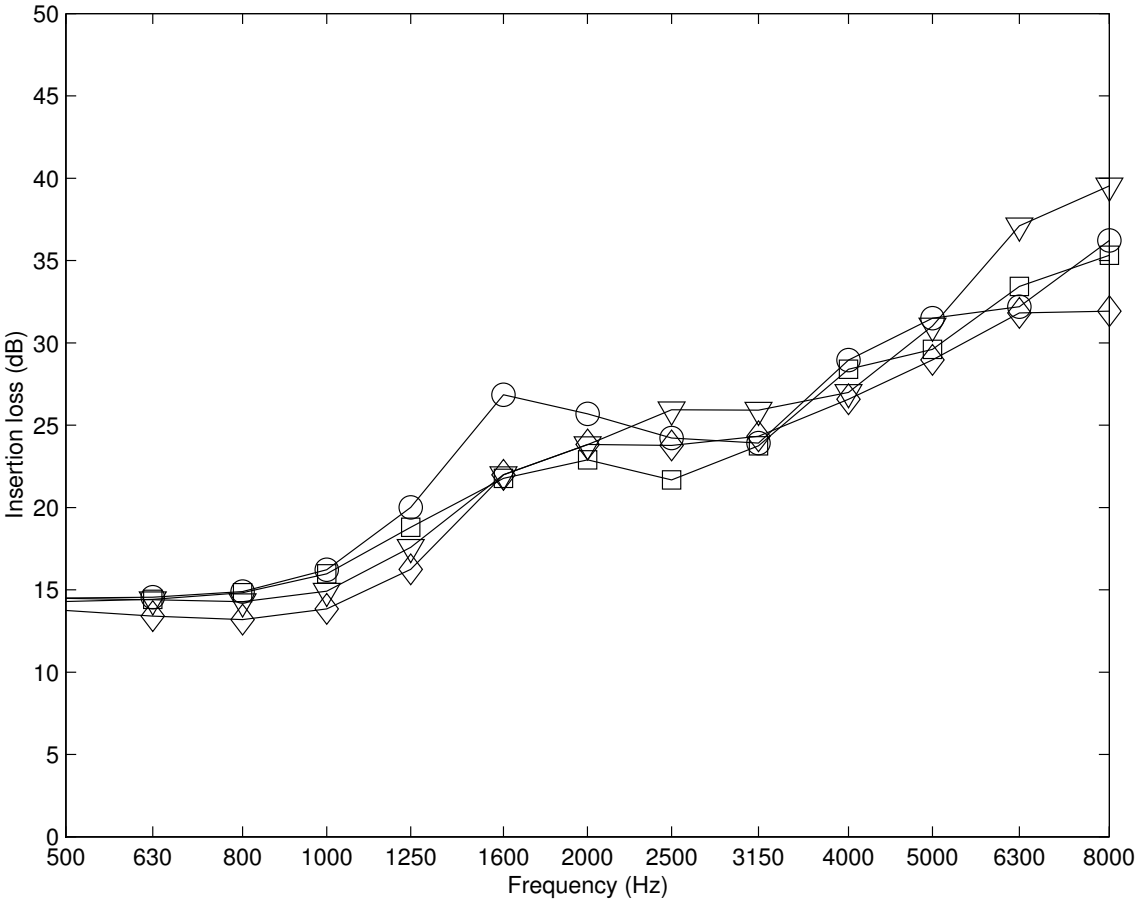

Figure 4.15. Space-averaged insertion loss over the receiver plane to the height of 60 cm (42 microphones): '□': square; '○': circle; '△': triangle; '▽': inverted triangle.

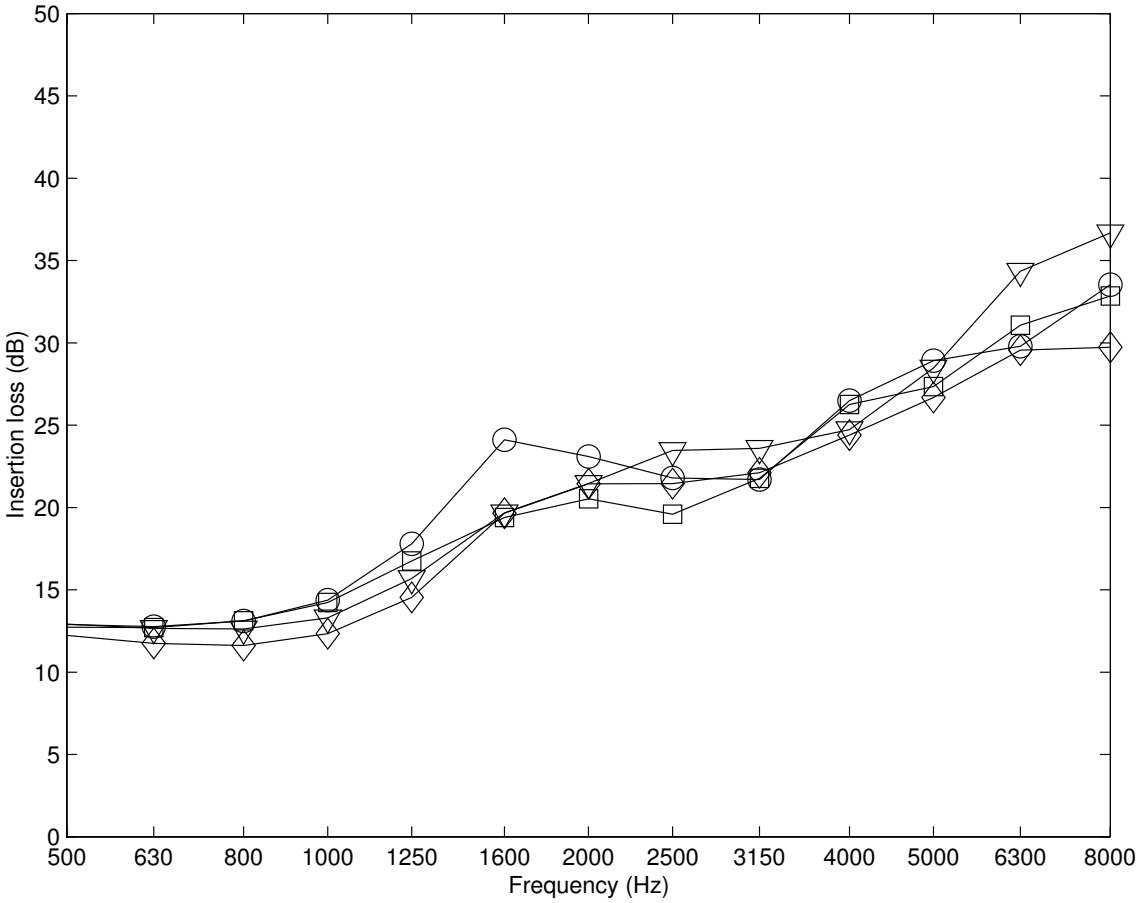

Figure 4.16. Spaced-averaged insertion loss over the receiver plane to the height of 90 cm (57 microphones): '□': square; '○': circle; '△': triangle; '▽': inverted triangle.

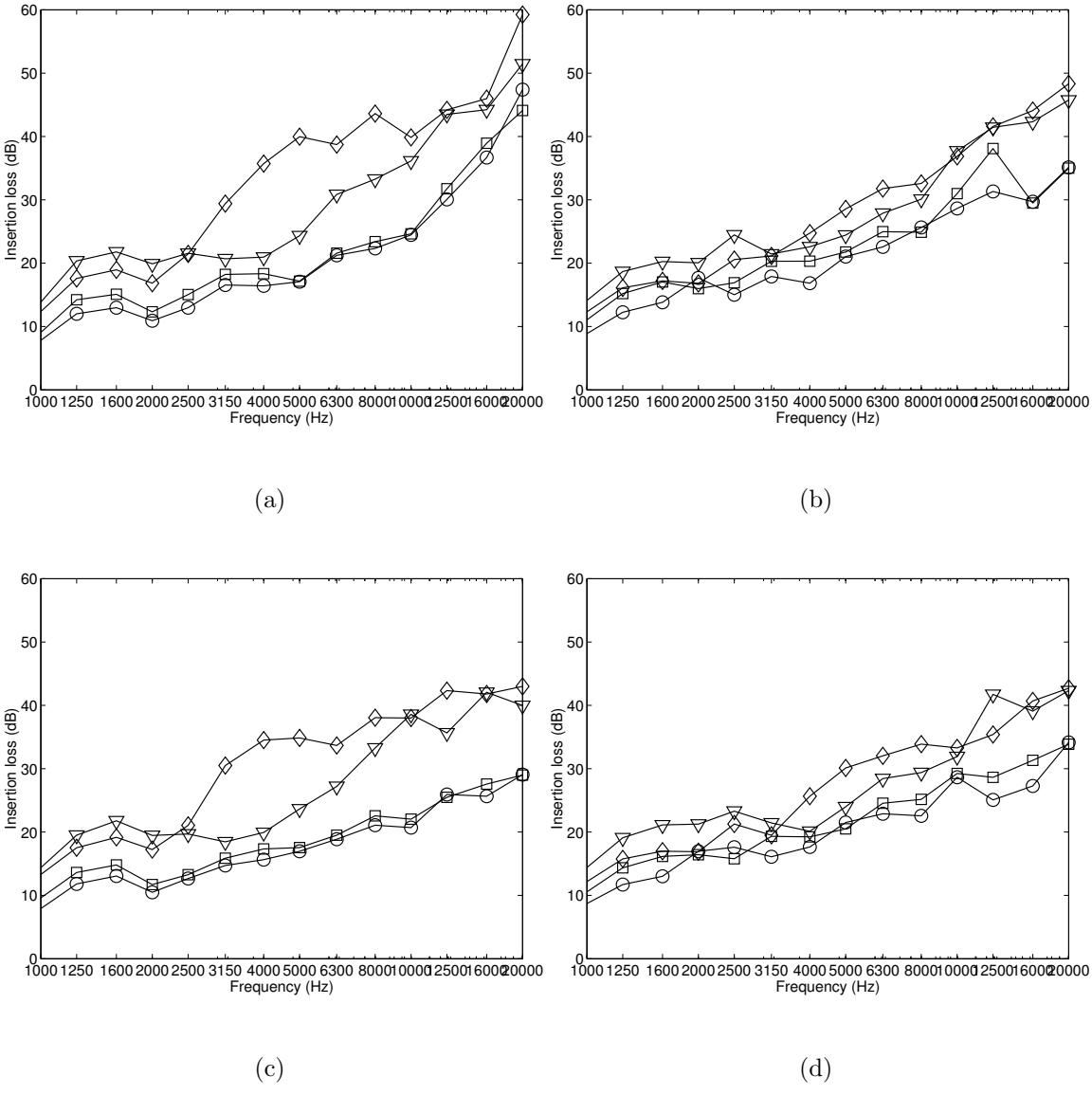

(a) (b)

(c) (d)

Figure 4.17. Insertion loss vs. frequency: '○': baseline barrier; '□': 5 cm linear extension; '◇': glassfiber; '▽': QUASH: (a) receiver 1 at $y = 0$ cm and $z = 0$ cm, (b) receiver 2 at $y = 30$ cm and $z = 0$ cm, (c) receiver 3 at $y = 0$ cm and $z =$ -50 cm, (d) receiver 4 at $y = 30$ cm and $z =$ -50 cm.

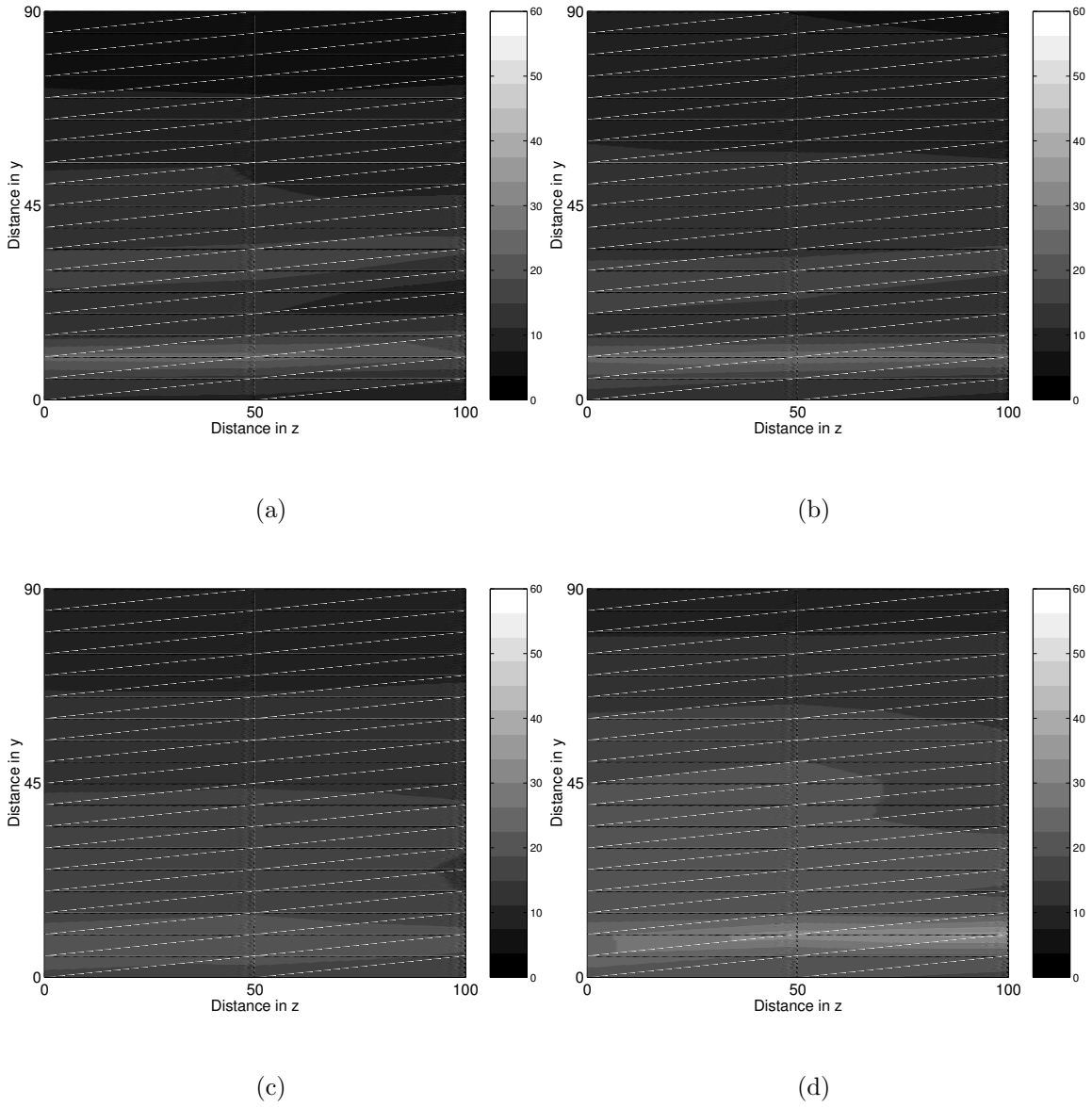

(a) (b)

(c) (d)

Figure 4.18. Insertion loss distribution over the receiver plane at the one-third octave band center frequency of 2000 Hz: (a) baseline barrier, (b) 5 cm linear extension, (c) glassfiber, (d) QUASH.

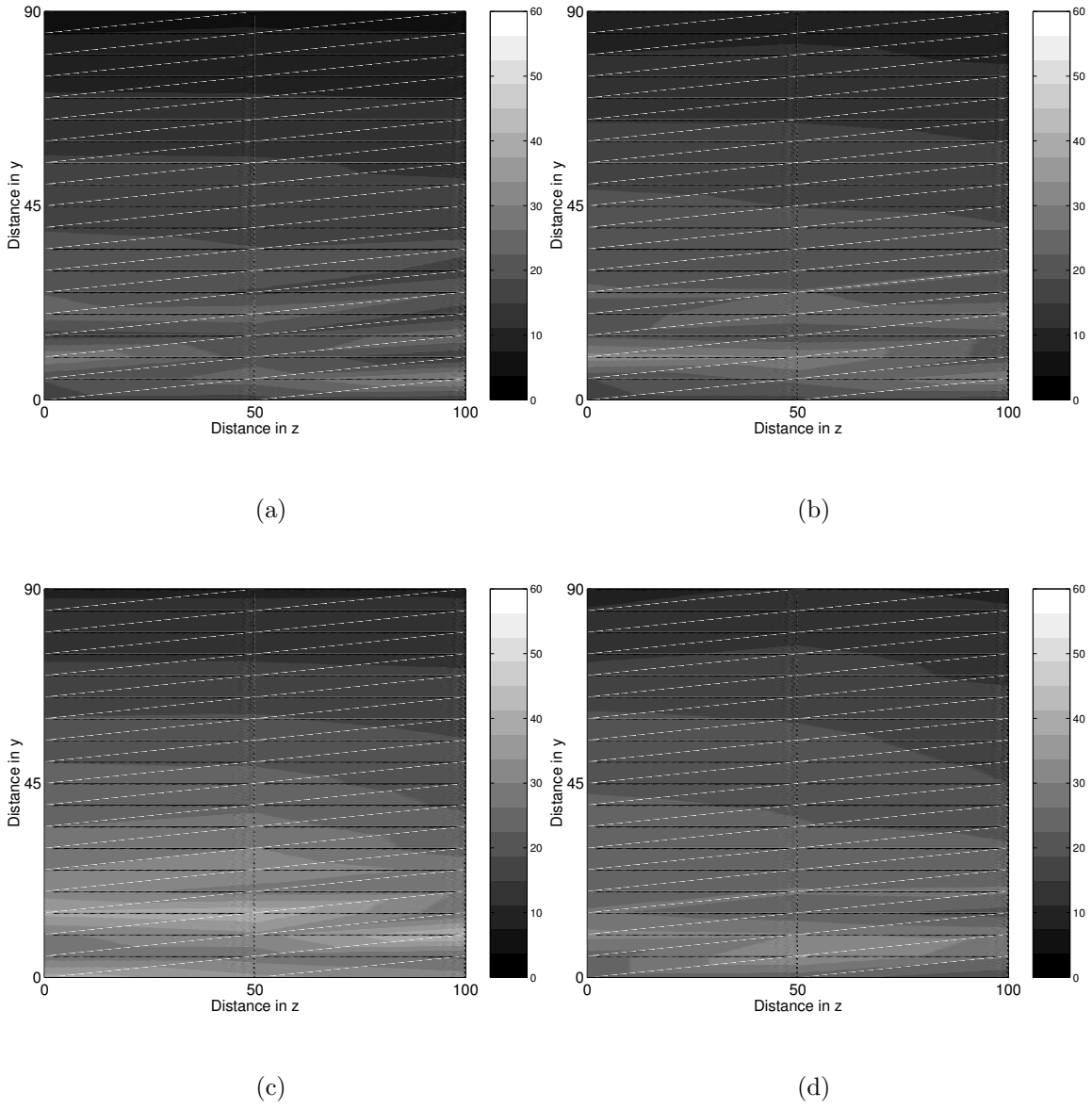

(a) (b)

(c) (d)

Figure 4.19. Insertion loss distribution over the receiver plane at the one-third octave band center frequency of 5000 Hz: (a) baseline barrier, (b) 5 cm linear extension, (c) glassfiber, (d) QUASH.

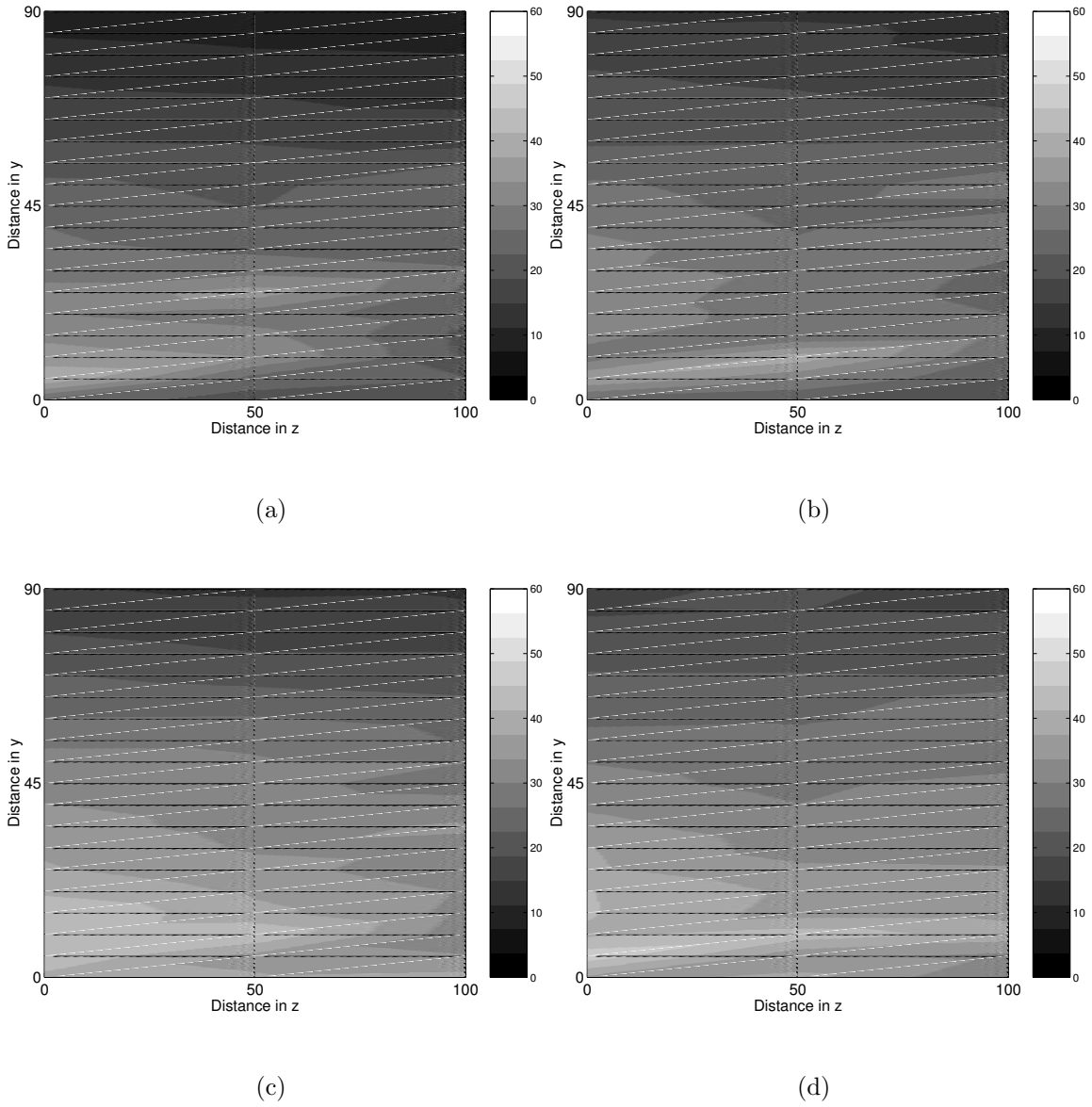

(a) (b)

(c) (d)

Figure 4.20. Insertion loss distribution over the receiver plane at the one-third octave band center frequency of 10000 Hz: (a) baseline barrier,(b) 5 cm linear extension, (c) glassfiber, (d) QUASH.

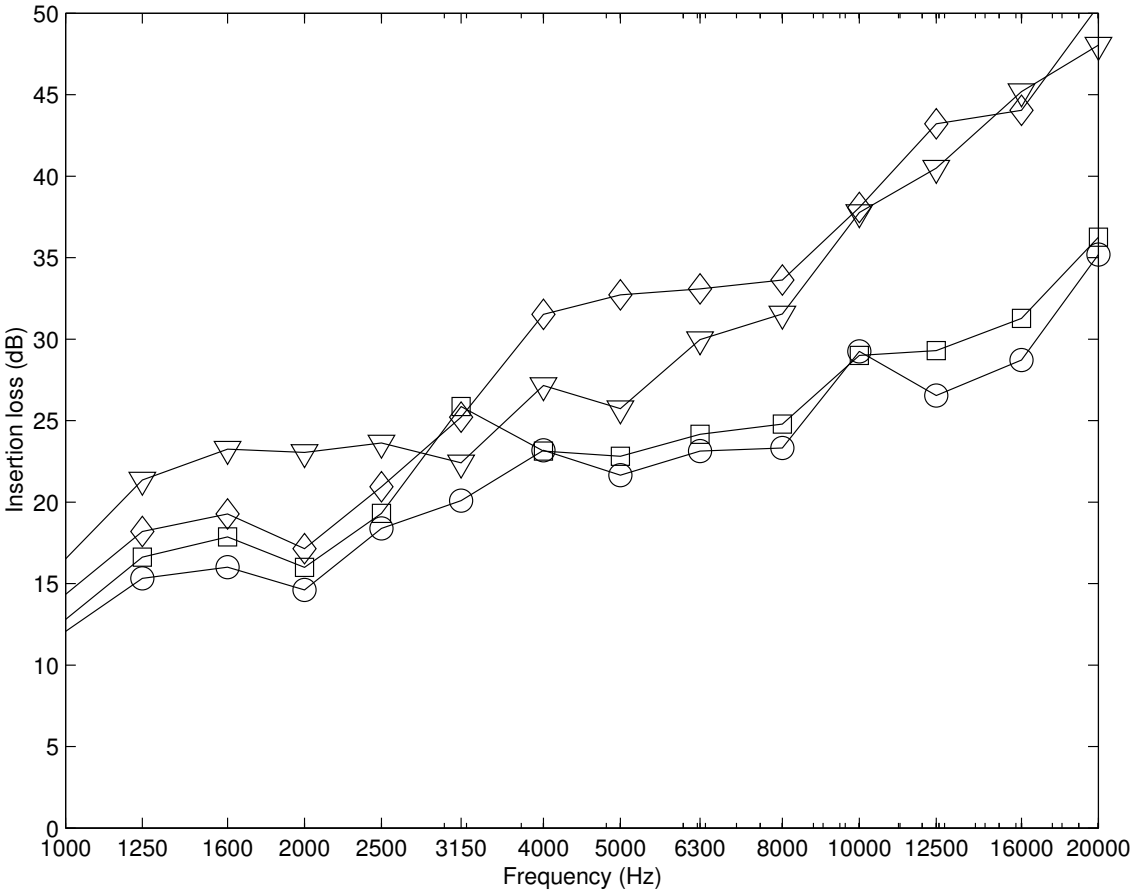

Figure 4.21. Space-averaged insertion loss over the receiver plane to the height of 30 cm (21 microphones): '$\circ$': baseline barrier; '$\square$': 5 cm linear extension; '$\diamond$': glassfiber; '$\bigtriangledown$': QUASH.

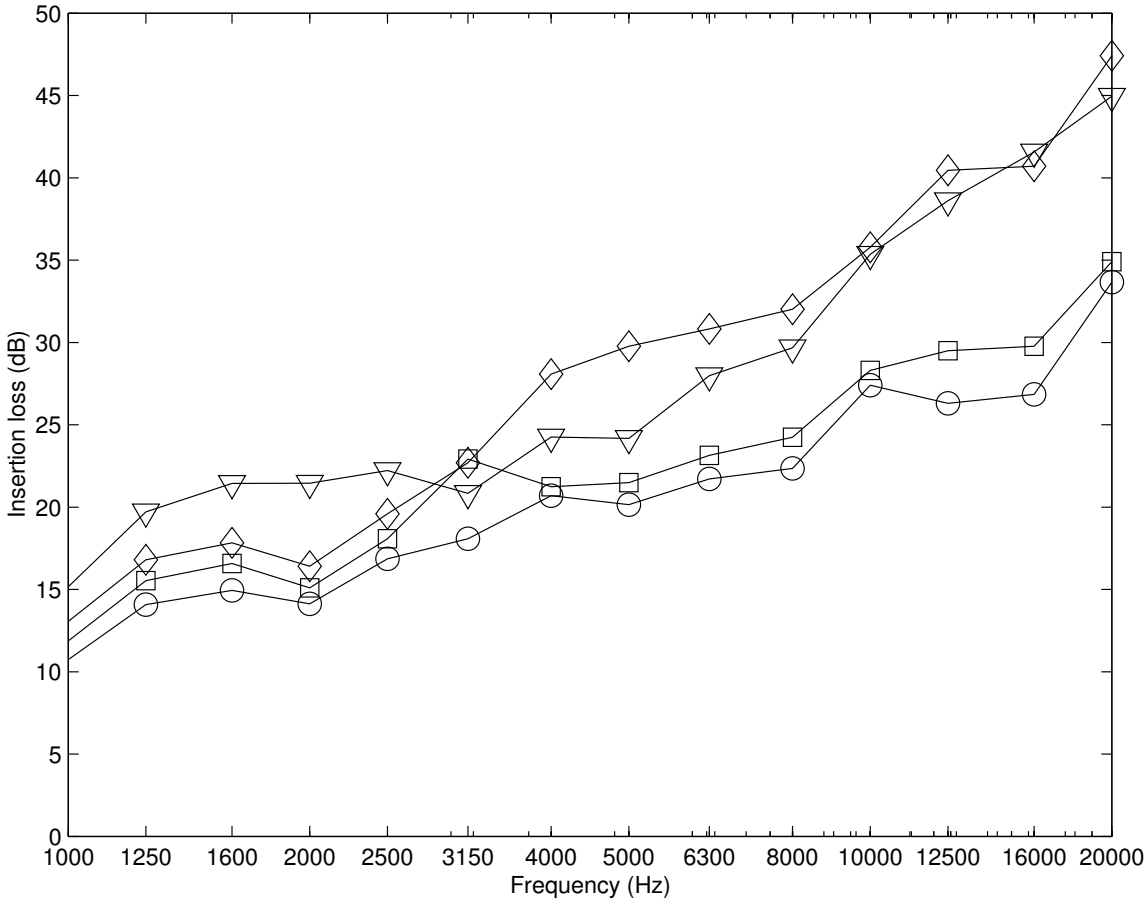

Figure 4.22. Space-averaged insertion loss over the receiver plane to the height of 60 cm (42 microphones): '$\circ$': baseline barrier; '$\square$': 5 cm linear extension; '$\diamond$': glassfiber; '$\bigtriangledown$': QUASH.

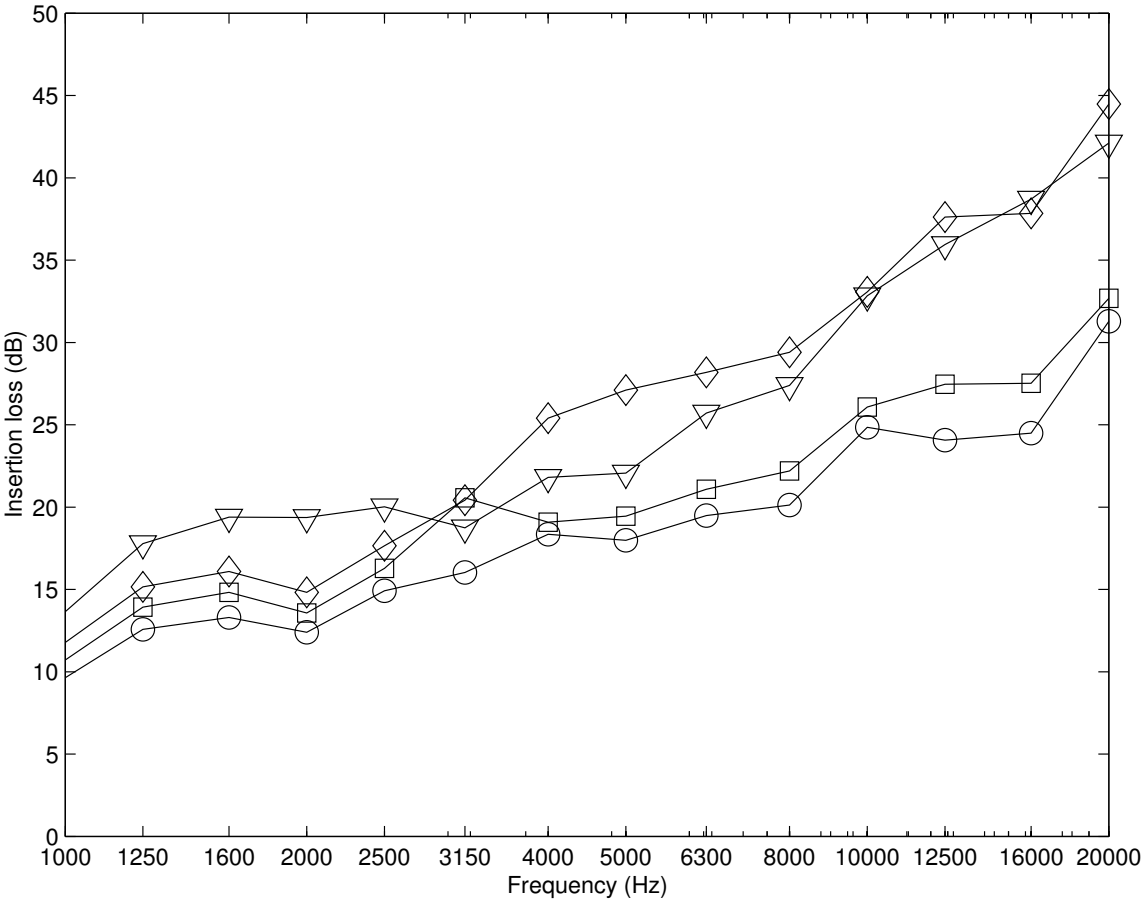

Figure 4.23. Spaced-averaged insertion loss over the receiver plane to the height of 90 cm (57 microphones): '$\circ$': baseline barrier; '$\square$': 5 cm linear extension; '$\diamond$': glassfiber; '$\bigtriangledown$': QUASH.

5. NUMERICAL ANALYSIS

A numerical model was created to predict the performance of rectangular barriers. A boundary element method was used in which it was assumed that the surrounding fluid medium was infinite in size and homogeneous. The models were developed using commercially available software [20]. The meshes for the boundary element model were refined to reduce calculation cost while ensuring proper resolution. The results from numerical predictions at different frequencies were averaged over one-third octave bands for comparisons with experimental data. The application of similar numerical models to include the effects of sound absorptive treatments was investigated.

5.1. Background on boundary element methods

Two types of boundary element methods are available for acoustical analysis [21]. The more traditional approach, the direct boundary element method (DBEM), is based on the classical Helmholtz integral equation [22]. To solve the Helmholtz integral equation numerically, the boundary of the barrier structure is discretized into a number of curvilinear elements. By using shape functions, the sound pressure and the particle velocity along the boundary can be expressed as a linear summation of nodal sound pressures and nodal particle normal velocities. This relationship is expressed as a global matrix equation; this process is called the collocation method. The acoustic pressure and the acoustic particle velocity constitute the primary variables in the DBEM. When this method is applied to a very thin body, the solution of the integral equation breaks down [23]. When the meshes on opposite sides of the structure are too closely spaced, the coefficient matrix becomes singular. Thus, the so-called indirect formulation was developed to avoid this difficulty. The difference in the pressure and the difference in the normal gradient of the pressure across the boundary

element model are used as the primary variables in the indirect boundary element method (IBEM). The mid-surface of the thin body is used instead of the surfaces on both sides of the body to compute the effect of the body on the sound field. The indirect formulation can be combined with a variational approach, after considering the boundary conditions, in order to derive the primary system of equations. The attractive feature of employing a variational approach is that the system of equations involved in the boundary element formulation is symmetric, which reduces computational effort. The thickness of the barrier is not considered in numerical models based on the indirect variational approach. In the case of a barrier placed on a hard surface, modeling of an infinite reflecting plane can be avoided by adopting an appropriate fundamental solution, often referred to as the half-space Green's function. The half-space Green's function is constructed by using the method of images.

5.2. Variable-size mesh

For the acoustic boundary element method, it is required to have a minimum of six linear elements per wavelength to obtain reasonable prediction accuracy. If the frequency of interest is increased, the element size decreases and the model size increases very quickly which increase the calculation since the calculation time increases as a power of the number of elements. Note that the boundary element method is a global method in the sense that each degree of freedom is connected to all others. As a result, the boundary element formulations involve complex system matrices. The fully populated matrices result in computationally intensive tasks. The number of degrees of freedom for an acoustic boundary element model needs to be kept a minimum. One of the characteristics of the boundary element method is that a matrix of equations needs to be solved for each frequency. Multiple boundary element models of varying mesh density may be created for various frequency ranges of interest. For example, the mesh size should be around 9 mm for a frequency of 6300 Hz according

to the six elements per wavelength rule. But a mesh size of only 90 mm is required for a solution at 630 Hz.

In the present study, linear rectangular elements were used. A total of 12 different mesh sizes were used. The mesh size and the number of elements for each case are listed in Table 5.1. Each step of the analysis was performed with different mesh sizes and result files were imported to MATLAB for postprocessing. The calculation time for a unique mesh model was compared to that for a variable-size mesh model. The unique mesh models featured a 9 mm mesh for all frequencies. The calculation was performed from 500 Hz to 6300 Hz at all the one-third octave bands center frequencies. In this instance, the calculation took 10 hours 20 minutes and 36 seconds with a unique size mesh model, while the same case using a variable-size mesh model took only 1 hour 9 minutes and 27 seconds with a dual CPU (AMD 1800) machine having 2 GB memory.

5.3. Narrow-band results for rigid barriers

The sound field in the shadow region features very complicated interference patterns, especially at locations near the reflecting ground. Due to limitations in computational resources, the narrow band analysis was limited to frequencies up to 2000 Hz. The numerical solution was obtained with a frequency resolution of 10 Hz. The results below 500 Hz were not included due to the inaccuracy of the experimental data (see section 4.2). Figure 5.1 shows the insertion loss obtained from the numerical predictions along with experimental results for frequencies ranging from 500 Hz to 2000 Hz. Four receiver locations were selected for the comparison, located within the x-y plane at different heights, (y=0 cm, 30 cm, 60 cm and 90 cm). Figure 5.1(a) shows data at a point directly on the ground, i.e., y=0 cm. The numerical model was able to predict the complicated interference pattern at this point. Figure 5.1(b) shows that 30 cm above the hard ground the numerical model predicted the exact number of destructive interferences up to 2000 Hz. Note that peaks in the insertion loss curve

mean that the sound pressure level is a minimum at that frequency. Figure 5.1(c) shows that the insertion loss higher from the ground is rather smooth, without any peaks or dips. The numerical prediction is in good agreement with the experimental result. At the shadow region boundary, the amplitude of the insertion loss is less than 10 dB for all frequencies of interest and the numerical results agree well in character with the experimental results: see Figure 5.1(d).

Similar results over a receiver x-y plane at z=50 cm are shown in Figure 5.2. As shown in Figure 5.2(a) the peaks were not as strong on the ground as in the $z = 0$ cm case. The model predictions agree well with measured data except at low frequencies. Figure 5.2(b) shows the results at a height of y=30 cm and z=50 cm off the midline of the barrier length. At these points, the numerical model yields very good results. The same good agreement can be seen in Figure 5.2(c) and 5.2(d) which shows the comparison at 60 cm and 90 cm above the hard ground, respectively.

5.4. One-third octave band results for rigid barriers

5.4.1. Insertion loss at selected locations

A comparison between numerical and experimental results at frequencies up to 2000 Hz was described in section 5.3. The boundary element method requires re-calculation of the system matrices for each frequency. Thus, the calculation time is directly proportional to the number of frequencies considered in the analysis. The insertion loss can be measured with a fine frequency resolution. But the same resolution can not be easily achieved using a numerical model due to limitations in computing resources. One possible approach is to present the data in octave bands. It should be noted, however, that the experimental results were averaged into one-third octave bands while the numerical calculations were only made at five discrete frequencies within each one-third octave band. Experimental results measured with a frequency resolution of 1.25 Hz were averaged into the one-third octave band for comparison.

The latter operation results in a "smoother" insertion loss frequency distribution. Figure 5.3 shows the comparison between the measurements and predictions at four points at $z = 0$.

At all locations, the numerical model successfully predicted the insertion loss as shown in Figs. 5.3(a) to 5.3(d). Comparisons made at four receiver locations at $z = 50$ cm also show the same trend: see Figure 5.4. When the comparison was made near the ground there are some errors at particular frequencies, for example, at 2500 Hz in Figure 5.4(a). It is believed that the limited amount of averaging in the numerical model was responsible for the discrepancies at this frequency. However, good agreement was obtained at $y = 30$ cm, as shown in Figure 5.4(b). The numerical model predicted the performance of the barrier relatively well for points relatively high in the shadow zone: see Figure 5.4(c) and 5.4(d).

5.4.2. Insertion loss distributions

Figure 5.5 illustrates the insertion loss distribution attained from numerical predictions and experimental data at 1000 Hz, 1250 Hz and 1600 Hz. Here the darker colors indicates that the insertion loss is small and that the area is not well protected by the barrier. The locations of largest insertion loss (illustrated in the figure as light colors) were located between the ground level and $y = 20$ cm. The numerical results exhibit trends which are similar to the experimental results but which are somewhat different in detail. Figure 5.6 shows the insertion loss distributions at 2000 Hz, 2500 Hz and 3500 Hz. Note that the location of high insertion loss zone was predicted accurately in all cases. The numerical predictions feature more complicated insertion loss patterns then the experimental results. It is believed that this difference is due to the frequency averaging procedure described earlier. Corresponding comparisons for frequencies of 4000 Hz, 5000 Hz and 6300 Hz are shown in Figure 5.7. The insertion loss distribution in Figure 5.7(b) shows an interference pattern comprising several strips stretched in the z-direction. Figure 5.7(a) shows that the numerical model

was able to predict this behavior. The insertion loss calculated from the numerical model, shown in Figure 5.7(c) and 5.7(e), are more complex than in the experimental results shown in Figure 5.7(d) and 5.7(f). This behavior might again be caused by the limited number of averages used in the numerical model.

5.4.3. Space-averaged insertion loss

The insertion loss at 20 locations from $y = 0$ to 30 cm were averaged to calculate the space-averaged insertion loss over a region after shadow zone: results are shown in Figure 5.8. The numerical prediction was in good agreement with the experimental data at all frequencies except at 2500 Hz, 3150 Hz and 4000 Hz. At those frequencies the numerical model underestimates the barrier performance by 3 to 5 dB. The space-averaged insertion loss from the experiment and the numerical model over a larger section of the receiver plane is shown in Figure 5.9. The discrepancy between the numerical prediction and the experimental results at 2500 Hz, 3150 Hz and 4000 Hz was reduced compared to the results shown in Figure 5.8. At other frequencies the comparison gave excellent results. Lastly, the insertion losses averaged over the entire receiver plane for the experiment and the numerical calculation were shown in Figure 5.10. The averaged insertion loss shows a monotonic increase with frequency from 1000 Hz to 6300 Hz. The numerical model predicted the measured performance of the scale barrier model progressively more correctly as the surface area of the receiver plane was increased.

5.5. Multi-domain boundary element models

5.5.1. Modeling of sound absorptive material

Many types of sound absorbing materials are used in noise control applications. Materials with a low density and a high flow resistivity are “limp”. Fiberglass materi-

als support only a single uni-directional wave type, and may be modeled as a dissipative fluid with a complex characteristic impedance and wave number. The acoustical properties of those materials can be characterized with two independent properties such as the complex density and the sound speed, derived from the characteristic impedance and the wave number. Bolton et al. [24] showed that a four-microphone, standing wave tube can be used for measurement of the normal incidence reflection and the transmission coefficient of porous materials satisfying the above assumptions. Later Song and Bolton [25] suggested a transfer-matrix approach which does not require an anechoic termination in a standing wave tube. Measured data available from the latter study for an aviation grade fiberglass of 2.5 cm thickness were used in the numerical model described below.

5.5.2. Sound intensity

Diffraction in the term is mostly commonly applied to the form of scattering produced by discontinuities of impedance presented to incident waves by the edges of barriers. The top of the barrier which introduces the impedance discontinuity can be thought of as the location of a secondary source in the sound field. Sound energy is important because it is a conserved quantity, unlike the sound pressure and particle velocity. The rate of generation of sound energy, i.e., the sound power, characterizes the strength of a sound source. The sound intensity in a specified direction is the amount of sound energy flowing through a unit area normal to that direction. The sound intensity is normally measured in watt per square meter. Some of the modern uses for intensity measurements include: total sound power estimation, component sound power measurement, transmission loss measurement and estimation of the absorption coefficients for materials. The benefits of adopting a sound absorptive top on a barrier was studied here. The sound intensity fields in the top region of barriers with and without sound absorptive materials were compared. The intensity was measured in the x and y directions at 10 points near the barrier top on a plane perpendicular

to the barrier along the center line by using a Brüel and Kjær intensity probe type 4181 with a 12 mm spacer which allows measurements to be made from 125 Hz to 5000 Hz. Ten points were taken at 20 cm behind the barrier from y = 12 to 47 cm. The interval between measurement locations was 5 cm.

5.5.3. Verification of numerical results

The relative amplitudes of the intensities near the barrier top were compared in the cases of rigid and sound absorptive extensions between the measurement and numerical predictions. The intensity measurements were performed at a limited number of locations for the verification of the numerical results. Figure 5.11 shows the intensity vectors at locations 20 cm behind the barrier from experiments and numerical predictions at 1000 Hz. Experimental results shows that the amplitude of the intensities at locations in the shadow region decreased without much change in the directions of vectors. It can be seen that the amplitude of the intensity vectors was smaller in the case of an absorptive extension than the rigid extension but the direction of the vectors were not consistent in the numerical results. A further comparison was made at 2000 Hz: see Fig. 5.12. At this frequency, the orientation of the intensity vectors change as sound propagates through the sound absorptive treatment, as shown in 5.12(b). This shows that the waves travelling through the fiberglass material travel at a lower speed than the sound waves in air.

5.5.4. Intensity distribution

A numerical model was implemented to study the change of sound intensity near the barrier top due to the sound absorptive treatment. The distribution of mean intensity is represented in Fig. 5.13 at 1000 Hz for rigid and absorptive extensions. The calculation was performed over a receiver plane of 20 cm by 20 cm from x = -0.1 to 0.1 m and from y=0.37 to 0.42 m. The interval between points was 1 cm both in the x- and y-directions. The intensity vectors indicate the way sound waves travel

around the rigid extension in Fig. 5.13(a). It is obvious that the rigid extension did not allow the penetration of sound waves. At the same frequency, the sound field behaved slightly differently with the absorptive extension as shown in Fig. 5.13(b). The direction of the intensity vectors was different in front of the absorptive extension, compared to the rigid case. The intensity vectors with the absorptive top show that the numerical model allows sound to travel through the absorptive extension. Thus the amplitude of the intensity vectors was greater in the case of an absorptive extension compared to the ones with the rigid extension. It should be noted that the amplitude of the intensity vectors is smaller at locations above the end of the barrier extension in the case of the absorptive edge. Figure 5.14(a) shows sound intensity vectors at 2000 Hz for rigid and absorptive extensions. The intensity plot shows that strong reflections off the rigid extension cause the sound wave to travel in the vertical direction in front of the extension. Another comparison was performed at 4000 Hz: see Fig. 5.15. Reflection from the rigid barrier extensions causes sound waves to travel in the negative x-direction as shown in Fig. 5.15(a). With the sound absorptive top, the direction of the intensity was in the positive x-direction as shown in Fig. 5.15(b). This was caused by the characteristics of the sound absorptive material used for the calculation. Fig. 5.15 shows that behind the barrier top, the intensity was larger with the absorptive top since there is a sound wave component travelling through the porous material with no interference between the sound wave travelling around and through the absorptive material. But gradually interference became significant and the amplitude of the intensity vectors with the absorptive top were about the same as the rigid top when the intensity were calculated 10 cm behind the barriers.

5.5.5. Space-averaged insertion loss

The insertion loss at 20 locations from $y = 0$ to 30 cm were averaged to calculate the space-averaged insertion loss in Figure 5.16. The numerical prediction is in good agreement with the experimental result except at 1000 Hz and 4000 Hz. At those

frequencies the numerical model underestimates the barrier performance by 2 to 6 dB. It should be noted that the numerical model also underestimated the performance of rigid barriers at certain frequencies. The space-averaged insertion loss over a larger receiver plane is shown in Figure 5.17. The discrepancy between the numerical predictions and the experimental results at 1000 Hz was reduced compared to that in Figure 5.16. The discrepancy at 4000 Hz was still present but the magnitude of error was reduced by 2 dB. This suggests that the multi-domain model fails to predict the performance of barrier with soft extension at the receiver locations near the ground or deep in the shadow region. However at other frequencies the comparison gave excellent results. Lastly, the insertion losses averaged over the entire receiver plane for the experiment and the numerical calculation are shown in Figure 5.18. The averaged insertion loss shows a monotonic increase with frequency from 1000 Hz to 6300 Hz. The numerical model including the sound absorptive material predicted the overall performance of the scale barrier model correctly.

Table 5.1. Mesh sizes and number of elements for variable-size mesh models

Frequency	Mesh size	Number of elements
500	113 mm	66
630	90.0 mm	108
800	70.8 mm	170
1000	56.7 mm	258
1250	45.3 mm	432
1600	35.4 mm	690
2000	28.3 mm	1131
2500	22.7 mm	1728
3150	18.0 mm	2720
4000	14.2 mm	4472
5000	11.3 mm	7095
6300	8.99 mm	11111

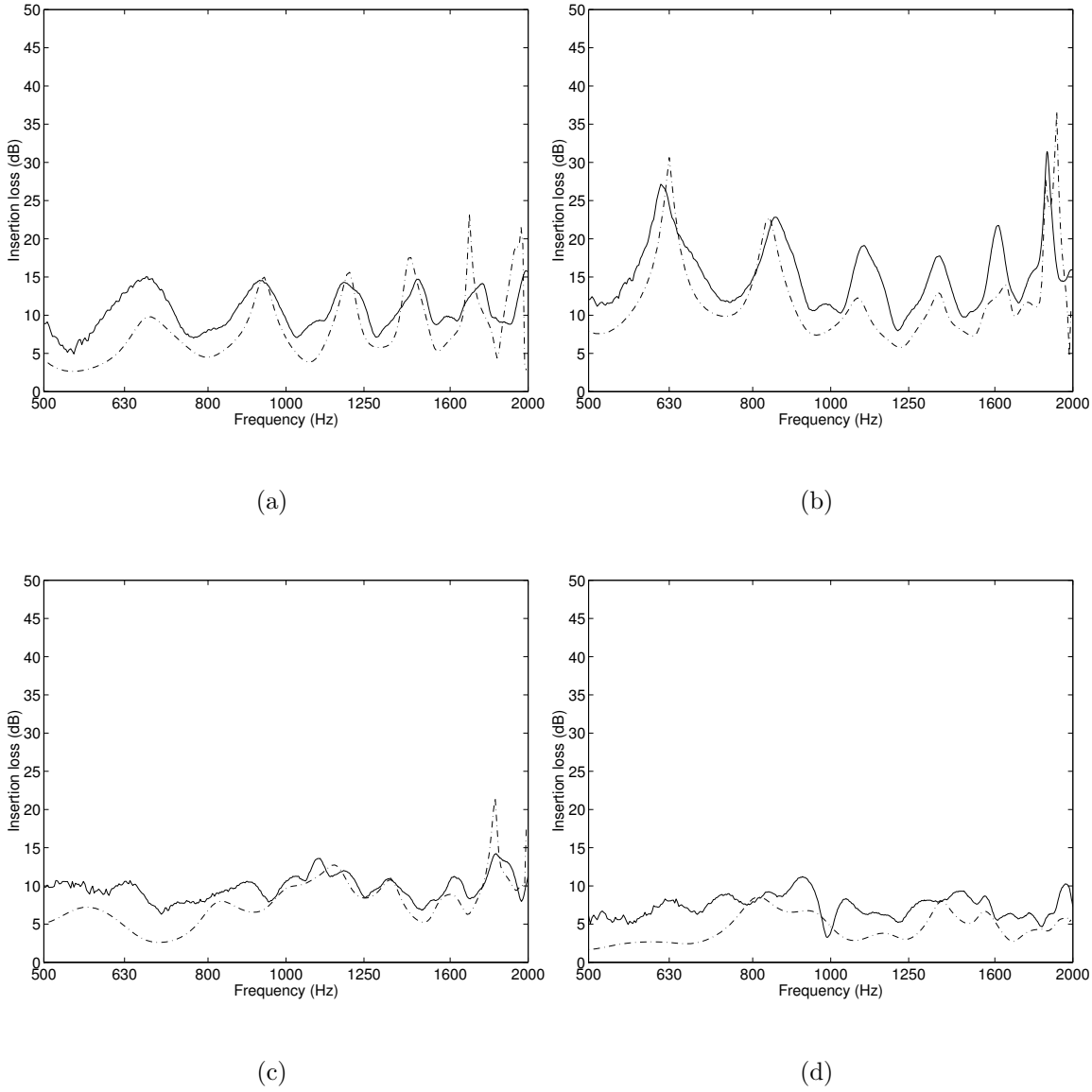

Figure 5.1. Comparison of insertion loss: '–': Experiment; '-·': Numerical prediction; (a) y = 0 cm and z = 0 cm, (b) y = 30 cm and z = 0 cm, (c) y = 60 cm and z = 0 cm, (d) y = 90 cm and z = 0 cm.

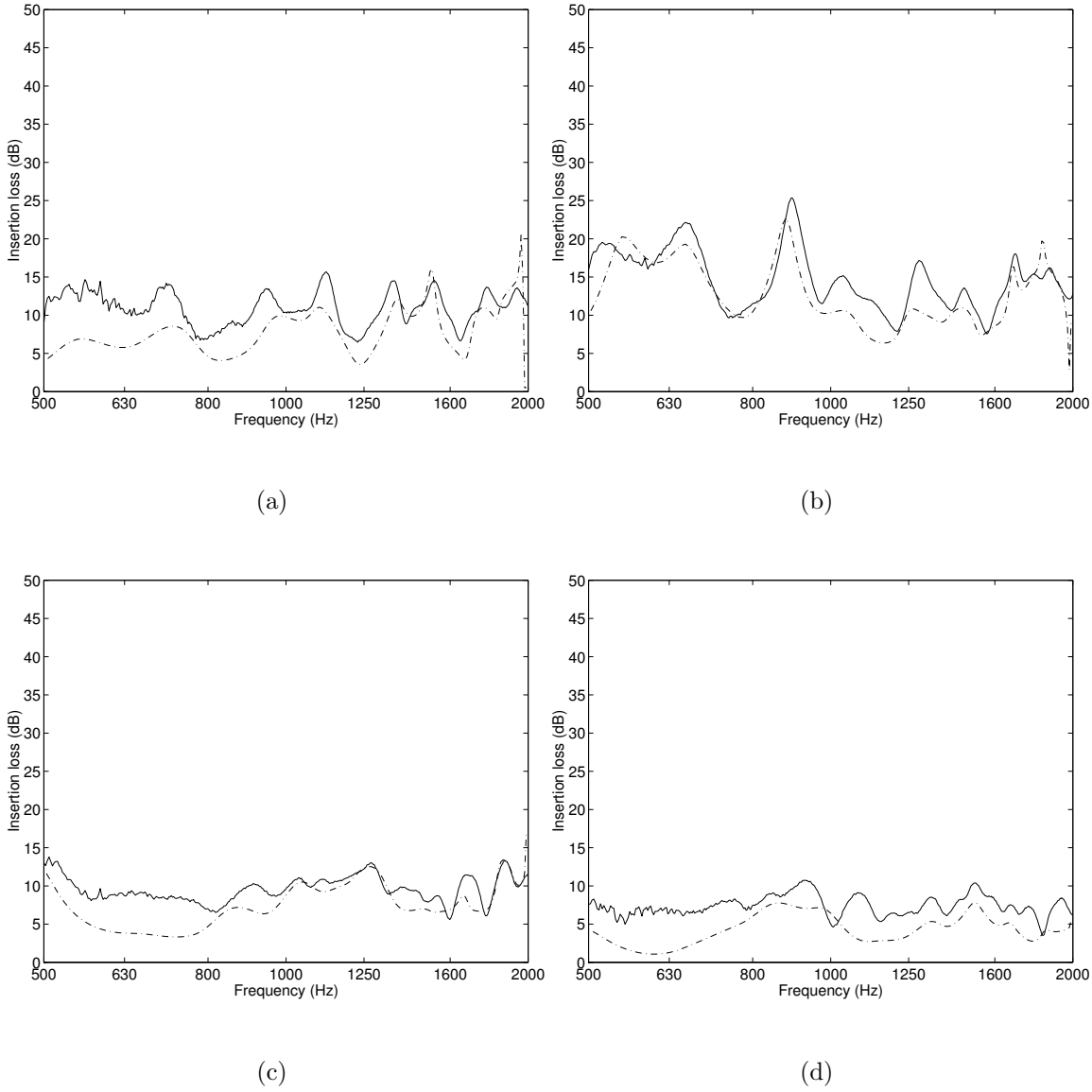

Figure 5.2. Comparison of insertion loss: '–': Experiment; '-·': Numerical prediction; (a) y = 0 cm and z = 50 cm, (b) y = 30 cm and z = 50 cm, (c) y = 60 cm and z = 50 cm, (d) y = 90 cm and z = 50 cm.

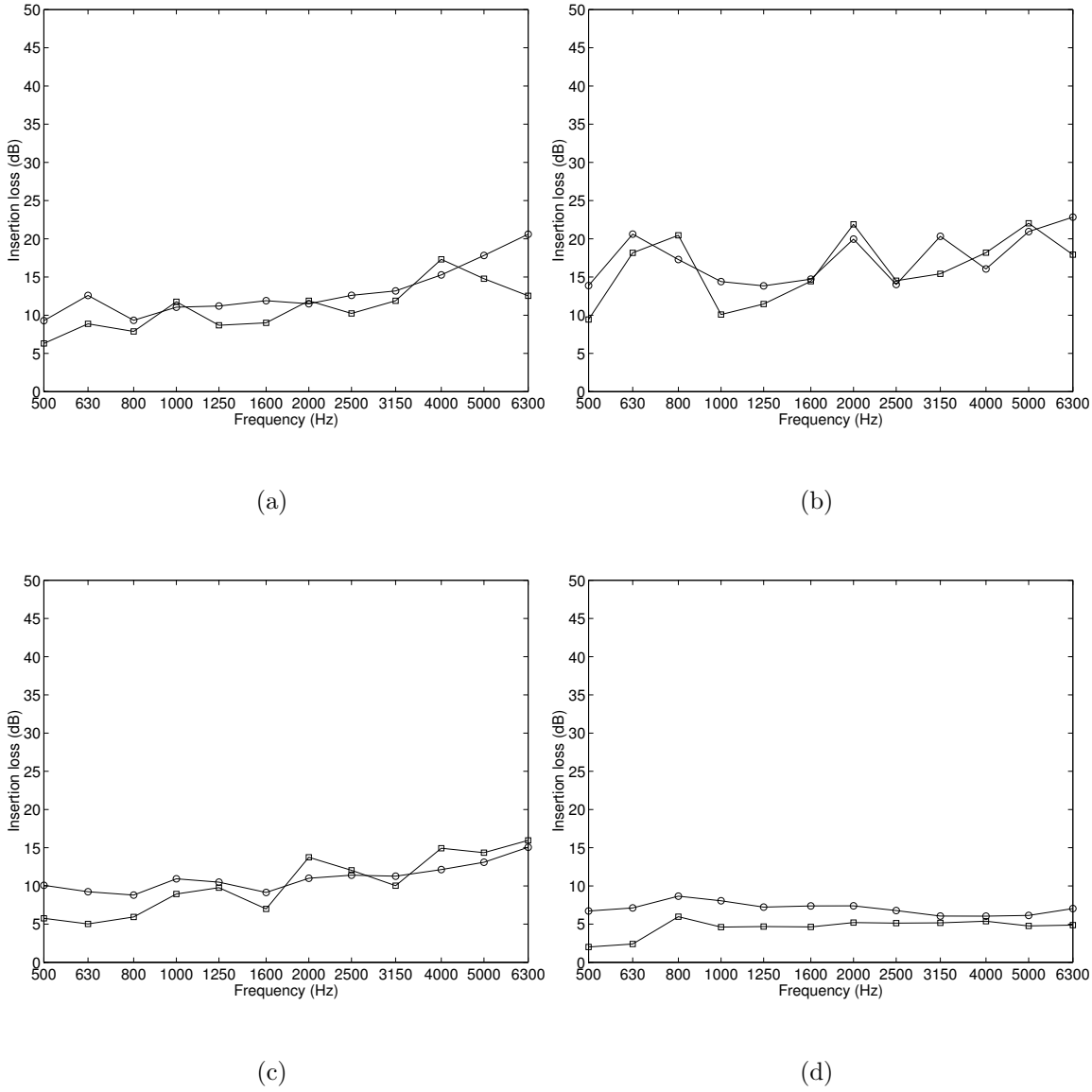

Figure 5.3. Comparison of insertion loss: '○': Experiment; '□': Numerical prediction; (a) y = 0 cm and z = 0 cm, (b) y = 30 cm and z = 0 cm, (c) y = 60 cm and z = 0 cm, (d) y = 90 cm and z = 0 cm.

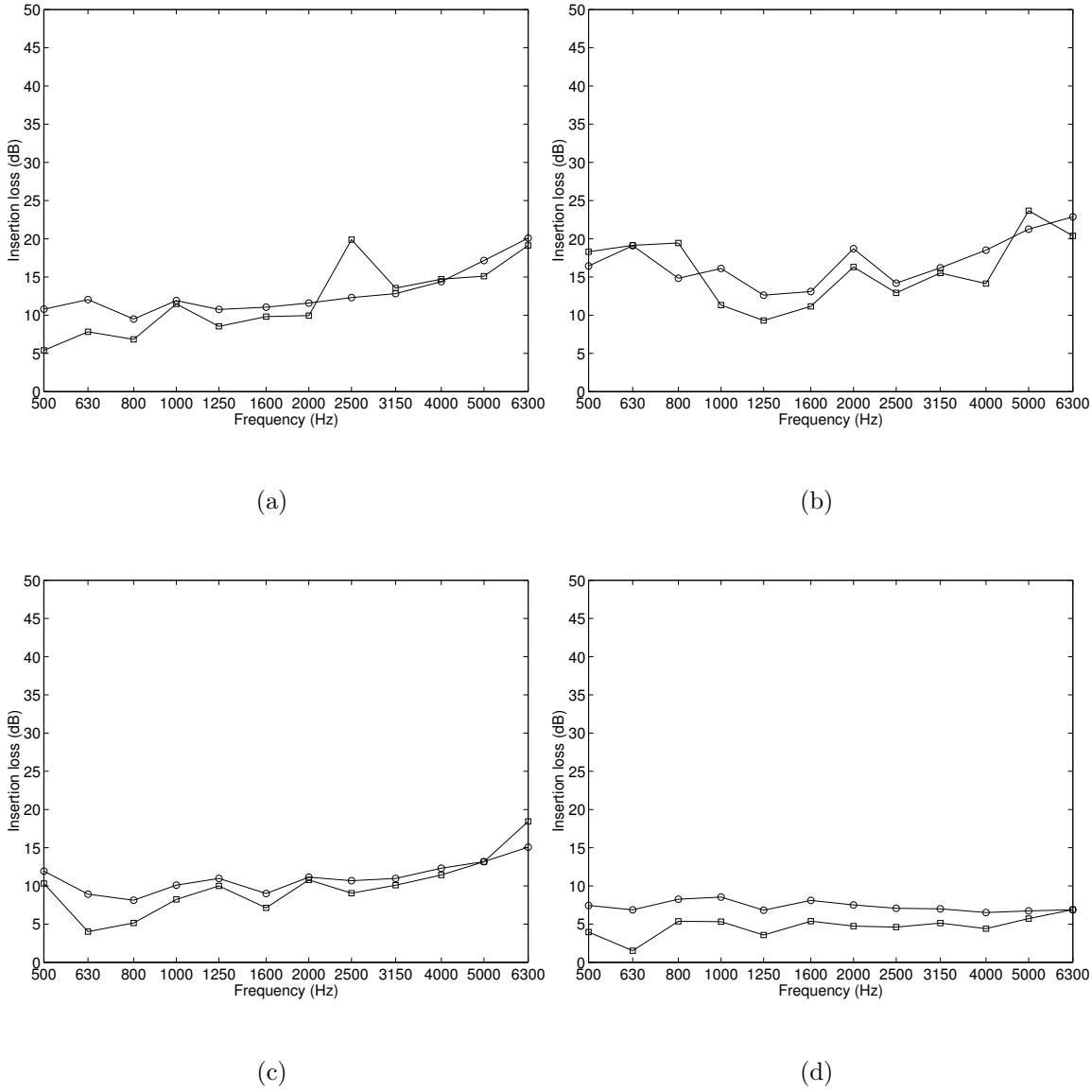

Figure 5.4. Comparison of insertion loss: '○': Experiment; '□': Numerical prediction; (a) y = 0 cm and z = 50 cm, (b) y = 30 cm and z = 50 cm, (c) y = 60 cm and z = 50 cm, (d) y = 90 cm and z = 50 cm.

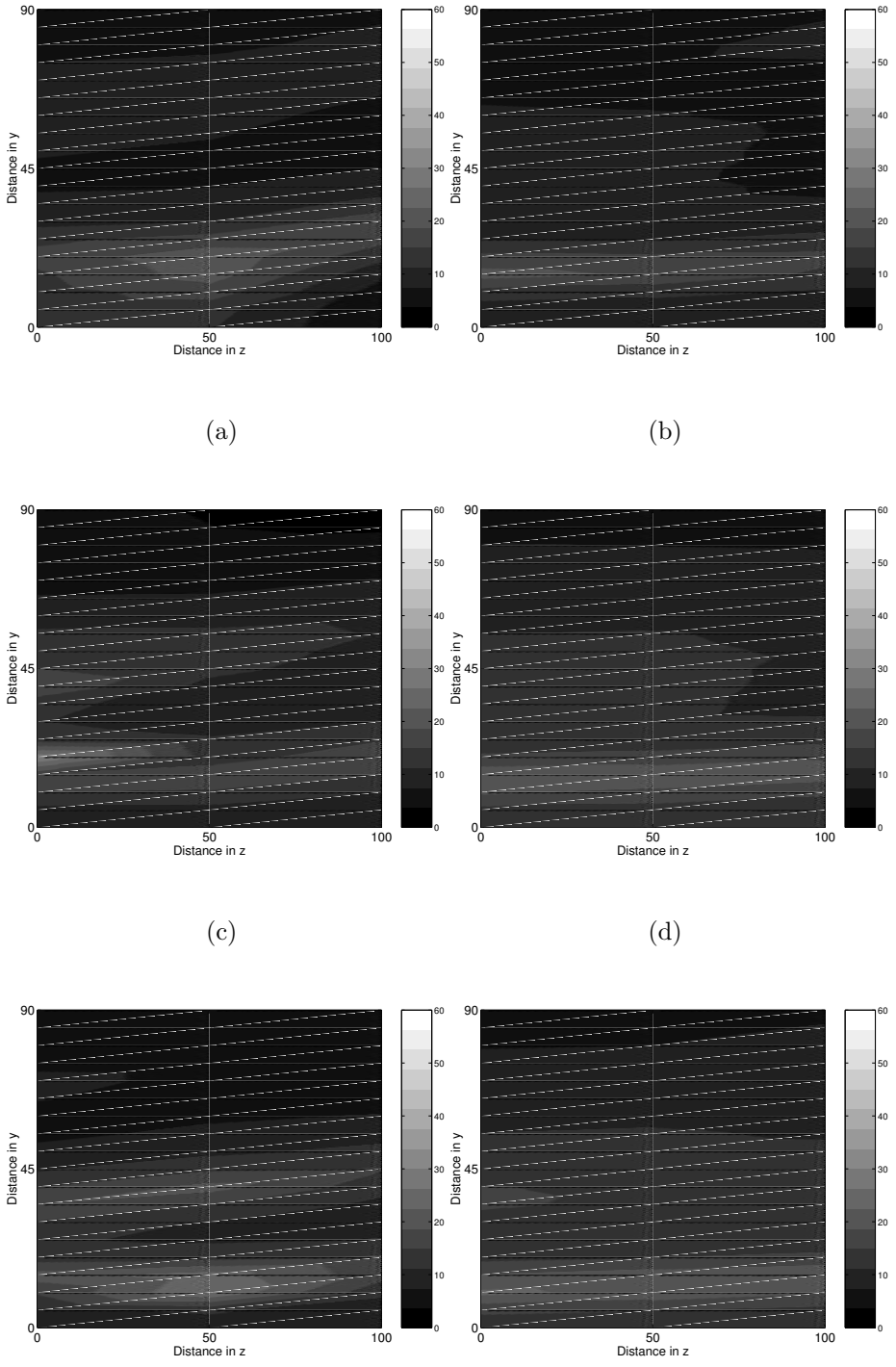

(a) (b)

(c) (d)

(e) (f)

Figure 5.5. Comparison of insertion loss distribution over the receiver plane; results shown in one-third octave bands, (a) Numerical prediction at $f_c = 1000$ Hz, (b) Experimental result at $f_c = 1000$ Hz, (c) Numerical prediction at $f_c = 1250$ Hz, (d) Experimental result at $f_c = 1250$ Hz, (e) Numerical prediction at $f_c = 1600$ Hz, (f) Experimental result at $f_c = 1600$ Hz.

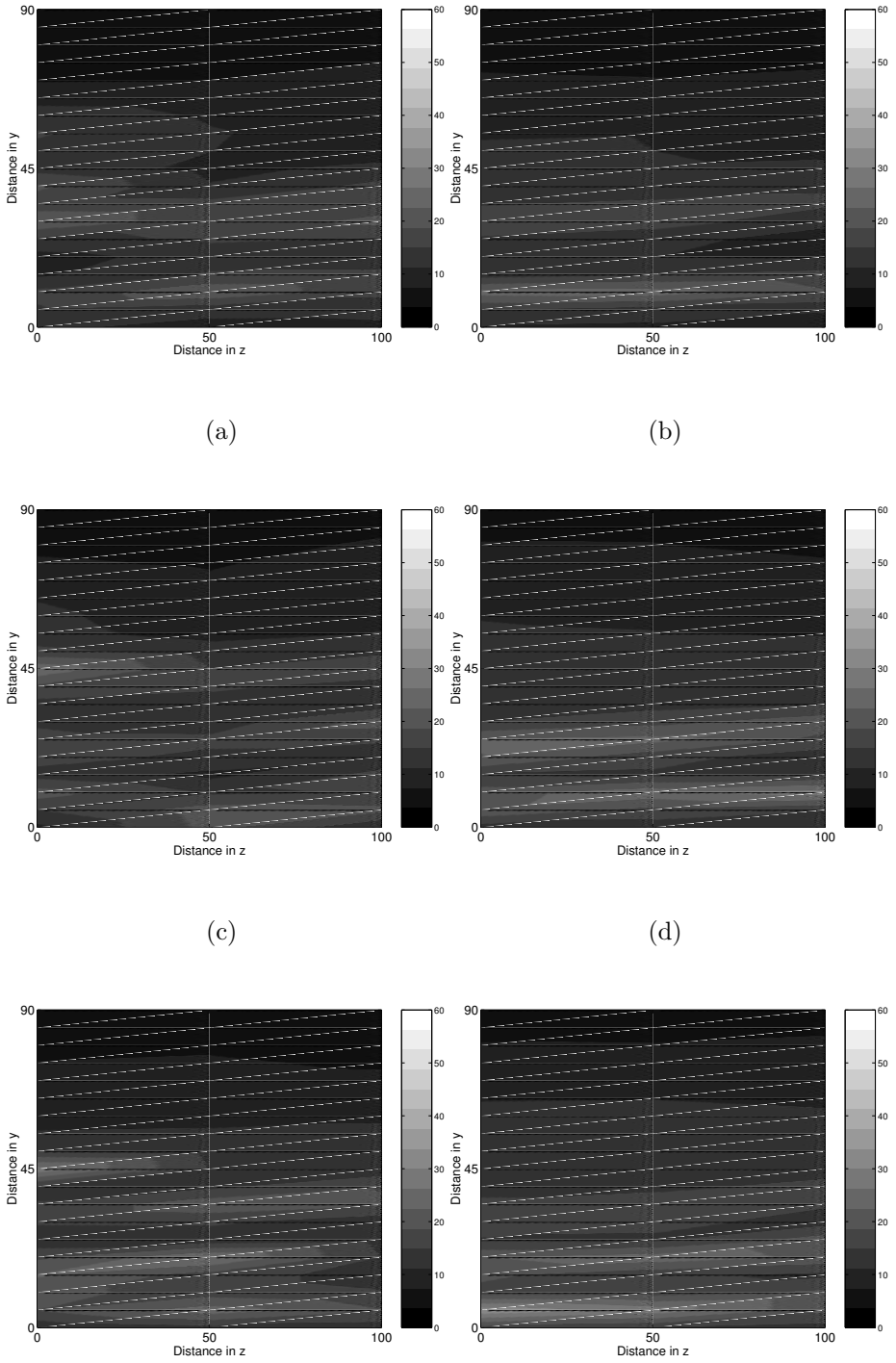

(a) (b)

(c) (d)

(e) (f)

Figure 5.6. Comparison of insertion loss distribution over the receiver plane; results shown in one-third octave bands, (a) Numerical prediction at $f_c = 2000$ Hz, (b) Experimental result at $f_c = 2000$ Hz, (c) Numerical prediction at $f_c = 2500$ Hz, (d) Experimental result at $f_c = 2500$ Hz, (e) Numerical prediction at $f_c = 3150$ Hz, (f) Experimental result at $f_c = 3150$ Hz.

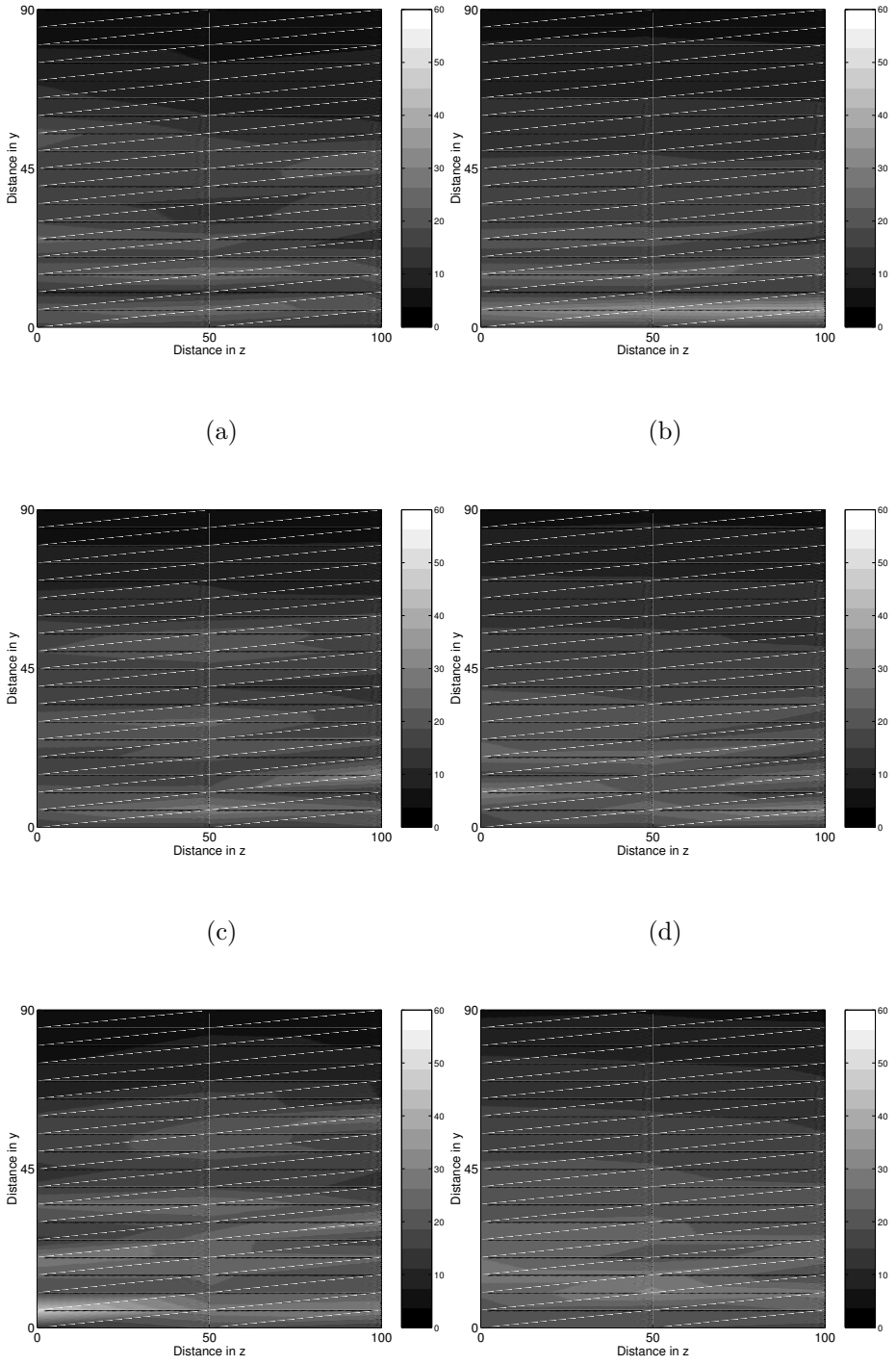

(a) (b)

(c) (d)

(e) (f)

Figure 5.7. Comparison of insertion loss distribution over the receiver plane; results shown in one-third octave bands, (a) Numerical prediction at $f_c = 4000$ Hz, (b) Experimental result at $f_c = 4000$ Hz, (c) Numerical prediction at $f_c = 5000$ Hz, (d) Experimental result at $f_c = 5000$ Hz, (e) Numerical prediction at $f_c = 6300$ Hz, (f) Experimental result at $f_c = 6300$ Hz.

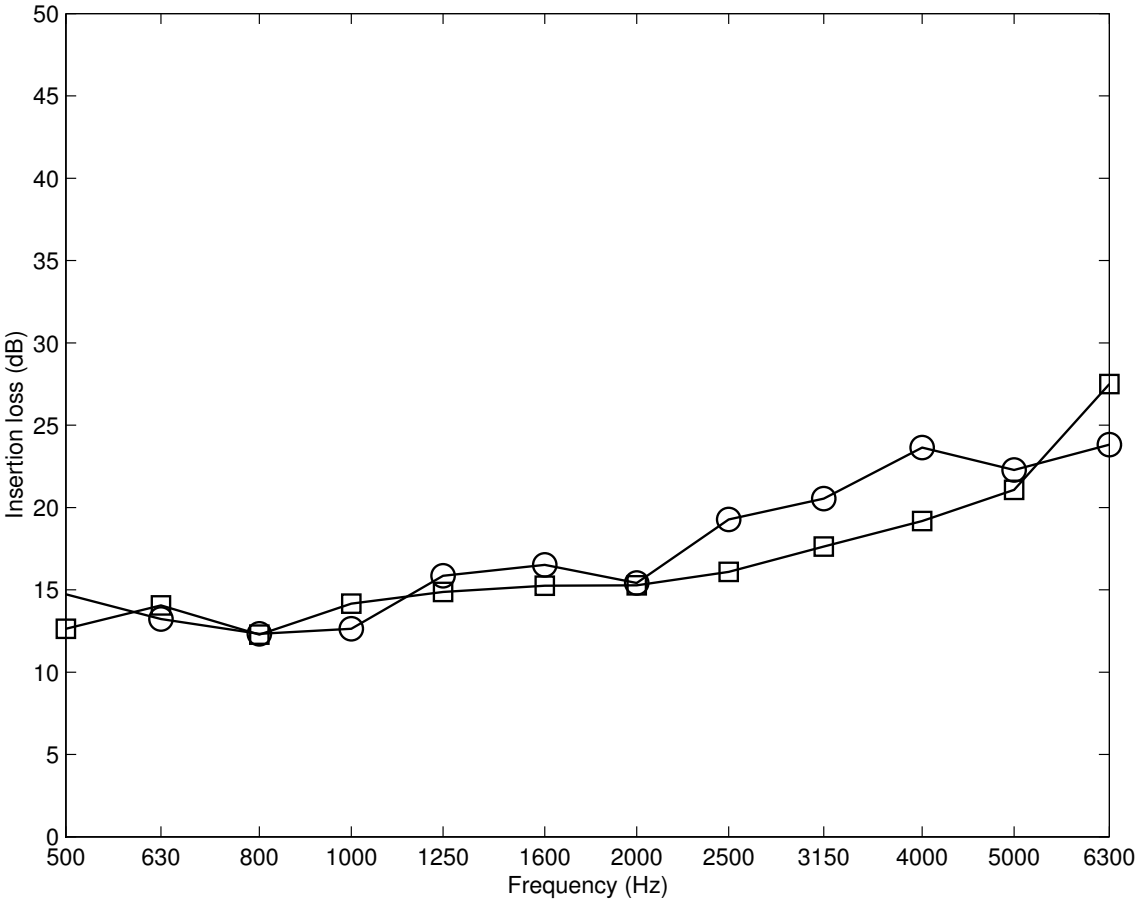

Figure 5.8. Space-averaged insertion loss over the receiver plane to the height of 30 cm (21 microphones):‘$\circ$’: Experimental result; ‘$\square$’: Numerical prediction.

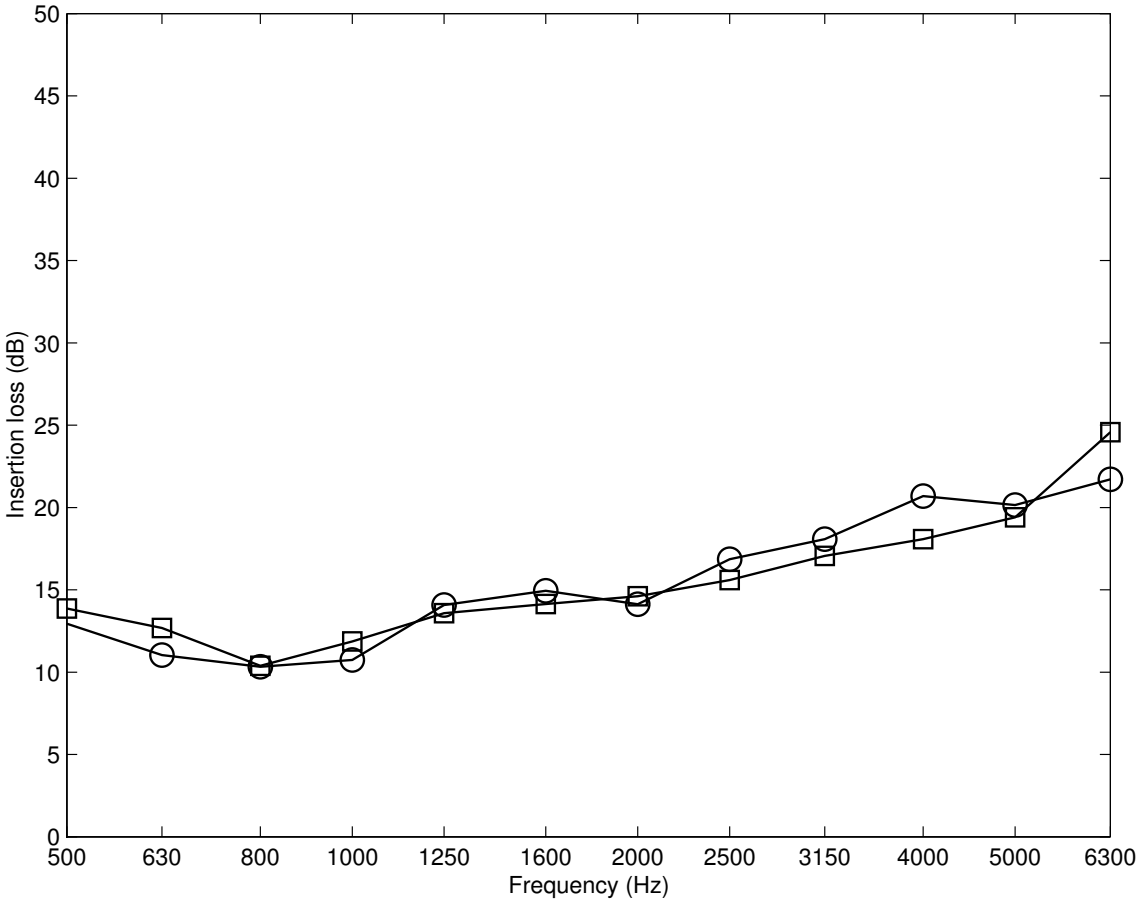

Figure 5.9. Space-averaged insertion loss over the receiver plane to the height of 60 cm (42 microphones):‘$\circ$’: Experimental result; ‘$\square$’: Numerical prediction.

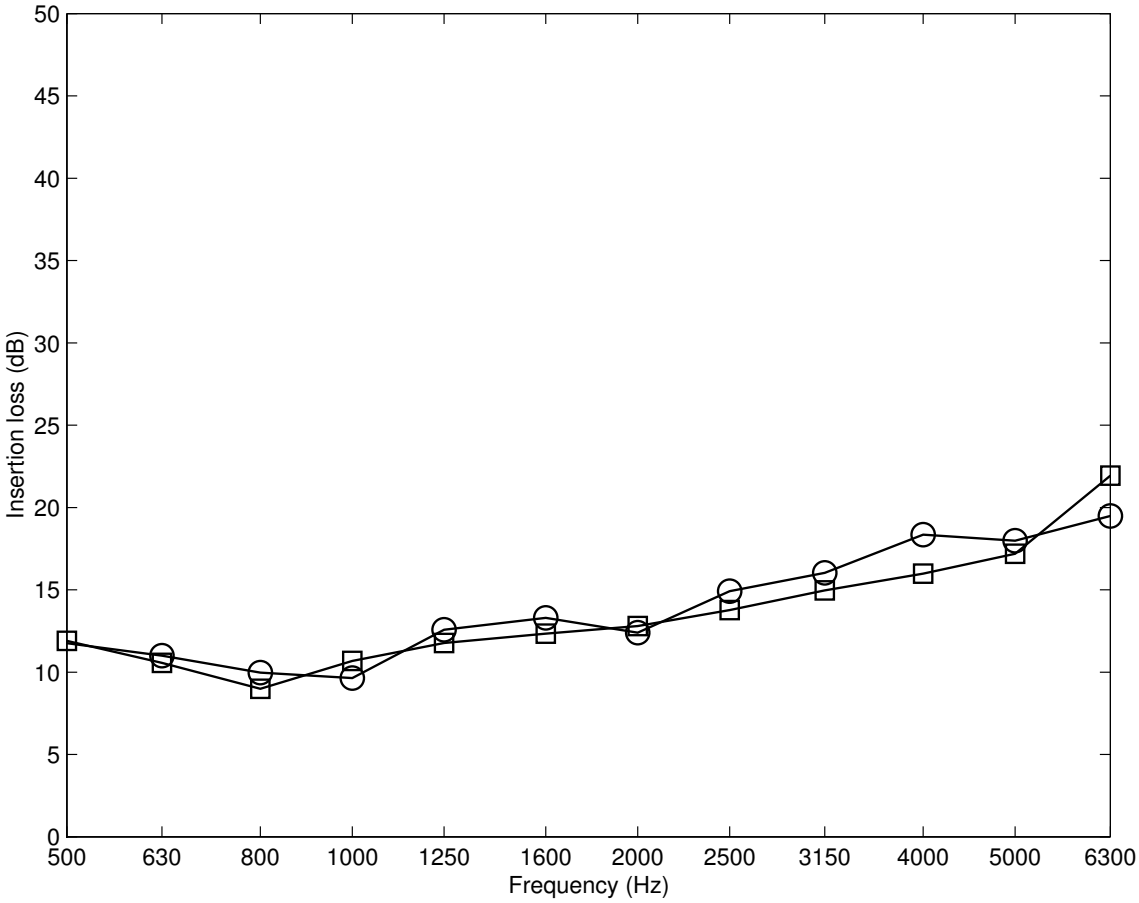

Figure 5.10. Space-averaged insertion loss over the receiver plane to the height of 90 cm (57 microphones):‘$\circ$’: Experimental result; ‘$\square$’: Numerical prediction.

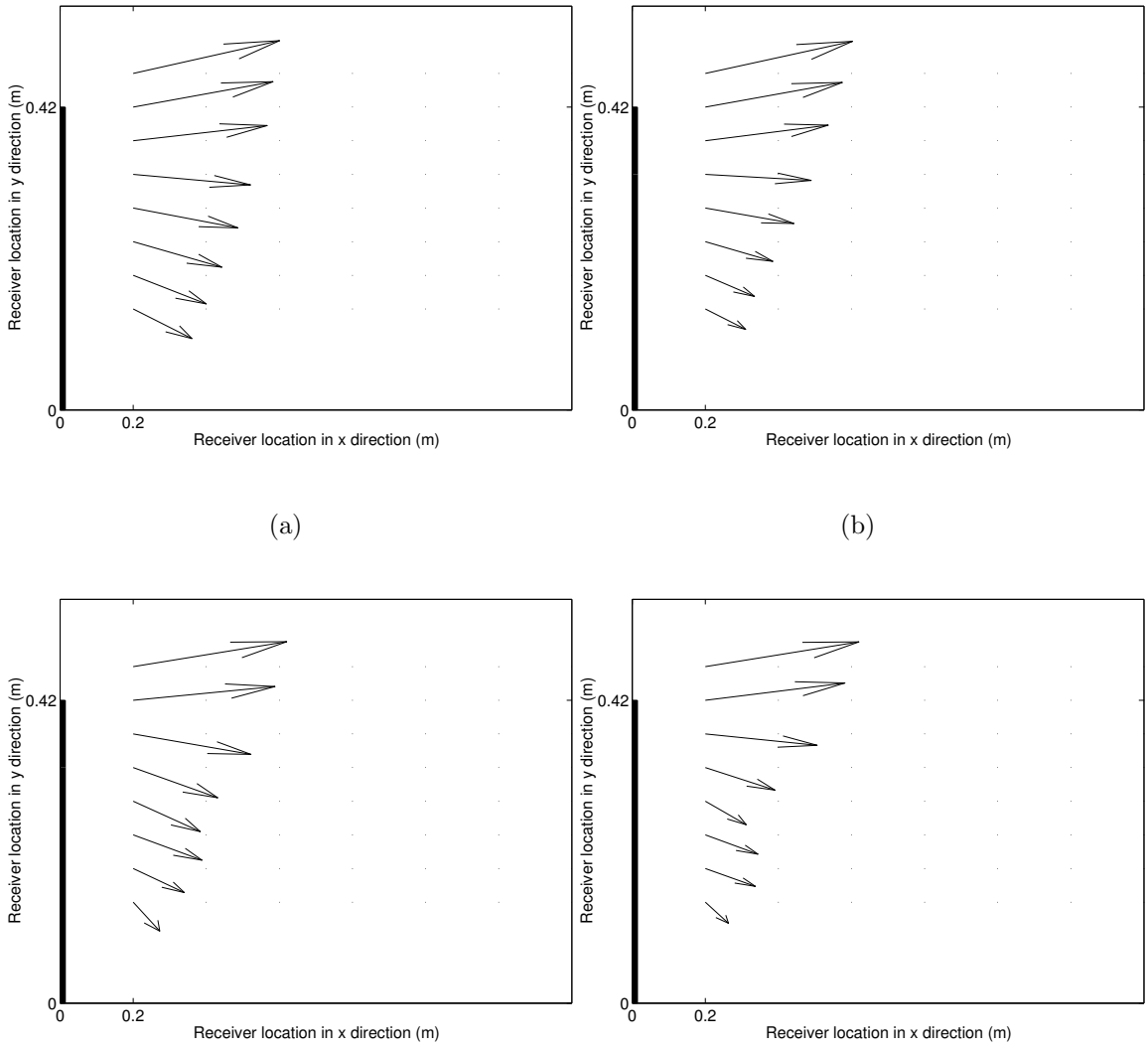

Figure 5.11. Distribution of mean intensity at 1000 Hz around the barrier extensions (vector scales $I^{1/2}$) (a) Rigid extension (Experiment), (b) Absorptive extension (Experiment), (c) Rigid extension (Numerical prediction), (d) Absorptive extension (Numerical prediction).

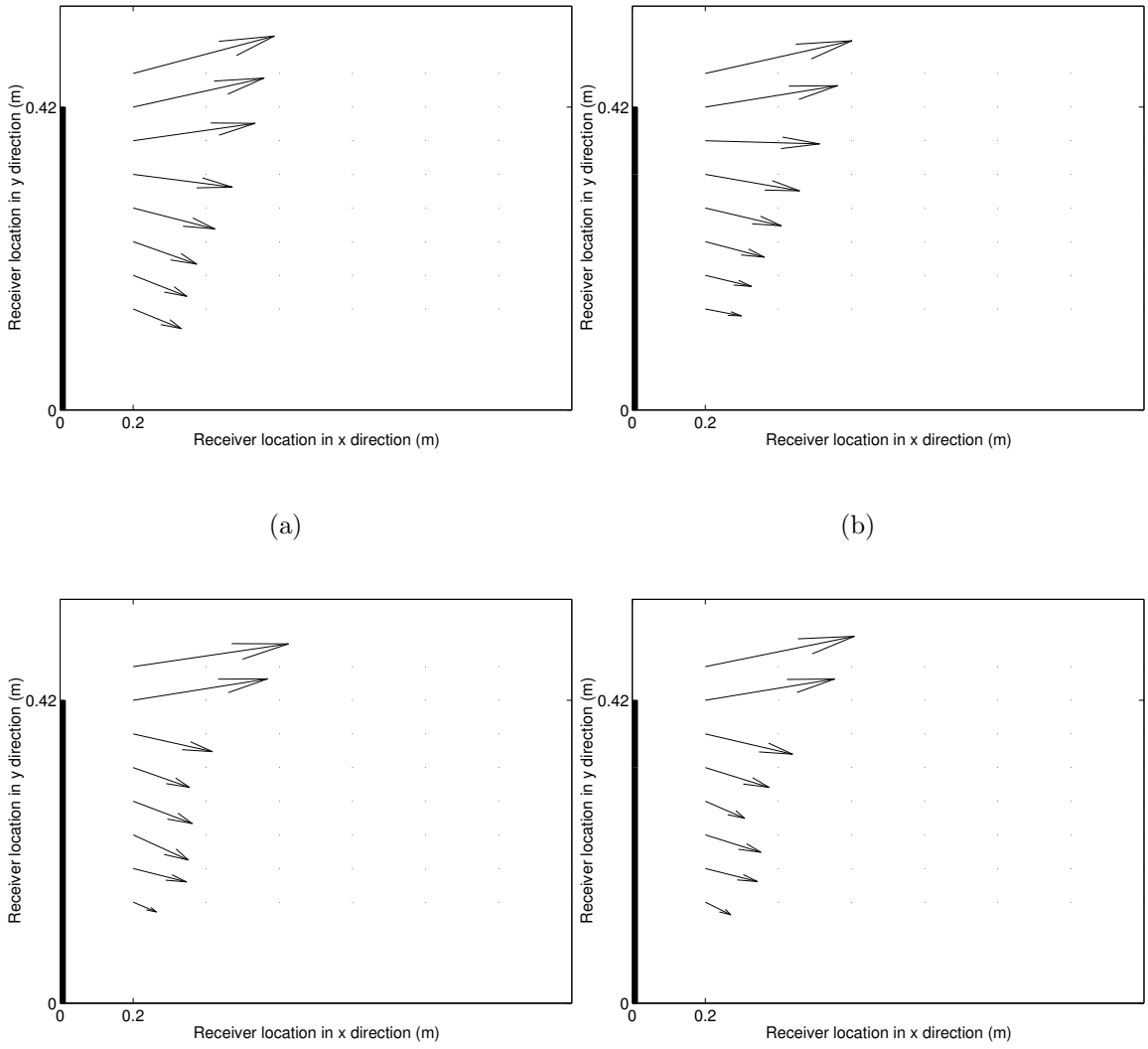

Figure 5.12. Distribution of mean intensity at 2000 Hz around the barrier extensions (vector scales $I^{1/2}$) (a) Rigid extension (Experiment), (b) Absorptive extension (Experiment), (c) Rigid extension (Numerical prediction), (d) Absorptive extension (Numerical prediction).

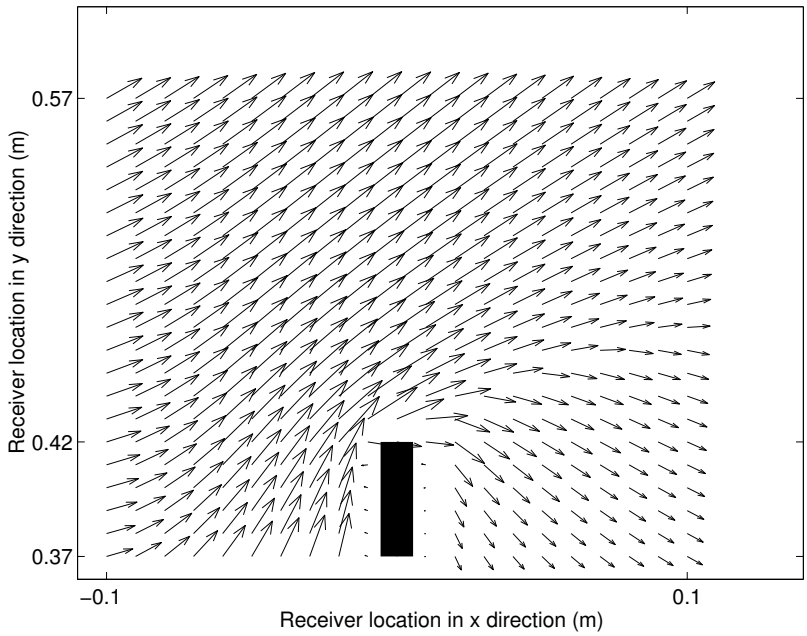

(a)

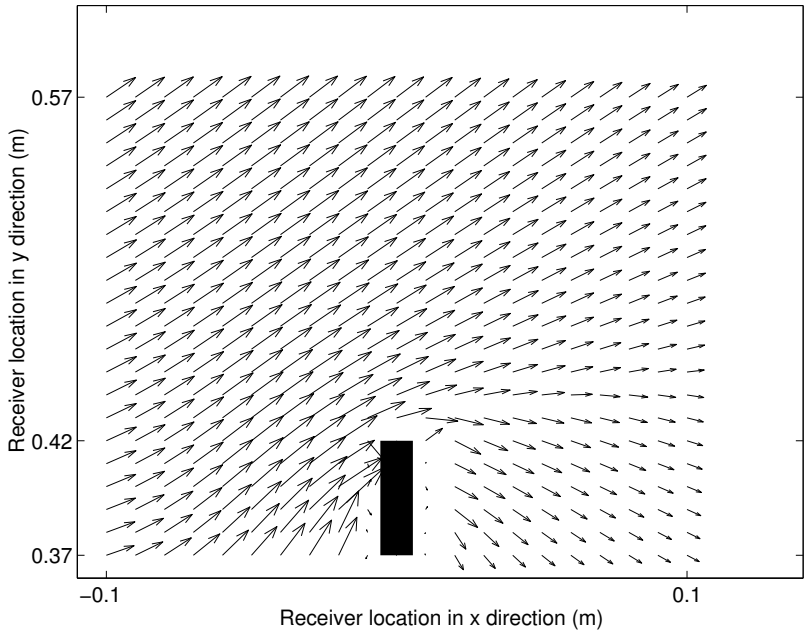

(b)

Figure 5.13. Distribution of mean intensity at 1000 Hz around the barrier extensions (vector scales $I^{1/2}$): (a) Rigid extension, (b) Sound absorptive extension.

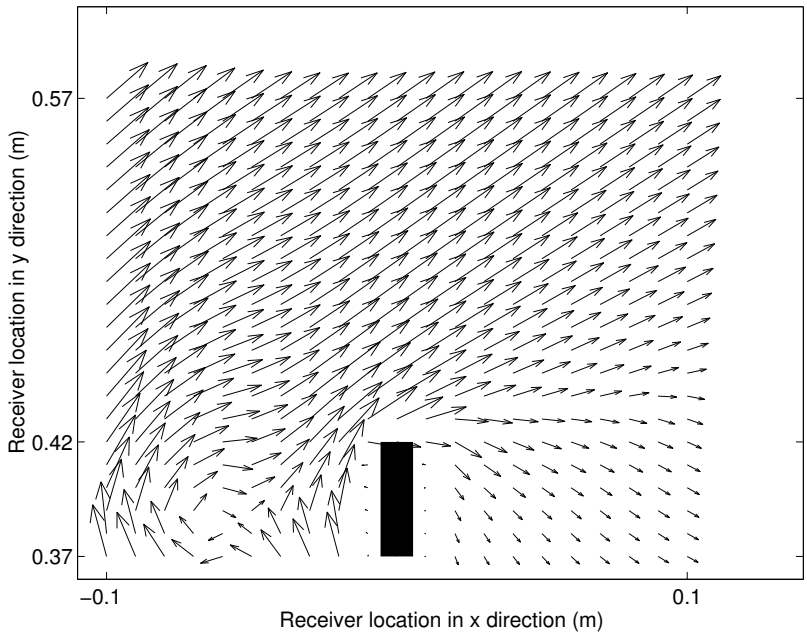

(a)

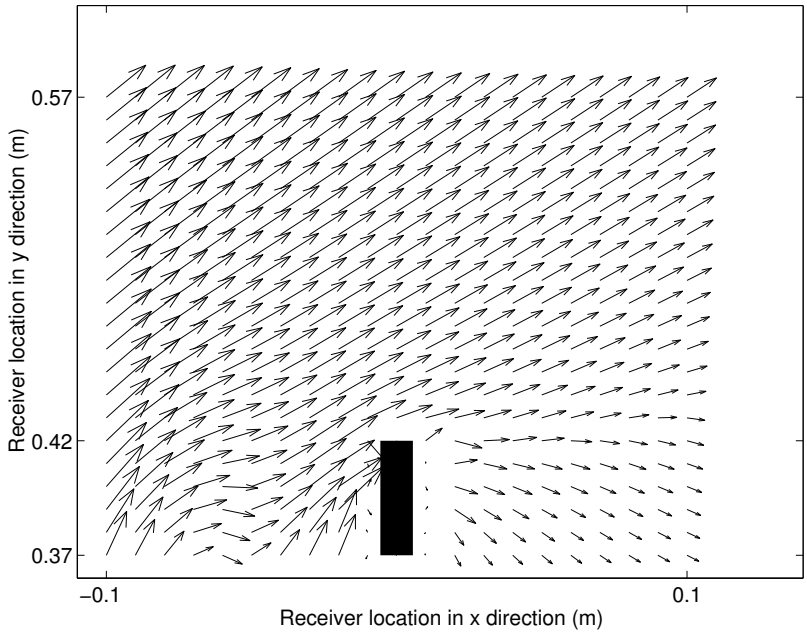

(b)

Figure 5.14. Distribution of mean intensity at 2000 Hz around the barrier extensions (vector scales $I^{1/2}$): (a) Rigid extension, (b) Sound absorptive extension.

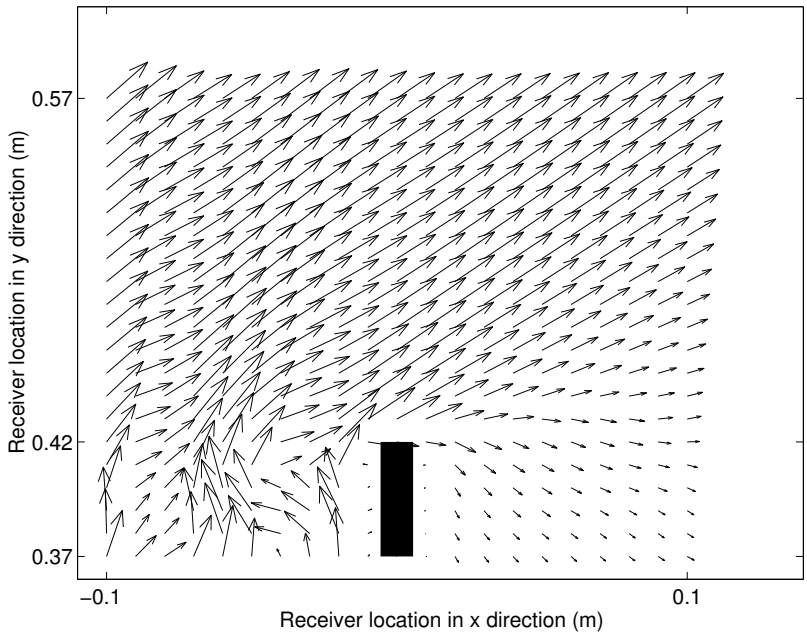

(a)

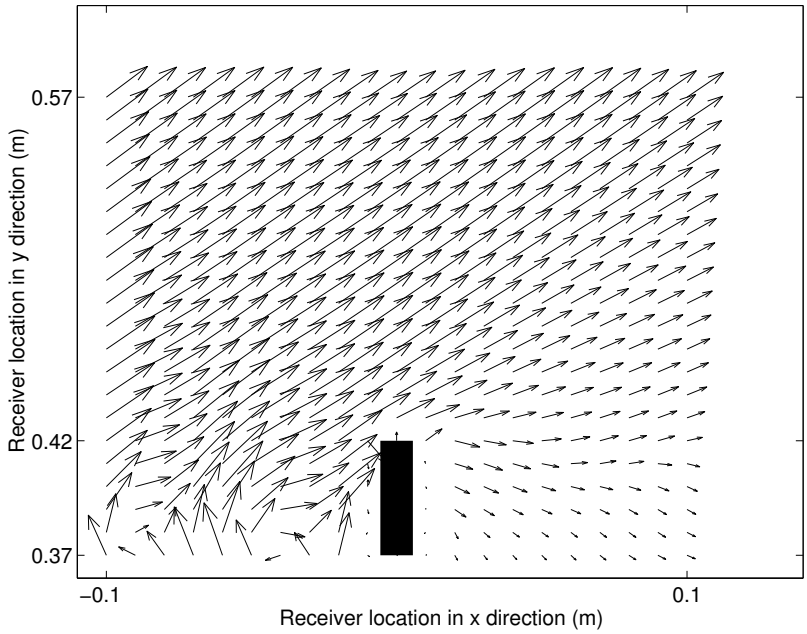

(b)

Figure 5.15. Distribution of mean intensity at 4000 Hz around the barrier extensions (vector scales $I^{1/2}$): (a) Rigid extension, (b) Sound absorptive extension.

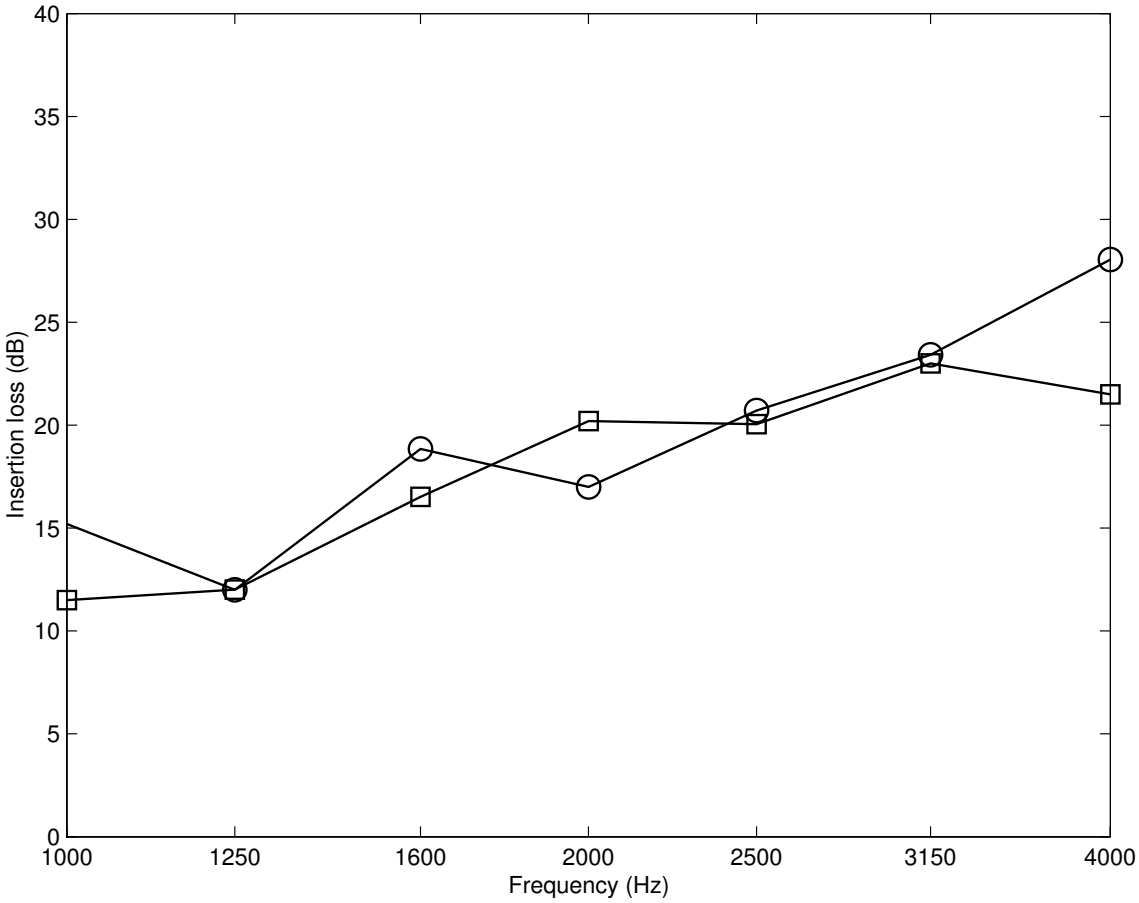

Figure 5.16. Space-averaged insertion loss over the receiver plane to the height of 30 cm (21 microphones):‘$\circ$’: Experimental result; ‘$\square$’: Numerical prediction.

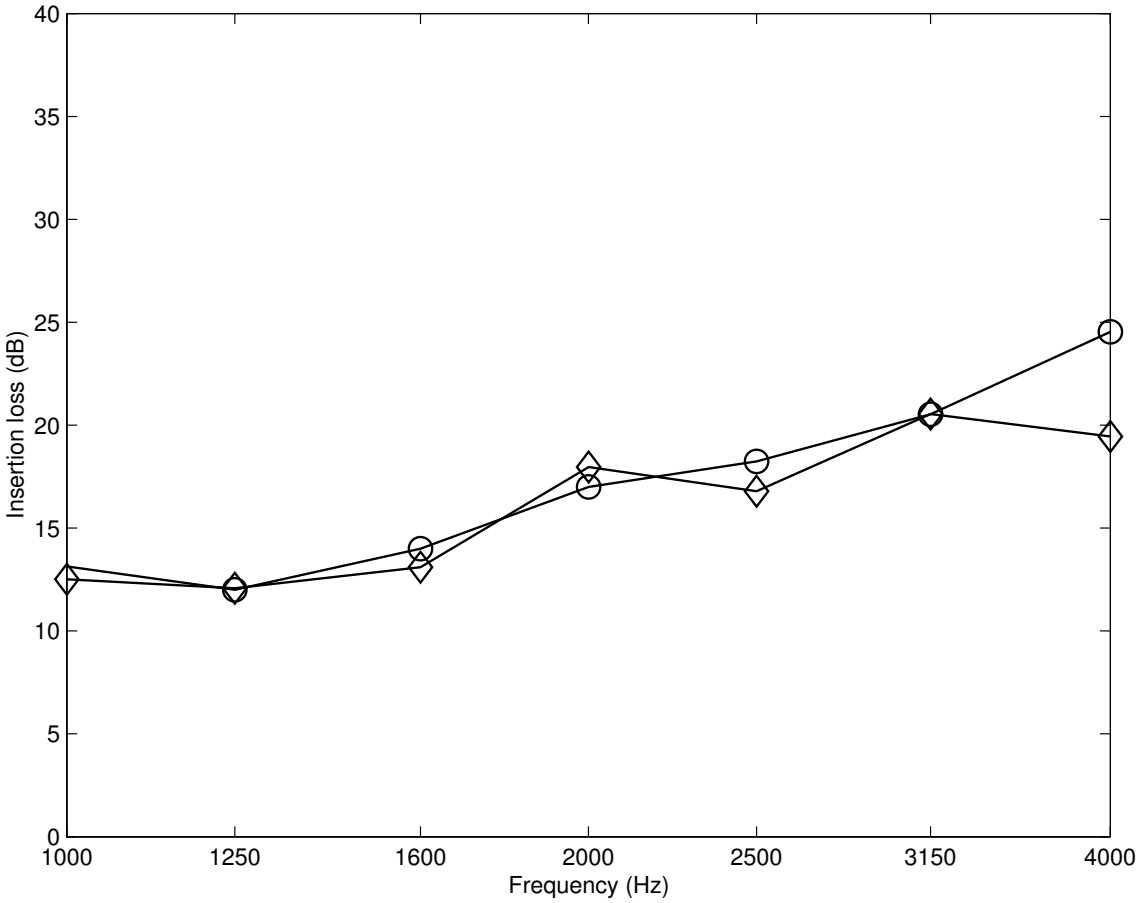

Figure 5.17. Space-averaged insertion loss over the receiver plane to the height of 60 cm (42 microphones):'$\circ$': Experimental result; '$\square$': Numerical prediction.

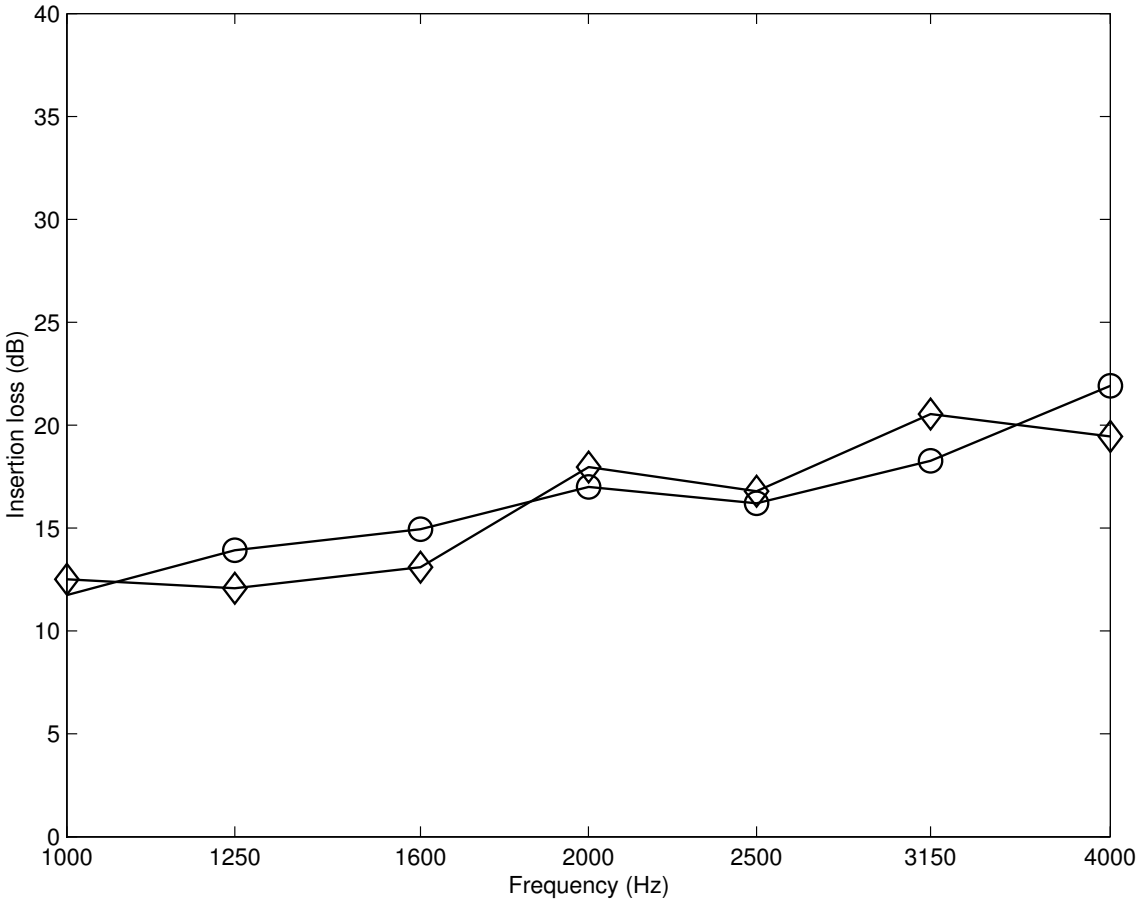

Figure 5.18. Space-averaged insertion loss over the receiver plane to the height of 90 cm (57 microphones):‘$\circ$’: Experimental result; ‘$\square$’: Numerical prediction.

6. FIELD MEASUREMENTS

Outdoor measurements were made along route US 20 in South Bend, Indiana on July 16, 2002. The goals of these preliminary measurements were: 1) to assess the performance of an existing barrier in the area, 2) to verify predictions from the Federal Highway Administration (FHWA) Traffic Noise Model (TNM), and 3) to select a suitable measurement location to evaluate the absorptive edge concept in the field.

6.1. Preliminary measurements

6.1.1. Measurement site selection

As suggested at the Study Advisory Committee meeting on June 3, 2002, the field measurements were planned along US 20 in South Bend, Indiana. The test site was visited on June 31, 2002 to survey the area and locate suitable measurement locations. Noise barriers are already installed along US 20 on both sides of the road. The existing barrier extends over a distance around 1.6 km. Figure 6.1 shows the area surrounding the section of US 20 where the noise barriers are installed. An apartment complex, the parking lot of a shopping mall, and a community park were identified as possible test sites. An additional 1.5 m high wooden barrier near to the apartment buildings would possibly have cause undesired reflections and thus this location was discarded. The ground surface of shopping mall was covered with asphalt, which might cause a large temperature gradient near the ground. It is well known that temperature gradients affects sound propagation. Generally, this phenomenon affects only sound propagation over distances of the order of 500 m. But sound propagation effects may occur for receivers at shorter distances when a very large temperature gradient is present. The outdoor measurements were planned to be carried on during the day

time in the summer. Thus the asphalt-covered measurement site was excluded. The community park featured a fairly large open space covered with grass. The roadside barrier height was 4.8 m above the highest point on the road. The ground level behind the barrier was approximately 3 m below the road level: see Figure 6.2. One possible problem was the presence of barrier gaps for emergency exits. But it was decided to perform the preliminary measurements at the community park, while making effort to minimize the influence from the gaps.

6.1.2. Field measurements

Four Brüel and Kjær 1.27 cm diameter microphones (types 4189 and 4190) were used for the measurements. Type 2639 and 2669 microphone preamplifiers were used with power supplies, type 5935. A sound level calibrator (type 4231) was used to calibrate the microphones before the measurement. A Brüel and Kjær Pulse data acquisition system connected to a Dell Inspiron 4000 laptop was utilized to perform one-third octave band measurements in real time. Measurements were made over one hour long time periods in the morning and afternoon of the same day. One microphone was located 1.5 m above the top of the barrier [26] to provide a reference sound pressure level. The other three microphones were located at 7.5 m, 15 m and 30 m [27] behind the barrier, at a height of 1.5 m above the local ground. A traffic classifier was installed on the roadway to measure traffic density and vehicle speed for different vehicle categories. A weather station from Davis Instruments was used to measure the atmospheric conditions.

The number of vehicles and their average speed for each category are shown in Table 6.1. Sound pressure levels measured at the reference microphone are shown in Figure 6.3 for one hour records. It can be seen that the shape of the frequency spectrum does not vary with the measurement time. This suggests that the average speed and percentage of the vehicle types are consistent, which can guarantee the repeatability of the field measurement. The sound pressure level difference between

reference and field microphone signals measured in the morning is shown in Figure 6.4. The sound pressure level difference is largest at location 3 between 2000 Hz and 6300 Hz. No significant differences can be observed at other frequencies. Figure 6.5 shows the same data measured in the afternoon of the same day. In this case, the sound pressure level difference is larger at locations 1 and 2 than that of location 3 at frequencies from 3150 Hz to 5000 Hz.

The atmospheric conditions are shown in Table 6.2. The direction of the barrier is North, this means that the wind was blowing from the barrier to the microphones.

6.1.3. Traffic noise model (TNM)

A detailed road map was acquired from the LaPorte district office to aid the design of the traffic noise model. The information about the height of the road relative to the ground, and the barrier geometry was obtained from the map and used to prepare TNM input file. The measured traffic data (see Table 6.1) was used to establish source strength. Table 6.3 shows the measured overall sound pressure levels, as well as corresponding TNM predictions. Note that one-third octave band results are not available from a TNM analysis. The relatively high sound pressure level at the reference microphone suggests that outdoor activity would be severely limited without the noise barriers in place. The sound pressure levels measured at the locations behind the barrier show that the barrier is fairly effective. Measured overall levels at the three microphones also show that there is less than a 1 dB difference in sound pressure level over these three locations. This suggests that all three measurement locations are fairly deep in the shadow zone of the barrier. The measured sound pressure levels at all points were well below the residential noise criterion of of 67 dBA.

It can be seen from Table 6.3 that TNM underestimates the reference sound pressure level by 0.4 dB for the record in the morning. At microphone location 2, located 7.5 m behind the barrier, TNM overestimates the level by 6.2 dB. Similarly,

the TNM calculation yielded 4.1 dB and 2.4 dB overestimates for the receivers 15 m and 30 m behind the barrier. For the afternoon period, the TNM prediction was 1.4 dB less than the measured sound pressure level at the reference location. The TNM predictions resulted in levels of 4.6 dB, 2.2 dB and 0.6 dB, respectively, in excess of the measured sound pressure levels for the receivers at 7.5 m, 15 m and 30 m. It should be noted that TNM predicts the same sound pressure level at the reference microphone for morning and afternoon periods, and only a 0.1 dB difference between levels at the three microphone locations. Table 6.1 shows that the total number of vehicles during measurement periods increased from 818 and 806 in the morning to 912 and 1028 in the afternoon, for eastbound and westbound traffic, respectively. But the percentage of heavy trucks decreased from 18 % and 15 % for eastbound to 20 % and 14 % for westbound traffic. It is believed that increased total number of vehicles was compensated by a lower percentage of heavy trucks in the afternoon.

Note that the wind direction was mostly from the receivers towards the wall during the measurement period in the morning, as shown in Table 6.2. This may have caused a slightly lower level than would have been measured under neutral atmospheric conditions. In the afternoon, the situation was reversed; the wind blew from the barrier to the receivers. The average wind speed was 0.5 m/s for both the morning and afternoon measurements in the direction normal to the barrier. Watts and Morgan [28] observed that noise levels may vary approximately 1 dB per 1 m/s of the normal component of the wind vector. The presence of wind might explain the higher measured sound pressures in the afternoon. The proximity of the measurement site to sources of community noise (i.e., a local road and children playing nearby) may also have been responsible for the discrepancies between predictions and measured data.

6.2. Measurements for TNM study

A different measurement location was investigated, further away from the sources of community noise in the same park. Measurements at the new location were made on August 30 and 31, 2002. The traffic data from these measurements is shown in Table 6.4. Measured traffic data show that there was more traffic later in the afternoon. The measurements made on August 30 include one reference microphone and one additional microphone located behind the barrier at one of three positions. The atmospheric conditions for the measurement period are shown in Table 6.5. A-weighted overall sound pressure levels are shown in Table 6.6. The TNM predictions of the reference sound pressure levels for August 30 are underestimated by 1.7, 1.4 and 1 dB for the 1 p.m., 2 p.m. and 3 p.m. records, respectively. The predictions at the three microphone locations for August 30 are overestimated by 0.5, 0.9 and 0.7 dB.

Another measurement was made at the same location on August 31. Note that three microphones were used at three different locations simultaneously. The traffic data for this measurement period can be found in Table 6.7. Note that the number of mid-sized and heavy trucks was reduced significantly, for example, compared to the 2 p.m. to 3 p.m. measurement on August 30 in Table 6.4, the number of mid-sized truck was reduced from 68 to 16 from the 1 p.m. to 2 p.m. measurement on August 31 in the eastbound traffic. The number of heavy trucks was also reduced from 118 to 44 for the same measurement duration times on the two dates. The atmospheric conditions for the measurement periods are shown in 6.8. TNM underestimates the reference sound pressure level by 2.5 dB for the 1 p.m. measurement on August 31 as shown in Table 6.9. Compared to the measurement on July 16 and July 30, the overestimation of TNM on the reference microphone was larger. The smaller amount of traffic may have caused this discrepancy. It should be noted that at the reference microphone all TNM predictions for 7 hour measurements on three different dates resulted in underestimates. Sound pressure levels are underestimated at microphones 2 and 4 by 0.7 and 0.8 dB and overestimated at microphone 3 by 0.6 dB for the 1 p.m.

measurement. TNM underestimated the sound pressure level at all three microphones for the measurement at 2 p.m.

6.3. Measurements with sound absorbing treatment

6.3.1. Experimental procedures

The barrier at the test site was not continuous, but was broken open for access purposes as shown in Figure 6.6. The two sections of the broken barriers overlapped, forming a narrow corridor parallel to the roadway. One vertical barrier edge at the opening was treated with sound absorptive material (Dow chemical QUASH: see Figure 6.7). Measurements were made on October 15, 2002 to verify the effects of the absorptive treatment. The shape of the treatment adopted was based on the findings from the scale model tests described in section 4.4. Figure 6.8 shows the completed installation on the vertical edge of one of two walls at the measurement site as shown. The installation height was 6.4 m along the vertical edge of the barrier.

Sound diffraction around a vertical edge was assumed to be generally analogous to diffraction around the top of the barrier, although ground effects and the presence of the corridor may have caused unusual sound propagation phenomena in this particular case. An effort was made to estimate the contribution from the top and the vertical edge of the barrier with a diffraction based model. The calculation was made with several point sources at various locations on the road first. The contribution of each point source to the receiver was calculated for each source location. It was concluded that one point source can simulate the effect of multiple point sources when the point source is located near the barrier section of interest. The receiver locations were chosen after comparing the contributions of the point source along two diffraction paths: over the barrier top and around the vertical edge of the barrier. Receiver locations in areas where there is little influence from diffraction over the top should allow the evaluation of the effectiveness of the vertical edge treatment. The reference

microphone was at the same position as before; microphones 1, 2 and 3 were located 7.5 m behind the barrier gap, 2.5 m apart from each other in order to ensure that the dominant component of the diffracted sound field was that from the vertical edge, relative to the possible contribution from the top of the barrier. The diffraction based model predicted an insertion loss of 46 dB, 45 dB and 43 dB for the barrier top at the three measurement locations. The diffraction around the vertical edge would cause 30 dB, 32 dB and 32 dB insertion losses at the same locations. The differences in insertion loss from two diffraction paths were larger than 10 dB at the three receivers.

6.3.2. Results

The sound pressure level at the reference microphone is shown in Figure 6.9. A 2 dB difference can be seen at all frequencies before and after the installation. Note that the traffic data was not collected for this measurement. The differences between sound pressure levels at the reference microphone and at each microphone location were used for the comparisons.

A comparison between the sound pressure level at reference microphone and at microphone 1 is shown in one-third octave bands in Figure 6.10. The sound absorptive treatment resulted in up to a 5 dB increase in sound pressure level difference at this receiver location. The same trend can be seen in Figure 6.11. The edge treatment yields an improvement over the existing barrier between 500 Hz and 6300 Hz. The improvement was insignificant between 500 Hz and 1600 Hz, as was also observed in the scale model experiments. The material used for the treatment was not expected to yield any benefit at low frequency. As shown in Figure 6.12, the largest sound pressure level difference was recorded at receiver 3, which was the deepest in the shadow zone among the three measurement locations.

A slightly larger sound pressure level difference was measured at microphone 3 (5 m to the right of microphone 1 which was placed behind the barrier vertical edge) as shown in Figure 6.13. This shows that the sound absorptive treatment was more

effective for receivers deeper in the shadow region, which also corroborated the scale-model results. Note that the frequency range over which the edge treatment is effective relies on the frequency dependent sound absorptive properties of the material.

Table 6.1. Measured traffic data on US 20 on July 16, 2002 (Δ_d=1 hour).

	11 a.m. - 12 p.m.	2 p.m. - 3 p.m.
Eastbound		
Number of cars	608	709
Average speed	99.3 kmph	99.0 kmph
Number of mid-sized trucks	62	70
Average speed	94.1 kmph	94.3 kmph
Number of heavy trucks	148	133
Average speed	95.8 kmph	96.6 kmph
Westbound		
Number of cars	590	815
Average speed	102.4 kmph	101.5 kmph
Number of mid-sized trucks	57	68
Average speed	97.7 kmph	98.5 kmph
Number of heavy trucks	159	145
Average speed	99.3 kmph	98.5 kmph

Table 6.2. Atmospheric conditions during the measurement on July 16, 2002.

Time	Wind(m/s)	Temp(° F)	Direction
11:00	0.9	88	S
11:10	0	89	SW
11:20	1.3	88	SW
11:30	1.8	91	S
11:40	2.2	90	S
11:50	0.2	91	SW
11:00	0.4	92	N
2:00	1.3	90	SW
2:10	1.3	92	NW
2:20	0.9	92	NW
2:30	0	90	N. A.
2:40	1.3	89	NW
2:50	0.9	90	NW
3:00	1.3	91	NW

Table 6.3. A-weighted overall sound pressure levels at four locations on July 16, 2002 (Δ_d=1 hour).

	11 a.m. - 12 p.m.		2 p.m. - 3 p.m.	
	Measurement	TNM	Measurement	TNM
Reference microphone	82.5	82.1	83.5	82.1
Microphone 1	55.0	61.2	56.8	61.2
Microphone 2	55.3	59.4	57.1	59.3
Microphone 3	55.8	58.2	57.5	58.1

Table 6.4. Measured traffic data on US 20 on August 30, 2002 (Δ_d=1 hour).

	2 p.m. - 3 p.m.	3 p.m. - 4 p.m.	4 p.m. - 5 p.m.
Eastbound			
Number of cars	796	941	1158
Average speed	96.9 kmph	96.9 kmph	97.2 kmph
Number of mid-sized trucks	68	75	56
Average speed	91.7 kmph	92.9 kmph	93.7 kmph
Number of heavy trucks	118	119	96
Average speed	93.2 kmph	93.7 kmph	92.1 kmph
Westbound			
Number of cars	891	1136	1389
Average speed	99.6 kmph	100.6 kmph	100.7 kmph
Number of mid-sized trucks	74	78	77
Average speed	95.8 kmph	95.6 kmph	97.2 kmph
Number of heavy trucks	148	157	145
Average speed	95.1 kmph	94.5 kmph	96.6 kmph

Table 6.5. Atmospheric conditions during the measurements on August 30, 2002.

Time	Wind(m/s)	Temp(° F)	Direction
14:00	0.9	95	E
14:10	0.4	98	E
14:20	0.9	90	E
14:30	0.9	91	E
14:40	0.9	91	E
14:50	0.9	92	E
15:00	1.3	90	E
15:10	1.3	91	E
15:20	0.9	93	E
15:30	0	92	E
15:40	1.3	91	E
15:50	0.9	90	E
16:00	1.3	89	E
16:10	1.3	89	E
16:20	0.9	89	E
16:30	0	88	E
16:40	1.3	89	E
16:50	0.9	88	E

Table 6.6. A-weighted overall sound pressure level at four locations on August 30, 2002 (Δ_d=1 hour).

	2 - 3 p.m.		3 - 4 p.m.		4 - 5 p.m.	
	Meas.	TNM	Meas.	TNM	Meas.	TNM
Reference microphone	79.9	78.2	80.0	78.6	79.7	78.7
Microphone 1	58.2	58.7				
Microphone 2			58.0	58.9		
Microphone 3					57.8	58.5

Table 6.7. Measured traffic data on US 20 on August 31, 2002 (Δ_d=1 hour).

	1 p.m. - 2 p.m.	2 p.m. - 3 p.m.
Eastbound		
Number of cars	789	780
Average speed	95.6 kmph	95.6 kmph
Number of mid-sized trucks	16	17
Average speed	88.8 kmph	90.0 kmph
Number of heavy trucks	44	28
Average speed	95.0 kmph	90.3 kmph
Westbound		
Number of cars	944	899
Average speed	99.6 kmph	99.8 kmph
Number of mid-sized trucks	30	17
Average speed	95.3 kmph	98.0 kmph
Number of heavy trucks	57	47
Average speed	90.0 kmph	96.6 kmph

Table 6.8. Atmospheric conditions during the measurements on August 31, 2002 (Δ_d=1 hour).

Time	Wind(m/s)	Temp(° F)	Direction
13:00	0.89	90	E
13:10	1.33	91	E
13:20	1.33	89	E
13:30	0.44	91	E
13:40	0.44	88	E
13:50	0.89	92	E
14:00	0	94	N.A.
14:10	0	93	N.A.
14:20	0.44	92	E
14:30	0	93	N.A.
14:40	1.78	89	E
14:50	1.33	89	E

Table 6.9. A-weighted overall sound pressure levels at four locations on August 31, 2002 (Δ_d=1 hour).

	1 p.m. - 2 p.m.		2 p.m. - 3 p.m.	
	Measurement	TNM	Measurement	TNM
Reference microphone	78.3	75.8	78.8	75.3
Microphone 1	56.6	55.9	57.7	55.2
Microphone 2	55.1	55.7	56.7	55.0
Microphone 3	56.3	55.5	57.8	54.8

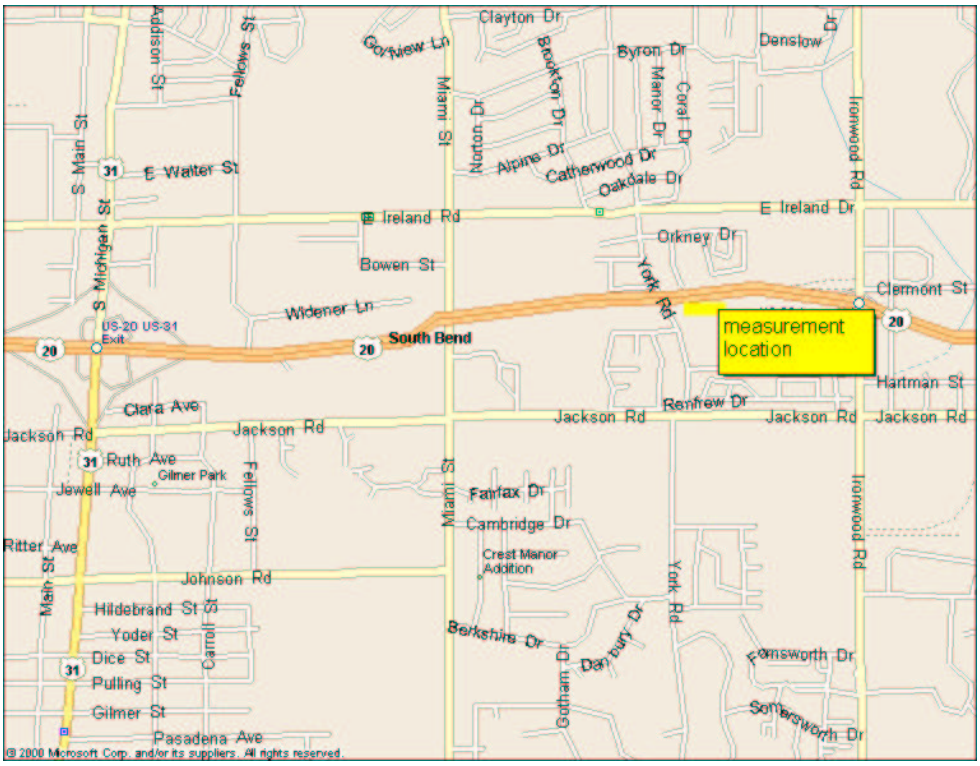

Figure 6.1. Map of the measurement location in South Bend, Indiana.

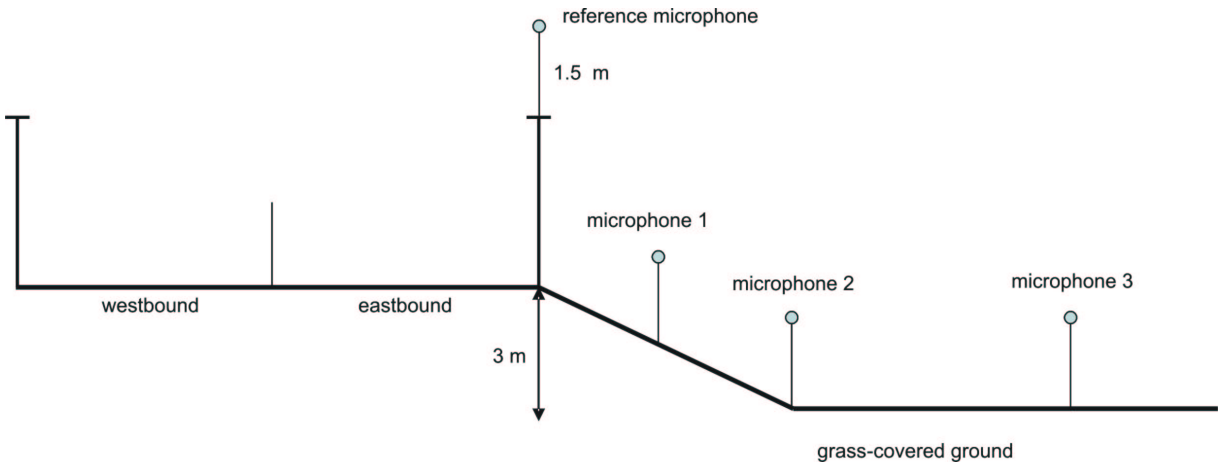

Figure 6.2. Cross-sectional view of the measurement location.

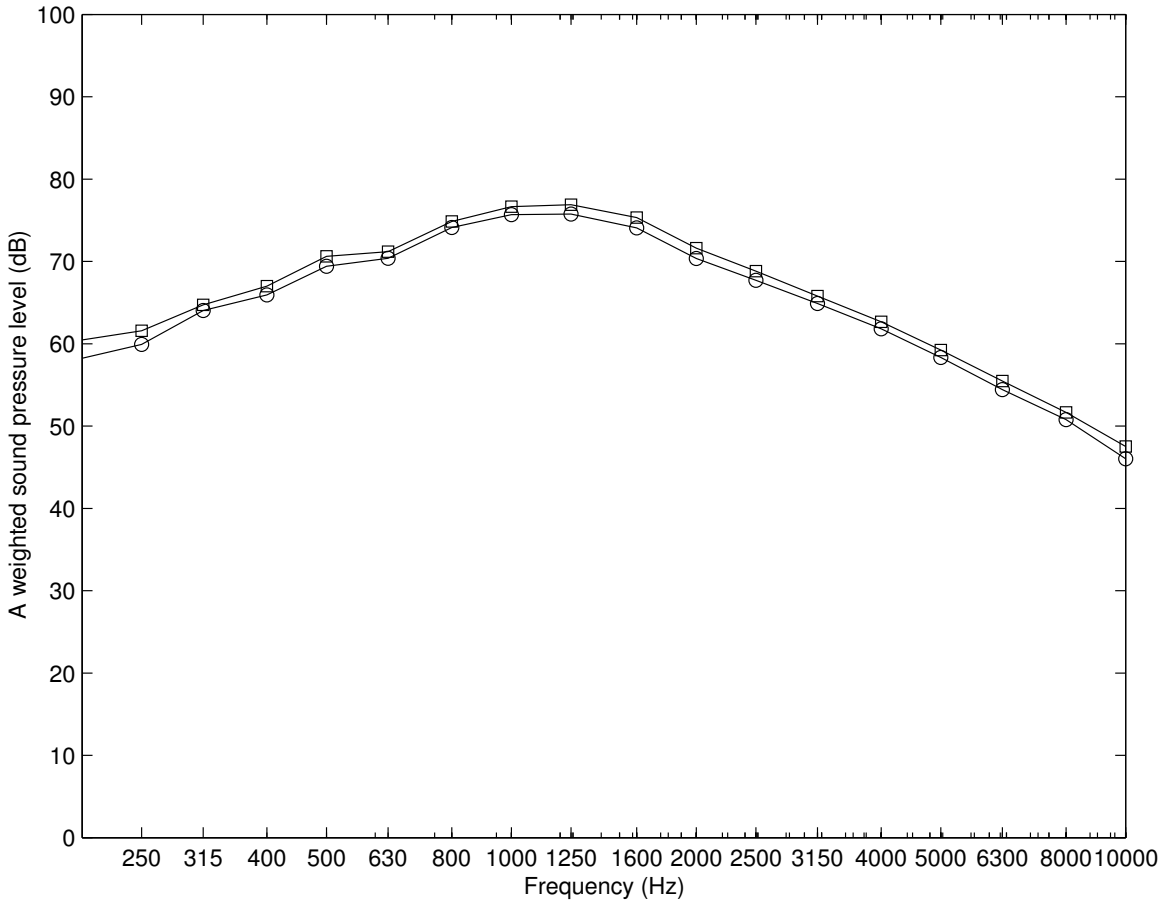

Figure 6.3. Sound pressure level vs. frequency; reference microphone on July 16. '○': in the morning; '□': in the afternoon.

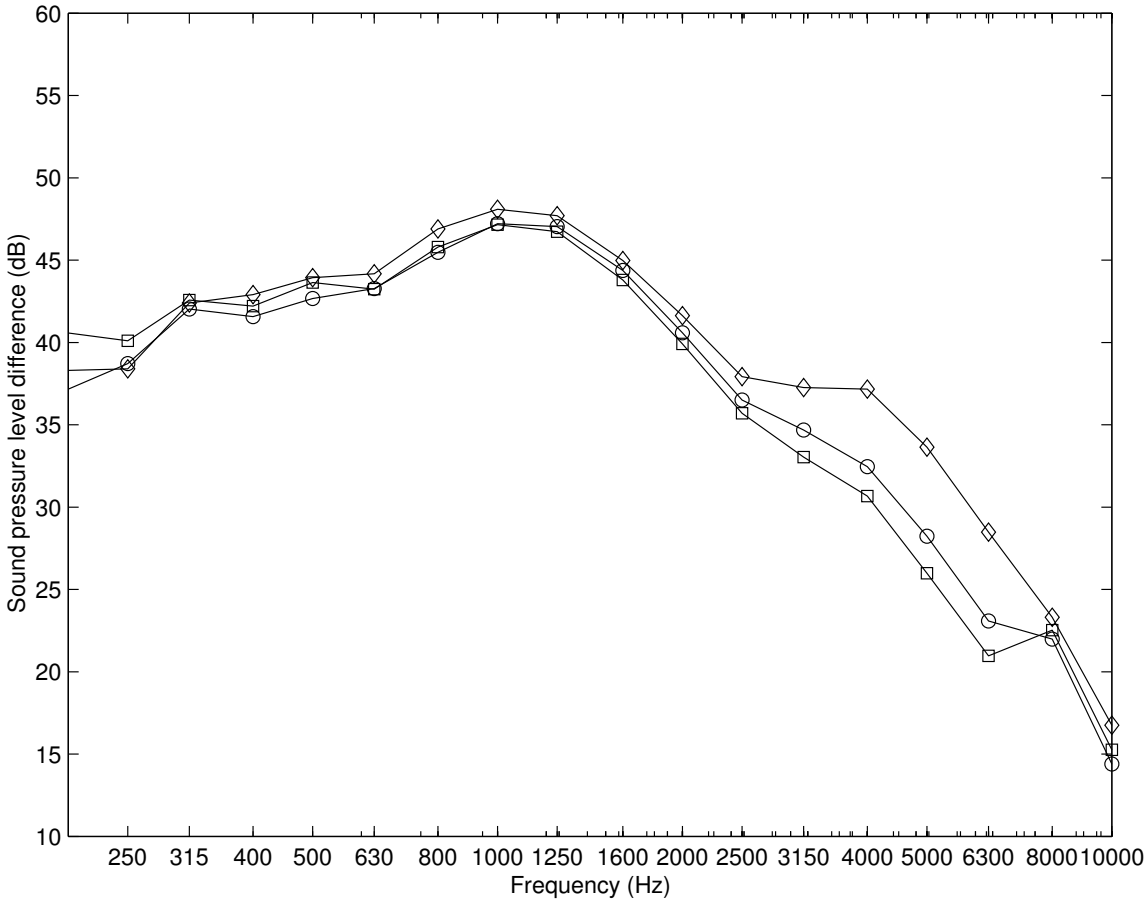

Figure 6.4. Difference between the sound pressure levels at the reference and the field locations. Morning on July 16. '○': microphone 1; '□': microphone 2; '◇': microphone 3.

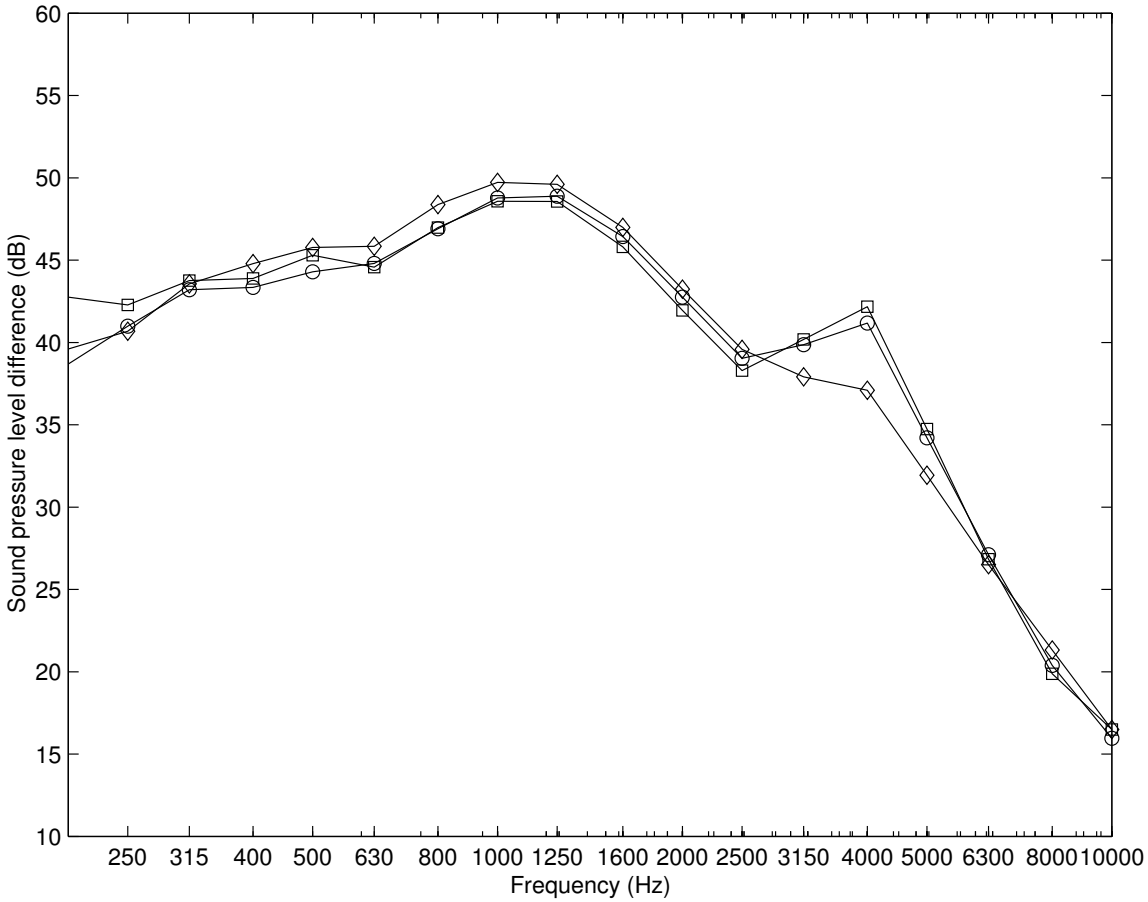

Figure 6.5. Difference between the sound pressure levels at the reference and the field locations. Afternoon on July 16. '$\circ$': microphone 1; '$\square$': microphone 2; '$\diamond$': microphone 3.

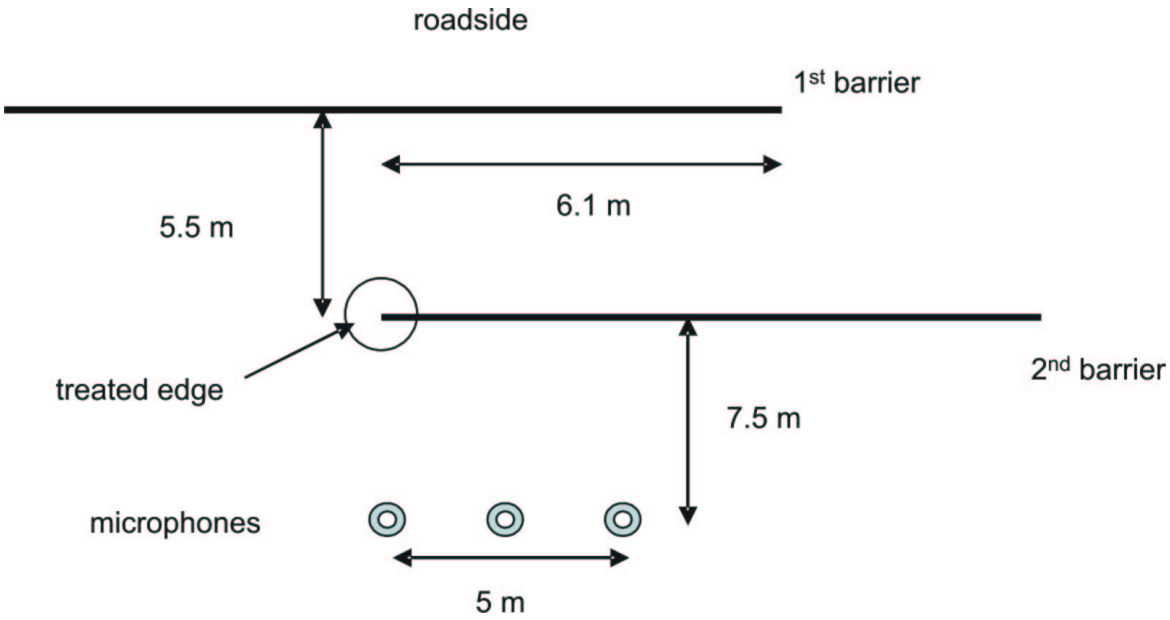

Figure 6.6. Top view of the measurement locations.

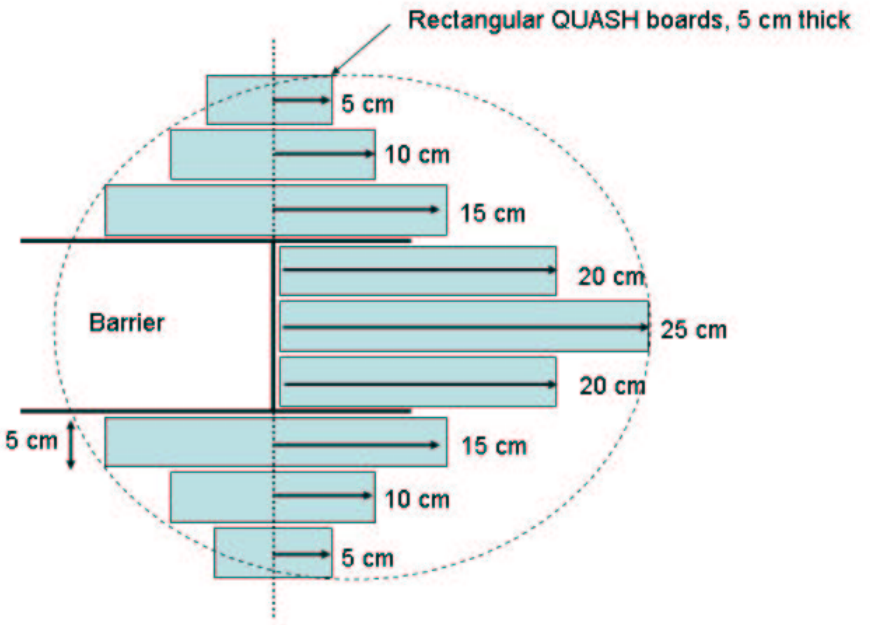

Figure 6.7. Cross section of the QUASH on the vertical edge of the barrier.

Figure 6.8. Installation of the absorptive QUASH treatment on the vertical edge of the barrier.

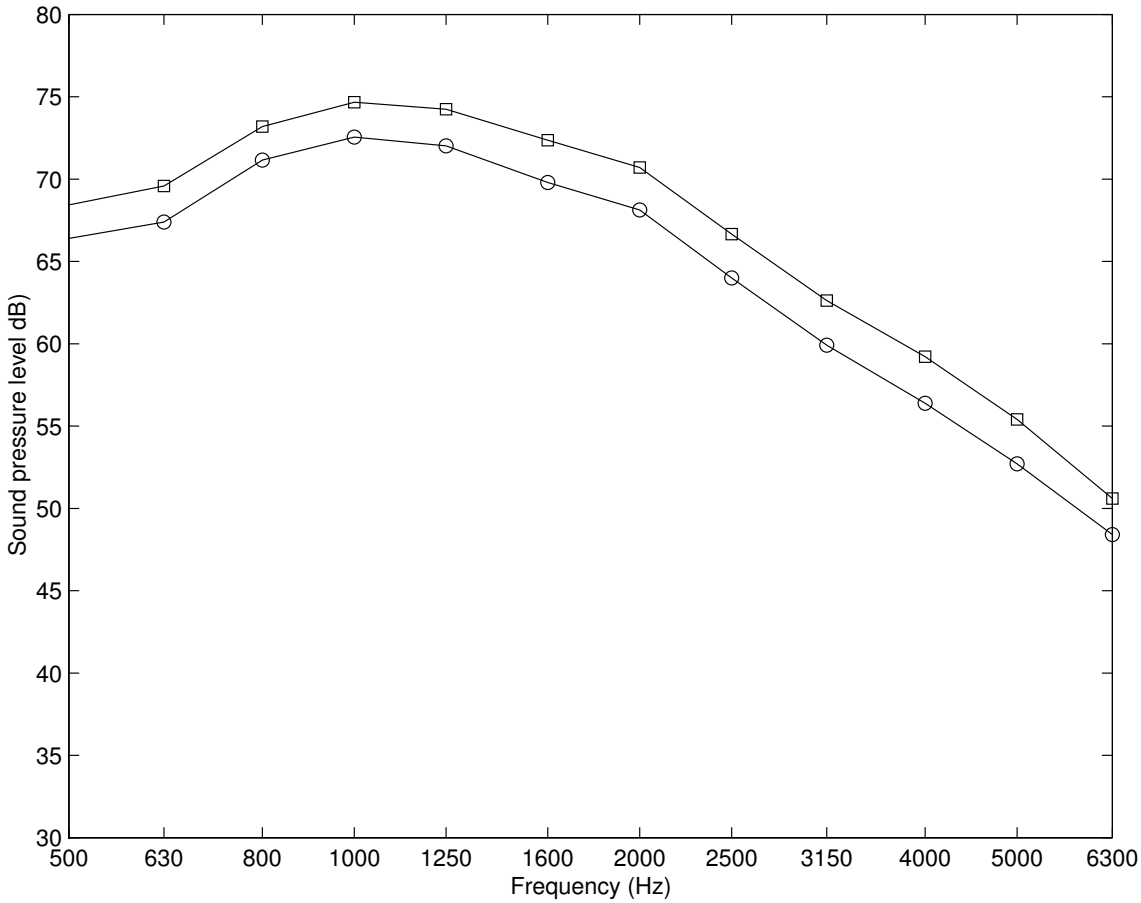

Figure 6.9. Sound pressure level vs. frequency at the reference microphone on October 15. '○': with absorptive treatment; '□': without absorptive treatment.

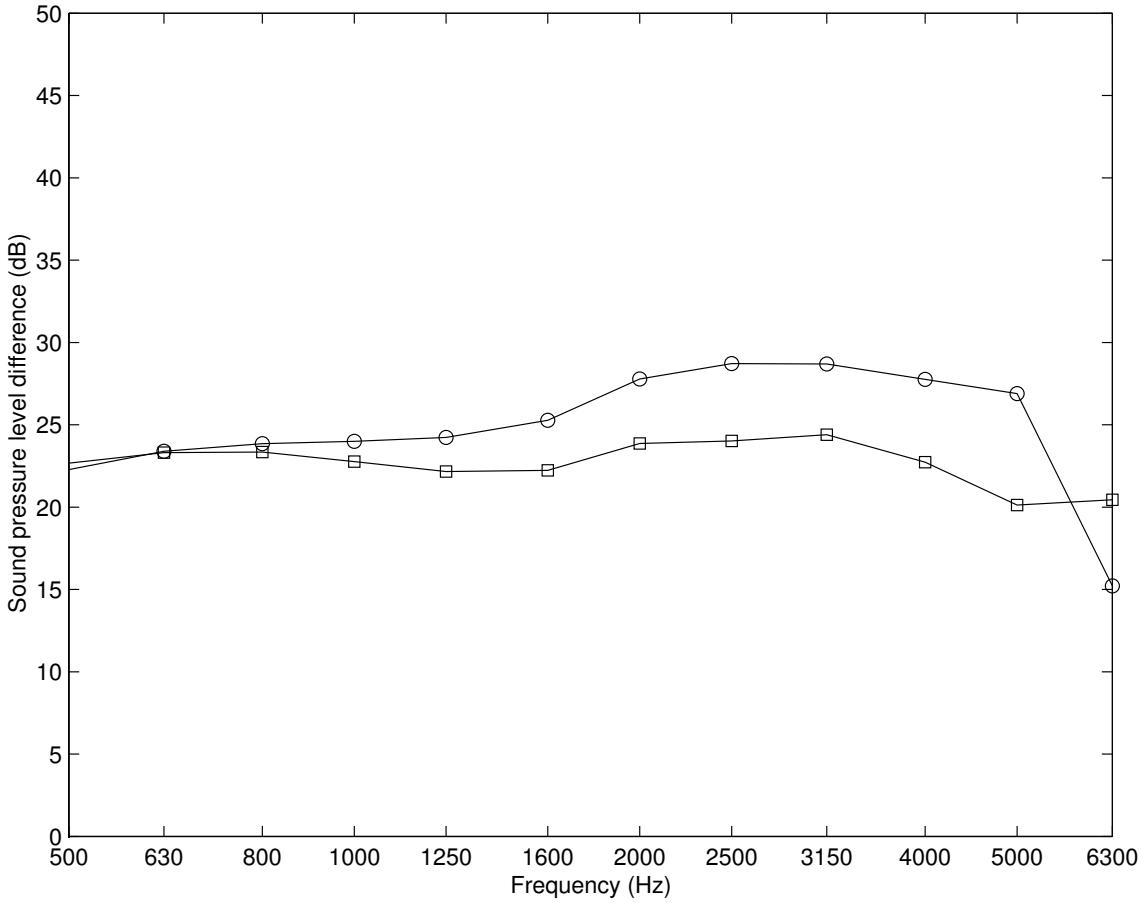

Figure 6.10. Difference between the sound pressure levels at the reference and the microphone 1 on October 15. '$\circ$': with absorptive treatment; '$\square$': without absorptive treatment.

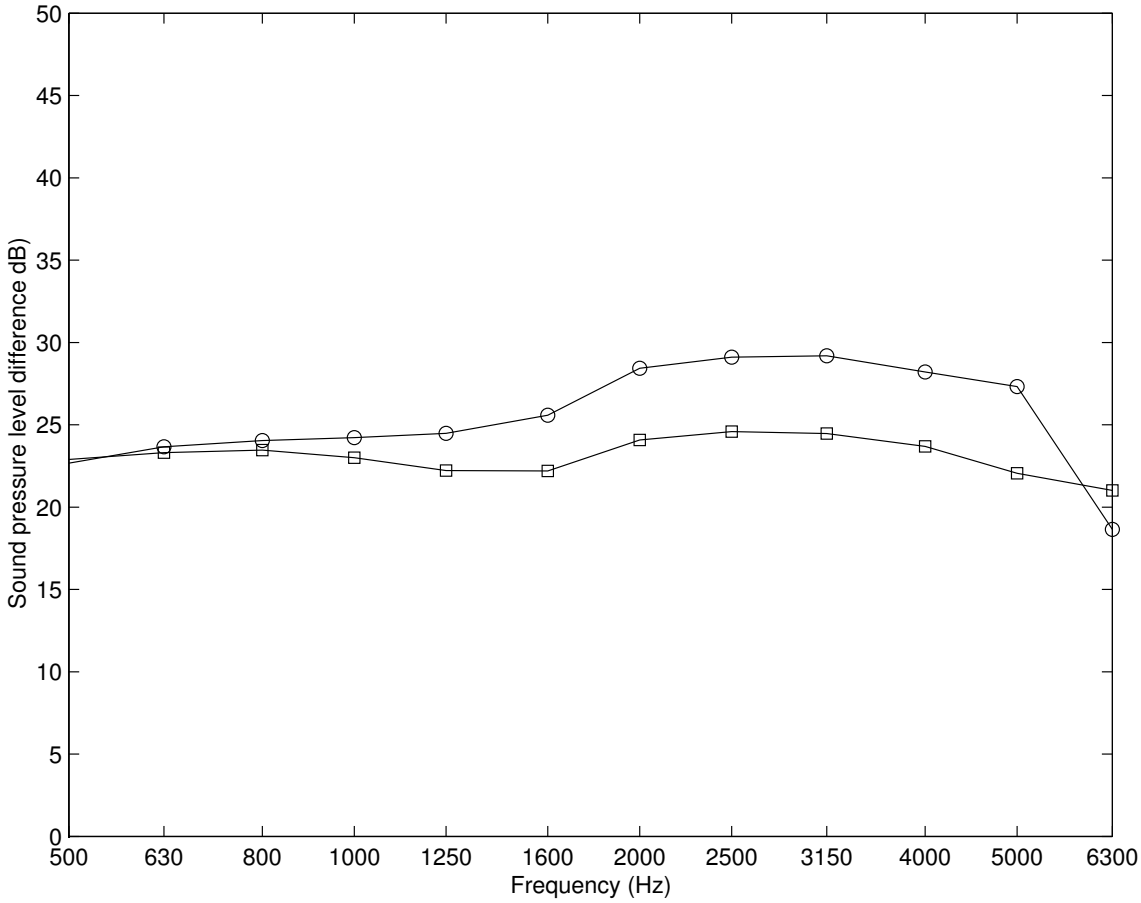

Figure 6.11. Difference between the sound pressure levels at the reference and the microphone 2 on October 15. '○': with absorptive treatment; '□': without absorptive treatment.

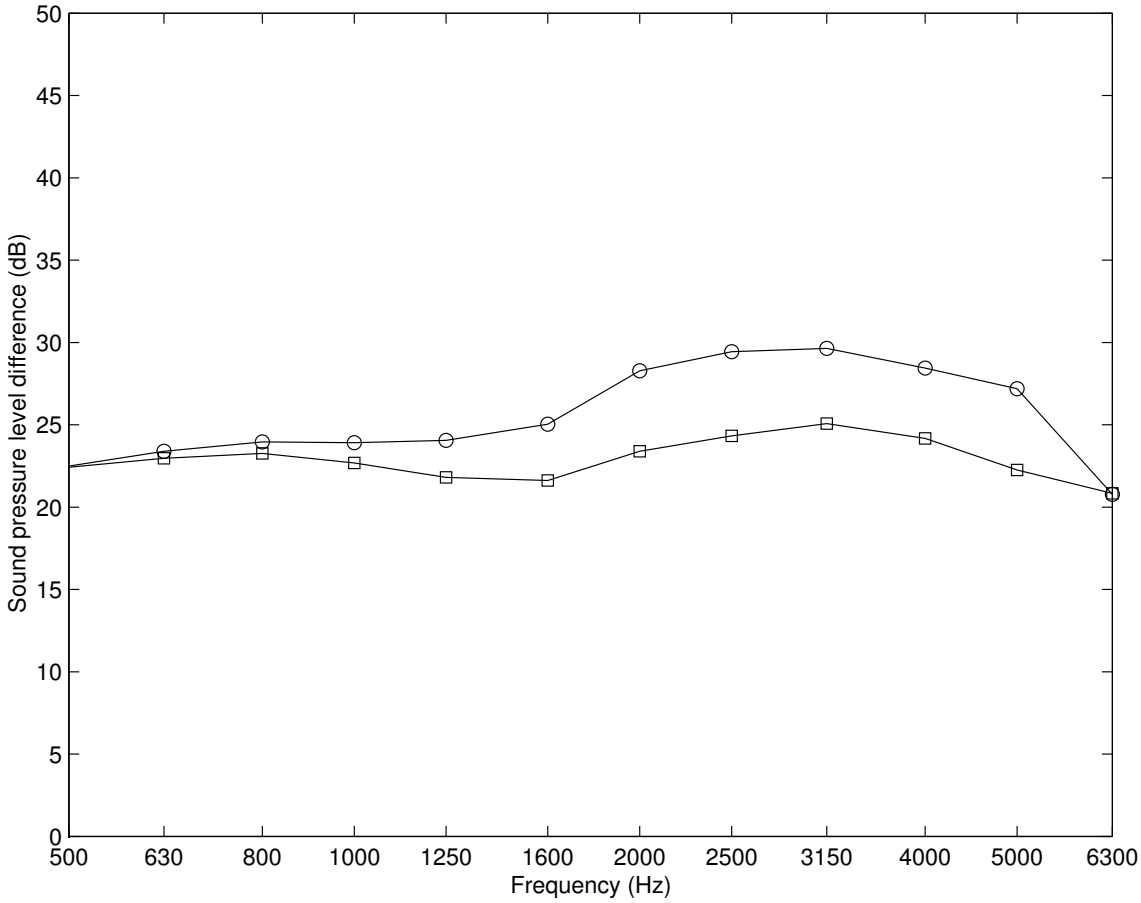

Figure 6.12. Difference between the sound pressure levels at the reference and the microphone 3 on October 15. '$\circ$': with absorptive treatment; '$\square$': without absorptive treatment.

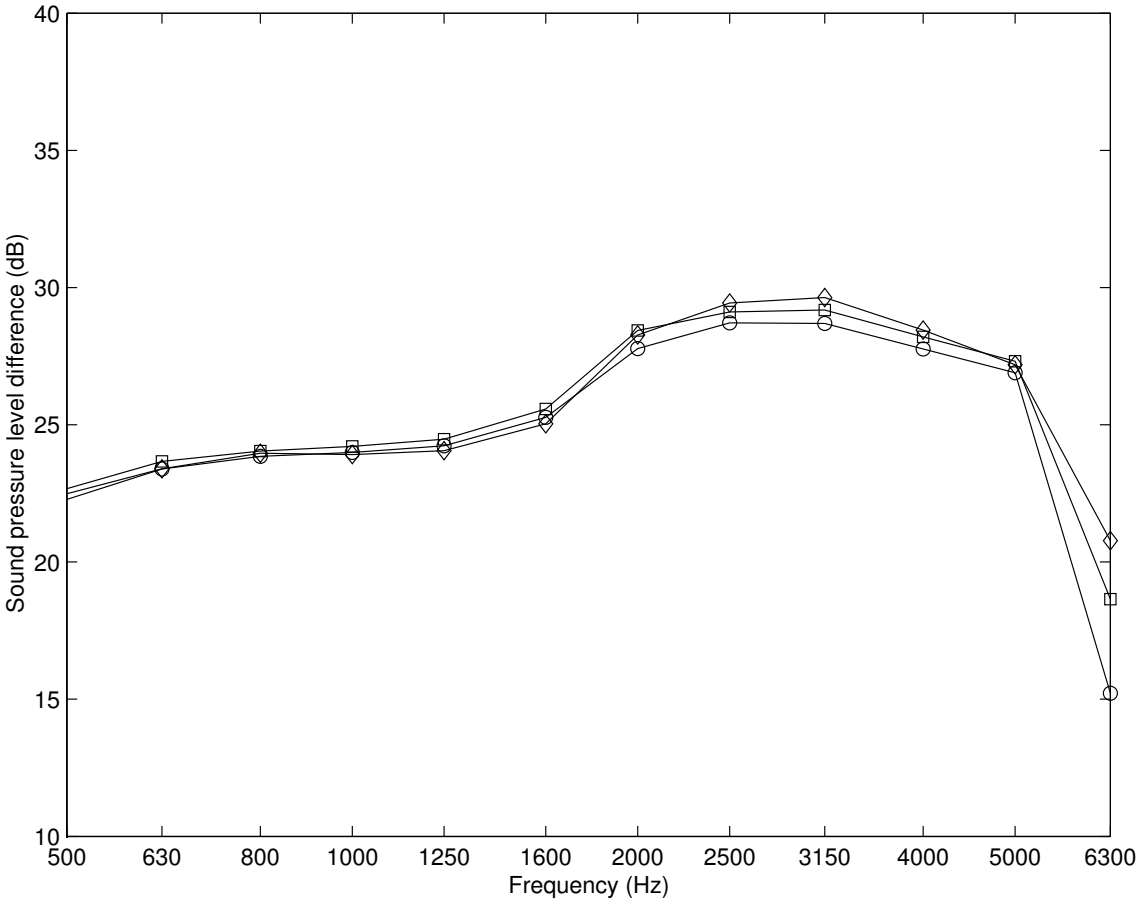

Figure 6.13. Difference between the sound pressure levels at the reference and the field locations on October 15. '○': microphone 1; '□': microphone 2; '◇': microphone 3.

7. CONCLUSIONS

The effectiveness of sound absorptive treatments on the top of rigid sound barriers was investigated for possible application to noise barriers along highways.

First, the relative insertion loss performance of various barrier configurations was compared experimentally. In particular, the insertion losses at selected receiver locations, the insertion loss distribution over the receiver plane and the space-averaged insertion loss were compared for different barrier designs. It was found that an absorptive treatment placed near the barrier edge increased the insertion loss at receiver locations in the shadow zone behind the barrier, and that the zone of insertion loss enhancement is apparently larger than that provided by straight or T-shape extensions of the same size as the absorptive treatment. The space-averaged insertion loss confirmed the conclusion.

Secondly, different shapes of acoustic treatment were evaluated in order to identify the best design. It was found that a circular shape performs best in an average sense among the four different shapes considered.

Two different absorptive materials were compared experimentally. The glassfiber performed better at higher frequencies, while QUASH made of polyolefin resulted in greater insertion loss at relatively low frequencies. The designs implemented with both of the absorptive materials yielded a much greater insertion loss compared to that of corresponding barrier designs with the same height made of rigid material.

Fourth, a numerical model was successfully implemented to predict the performance of sound barriers with absorbing tops. Frequency averaging over octave bands was used to facilitate the comparison between the numerical results and experiments. The predictions from the boundary element model were in good agreement with the experimental results.

Lastly, outdoor measurements were performed along US 20 in South Bend, Indiana. Measurements made in an area protected by an existing barrier showed a benefit between 2 dB and 5 dB at frequencies from 2000 Hz to 5000 Hz when an add-on device made of QUASH was attached to the existing barrier's edge.

Further work is needed to assess the benefits of sound absorptive treatments in the field, and evaluate their practicality, for example, cost and susceptibility to environmental exposure.

LIST OF REFERENCES

[1] S. Suh, L. Mongeau, and J. S. Bolton. Study of the performance of acoustic barriers for indiana toll roads. Technical Report JTRP-2001/20, Indiana Department of Transportation, Division of Research, 2001.

[2] G. F. Butler. A note on improving the attenuation given by a noise barrier. *Journal of Sound and Vibration*, 32(3):367–369, 1974.

[3] A. D. Rawlins. Diffraction of sound by a rigid screen with a soft or perfectly absorbing edge. *Journal of Sound and Vibration*, 45(1):53–67, 1976.

[4] A. D. Rawlins. Diffraction of sound by a rigid screen with a soft or perfectly absorbing edge. *Journal of Sound and Vibration*, 47(4):523–541, 1976.

[5] G. R. Watts. Acoustic performance of parallel traffic noise barriers. *Applied Acoustics*, 47(2):95–119, 1996.

[6] G. R. Watts and N. S. Godfrey. Effects on roadside noise levels of sound absoprtive materials on nosie barriers. *Applied Acoustics*, 58:385–402, 1999.

[7] K. Fujiwara and N. Furata. Sound shielding efficiency of a barrier with a cylinder at the edge. *Noise control engineering journal*, 37(5):5–11, 1991.

[8] T. Okubo and K. Fujiwara. Efficiency of a noise barrier on the ground with an acoustically soft cylindrical edge. *Journal of Sound and Vibration*, 216(5):771–790, 1998.

[9] T. Okubo and K. Fujiwara. Efficiency of a noise barrier with an acoustically soft cylindrical edge for practical use. *Journal of Acoustical Society of America*, 105(6):3326–3335, 1998.

[10] T. Okubo and K. Fujiwara. Efficiency of a noise barrier with an acoustically soft cylindrical edge for practical use. *Journal of Acoustical Society of America*, 105(6):3326–3335, 1999.

[11] K. Fujiwara. Noise shielding efficiency of barrier with multiple absorbing edge obstacle. In *INTER-NOISE 1999*, 1999.

[12] M. Moser and R. Volz. Improvement of sound barriers using headpieces with finite acoustic impdeance. *Journal of Acoustical Society of America*, 106(6):3049–3060, 1999.

[13] W. Bowlby, J. Higgins, and J. Reagan. Noise barrier cost reduction procedure: Stamina2.0 / optima: User's manual. Technical Report FHWA-DP-58-1, U.S. Department of Transportation Federal Highway Administration, Arlingoton, VA, 1982.

[14] U. J. Kurze and G. S. Anderson. Sound attenuation by barriers. *Applied Acoustics*, 4:35–53, 1971.

[15] G. S. Anderson, C. S. Y. Lee, G. G. Fleming, and C. W. Menge. FHWA traffic noise model, user's guide. Technical Report FHWA-PD-96-09, U.S. Department of Transportation Federal Highway Administration, Washington D.C., 1998.

[16] B. A. DeJong, A. Moerkerken, and J. D. van der Toorn. Propagation of sound over grassland and over an earth barrier. *Journal of Sound and Vibration*, 86(1):23–46, 1983.

[17] J. L. Rochat. Observations of highway traffic noise measurements behind barriers and comparisons to FHWA's traffic noise. In *INTER-NOISE 2001*, 2001.

[18] R. L. Wayson, J. M. MacDonald, W. Arner, C. Corbisher, P. Tom, D. S. R. K Srinivas, and Brian Kim. Noise barrier measurement, modeling and evaluation at multiple sites in florida. In *INTER-NOISE 2001*, 2001.

[19] P. Menounou, M. R. Bailey, and D. T. Blackstock. Edge wave on axis behind an aperture or disk having a ragged edge. *Journal of Acoustical Society of America*, 107(1):103–111, 2000.

[20] LMS International, Leuven, Belgium. *SYSNOISE User's Guide*, 5.5 edition, 2001.

[21] C. A. Brebbia and J. Dominguez. *Boundary elements an introductory course*. Computational Mechanics Publications, Southampton, third edition, 1992.

[22] R. D. Ciskowski and C. A. Brebbia, editors. *Boundary element methods in acoustics*. Computational Mechanics Publications, Southampton, 1991.

[23] T. W. Wu, editor. *Boundary element acoustics: Fundamentals and computer codes*. WIT press, Southampton, 2000.

[24] J. S. Bolton, R. J. Yun, J. Pope, and D. Apfel. Development of a new sound transmission test for automotive sealant materials. *SAE Transaction, Journal of Passenger Cars*, 106:2651–2658, 1997.

[25] B. H. Song and J. S. Bolton. A transfer-matrix approach for estimating the characteristic impedance and wave numbers of limp and rigid materials. *Journal of Acoustical Society of America*, 107(3):1131–1152, 2000.

[26] Methods for determination of insertion loss of outdoor noise barriers. Technical Report ANSI-S12.8-1998, American National Standards Institute, 1998.

[27] C. S. Y. Lee and G. G. Fleming. Measurement of highway related noise. Technical Report FHWA-PD-96-046, John A. Volpe National Transportation Center, 1996.

[28] G. R. Watts and P. A. Morgan. Acoustic performance of an interference-type noise-barrier profile. *Applied Acoustics*, 49(1):1–16, 1996.